The Rational Design of a Bio-electrochemical System

A quantitative investigation into the design of a commercially viable microbial electrolysis cell for domestic wastewater treatment and hydrogen production

Daniel C. Aiken

A thesis presented for the degree of
Doctor of Engineering

School of Engineering
Newcastle University
United Kingdom
March 2020

Abstract

Reducing energy use is a key challenge for the wastewater industry. Microbial electrolysis cells (MEC) may provide a solution. No commercially viable bio-electrochemical has yet been developed, despite over 40,000 publications. This thesis seeks to serve as a guide to a commercially viable MEC design. Cost-performance targets are presented for MEC to be financially competitive with activated sludge treatment (AS). By reducing the cost of the anode and current collector by 90%, a viable organic loading rate (OLR) is shown to be between 800 and 1,400g-COD/m^3/d, if MEC serve a 20 year lifetime. An order of magnitude greater than previously achieved in pilot reactors - although acetate concentrations, a known direct food source for electrogenic species, are typically low (c.10mg-COD/l). A high performance MEC will be dependent upon sufficient concentrations of readily-digestible substrate close to a colonisable anode surface. To quantify a viable MEC design, a macro-model was developed using the Navier-Stokes equations and Monod kinetics. The model predicts MEC performance over a range of acetate concentrations and anode interstices distances, the space between anodes. To calibrate the model and differentiate biofilm kinetics from total microbial kinetics, the concept of current degradation rate is introduced. Models were calibrated against empirical observations of MEC performing under controlled conditions, analogous to those found in domestic wastewater, with a mean accuracy of 85.6%. Acetate concentrations (10-50mg-COD/l), conductivity (770$\pm$15μS/cm), temperature (10$\pm$0.5°C) and pH (7.50$\pm$0.05) were carefully controlled. Maximum acetate degradation rates of 10mg-COD/l were observed. Coulombic efficiencies and current densities were both observed to increase with concentration. To achieve the current produced in the laboratory, biofilms must have had higher local ORR than found in the bulk microbial community. As such, decreasing anode interstices distances significantly improved ORR for all modelled concentrations. In combination with pre-treatment technologies, MEC may surpass target ORR. However, material costs to break-even are low due to the requirements for additional anode materials.

Acknowledgements

My first thanks go to the countless people who have tirelessly worked to provide the conditions and knowledge for our continued development. I would like to extend my gratitude to Tom Curtis for initially believing in my academic potential and for his continued support and assistance throughout this project. I'd like to thank Jaime Amezaga for first organising this opportunity with the STREAM programme and for his sage advice. I'd also like to thank Chris Jones for his initial backing of the project and continued interest and support. My thanks also extend to my supervisor Elizabeth Heidrich whose help in practical matters and editing was of great assistance. I'd also like to thank Jan Dolfing for his assistance with technical details earlier in the project. A strong recognition goes to my colleagues Carolina Osprey for conducting the DNA extractions, Polly Moreland for conducting conducting the gel electrophoresis, to Andrew Nelson from NUOmics for the Illumina sequencing and Sarah Cotterill for her initial guidance with her pilot reactor.

I'd like to thank the EPSRC and Northumbrian Water for their funding, without whom this work would not have been possible. I'd also like to extend thanks to the staff at Northumbrian Water for their forthcoming provision of facilities and data that helped keep this project grounded. Specific thanks go to Andrew Moore, Trevor Fenwick, Peter Gill, Steve and Chris.

I'm also greatly appreciative to the staff associated with the STREAM project: Paul Jeffrey, Ewan McAdam, Tania Rice, Pablo Campo Moreno, Rachel Whitton and Mike Templeton for their organisation and commitment to providing career development. Especial thanks go to Justine Easten whose unwavering diligence in organisational matters did not go unrecognised. I'm also grateful to my friends and colleagues on the STREAM programme Dominic Carver, Shaun Boatwright, Thomas Collin, Aiden Robson and Rob Birch for their good company and humour.

My thanks extend to the laboratory support staff at Newcastle University: Dave Race, Amy Bell, Sarah Smith, Lisa Deveaux-Robinson, Amy Roberts, Henriette Christensen and Stephen Allen for their advice, organisation and assistance. I'd also like to give a very warm thanks to Daniel Leicester, Carl Samuel, Carolina Osprey, Vincenzo Padricello, Florence Jong, Emy Ekwenna and Matt Bell for their company and advice during the long laboratory hours.

And finally, I'd like to give thanks to my friends and family who have supported me through the ups and downs of not just the last few years, but throughout my life, and without whom I'd surely have lost my marbles years ago.

Contents

Abstract i

Acknowledgements iii

Acronyms xiii

1 Introduction 1

1.1 The need for sustainable wastewater treatment . . . 1
1.2 Bio-electrochemical systems . . . 2
1.2.1 Thermodynamics . . . 2
1.2.2 Microbial fuel cells . . . 3
1.2.3 Microbial electrolysis cells . . . 4
1.3 Managing microbial electrolysis cell performance . . . 5
1.3.1 Key reaction rates . . . 5
1.3.2 Biochemical performance and microbiology . . . 7
1.3.3 Electrode surface area . . . 8
1.3.4 Electron losses . . . 9
1.4 State of affairs: bio-electrochemical research . . . 11
1.4.1 Modelling . . . 14
1.5 Key challenges facing MEC development . . . 16
1.6 Aims, Objectives and Research Questions . . . 18

2 Avenues to the financial viability of microbial electrolysis cells (MEC) for domestic wastewater treatment and hydrogen production 19

2.1 Introduction . . . 19
2.2 Methodology . . . 20
2.2.1 Case study . . . 20
2.2.2 Material investment costs . . . 21
2.2.3 Energy costs and revenue . . . 23
2.2.4 Hydrogen production . . . 23
2.2.5 Activated sludge comparison . . . 23

2.2.6 NPV calculation comparison . . . 24
2.2.7 MEC scenarios . . . 24
2.2.8 Target Finder . . . 25
2.3 Results and Discussion . . . 26
2.3.1 Current state of financial feasibility . . . 26
2.3.2 Material costs . . . 27
2.3.3 Hydrogen production . . . 27
2.3.4 Applied voltage . . . 29
2.3.5 Future energy prices . . . 29
2.3.6 Asset recovery . . . 29
2.3.7 Maintenance: Replacement costs . . . 30
2.3.8 Maintenance: Personnel . . . 30
2.3.9 Space . . . 30
2.3.10 Making financially viable MECs . . . 31
2.4 Conclusion . . . 32

3 Limitations of acetate concentration on electrogenic biofilm activity 33
3.1 Introduction . . . 33
3.2 Methodology . . . 35
3.2.1 Set-up . . . 35
3.2.2 Operation . . . 38
3.2.3 Analysis . . . 39
3.3 Results and Discussion . . . 43
3.3.1 Acetate degradation . . . 43
3.3.2 Maximum current density . . . 46
3.3.3 Time until maximum current . . . 47
3.3.4 Current degradation rate . . . 51
3.3.5 Coulombic efficiency . . . 53
3.3.6 Two-electrode and three-electrode systems . . . 55
3.4 Conclusion . . . 63

4 Designing a viable microbial electrolysis cell (MEC) 65
4.1 Introduction . . . 65
4.2 Methods . . . 68
4.2.1 Phase one: CFD-biofilm model and discretisation . . . 68
4.2.2 Phase two: Calibration . . . 73
4.2.3 Phase three: Extrapolation . . . 78

4.3 Results and Discussion . . . 81
4.3.1 Organic removal rates . . . 81
4.3.2 Energy recovery . . . 84
4.3.3 Capital costs and design . . . 87
4.3.4 Input parameters . . . 91
4.3.5 Calibration accuracy . . . 93
4.4 Conclusion . . . 97

5 Conclusion **99**
5.1 Background . . . 99
5.2 The challenge . . . 100
5.3 Commercial viability and other findings . . . 100
5.4 Review . . . 103
5.5 Further research . . . 104

Bibliography **107**

Appendices **123**

A Supporting information for Chapter 1 **125**

B Supporting information for Chapter 3 **127**

C Supporting information for Chapter 4 **139**

List of Figures

1.1 Number of results for search terms in ScienceDirect, 23^{rd} October 2020 13
1.2 Reported current densities in literature fed with acetate and wastewater (Bibliography for current density literature study) 15

2.1 Target cost-performance ratios for financially competitive MECs treating domestic wastewater 27
2.2 Percentage of components costs compared to total material costs (left) compared to early estimates (Rozendal et al., 2008) (right) 29
2.3 Cost-performance ratio curves for eight scenarios of a financially competitive MEC** 31

3.1 Monod substrate degradation rate distribution against COD concentration 44
3.2 Maximum current density with respect to concentration 47
3.3 Time taken from feeding to reach maximum current density 48
3.4 Calculated feed times for each reactor over each run 49
3.5 Acetate concentrations during feeding runs 50
3.6 Smoothed current dose-responses following feeding for all 6 runs and fit to exponential decay curves 52
3.7 Substrate degradation rate against COD concentration 53
3.8 Coulombic efficiency against COD concentration 54
3.9 Substrate degradation rates against COD concentration in 2ES and 3ES 56
3.10 Current densities, current degradation rates and coulombic efficiencies for 2ES and 3ES 57
3.11 Cell voltages and anode potentials in 2ES and 3ES versus current density 59
3.12 Power and resistances in 2ES and 3ES versus current density 59
3.13 Changes in microbial community between runs 61
3.14 Observed species and coulombic efficiency 62
3.15 Simpson's diversity and coulombic efficiency 62

4.1 ORR at 90% substrate removal and anode chamber width under no growth and linear growth scenarios fed with three different acetate concentrations 81
4.2 Net energy projections with an additional voltage of 1.0V 84
4.3 Comparative net energy projections for MEC vs. AS 85

4.4 Projected hydrogen yields from MEC . . . 85
4.5 Projected CO2 equivalent emissions removed with 1.0V applied . . . 86
4.6 Allowable unit costs to break-even over a 20 year lifetime . . . 87
4.7 Time until 90% substrate removal . . . 88
4.8 Anode surface area required per volume per hour . . . 89
4.9 Allowable anode area costs to break-even over a 5, 10 and 20 year lifetimes. . . . 90
4.10 Violin plot of input ranges for models with good fit to all observation means . . . 92
4.11 Model accuracies found during calibration process . . . 94
4.12 Substrate degradation rate . . . 95
4.13 Maximum current densities . . . 95
4.14 Current degradation rate . . . 96
4.15 Coulombic efficiency . . . 96

B.1 Schematics for experimental 3D printed reactor chamber . . . 127
B.2 Gel electrophoresis imaging to detect proteins in samples . . . 128
B.3 Standard curves used for acetate concentrations . . . 129
B.4 Starting acetate concentration analysis into variation . . . 130
B.5 Q-Q plot for substrate concentrations on raw data and with run means, and reactor means removed . . . 131
B.6 Q-Q plot for substrate degradation rates . . . 132
B.7 Linear sweep voltammetry to determine stable potential range . . . 132
B.8 Smoothed current dose-responses following feeding for all 6 runs and fit to exponential decay curves . . . 133
B.9 Calculated feed times for each reactor over each run . . . 134
B.10 Profile qualities in forward runs . . . 135
B.11 Profile qualities in reverse runs . . . 136
B.12 Learning errors in forward runs . . . 137
B.13 Learning errors in reverse runs . . . 138

C.1 Discretised scheme with biomass placements . . . 139
C.2 Outputs for substrate, maximum current density, coulombic efficiency, and cpu time elapsed for most accurate permutation . . . 140
C.3 Substrate removal over time in most accurate model . . . 140
C.4 Current production over time in most accurate model . . . 141
C.5 Biofilm placement in new scheme . . . 141
C.6 Mesh independence test for a range of concentrations and widths . . . 141

List of Tables

1.1 Pilot reactor performances 14

2.1 List of components, material, price and source 21
2.2 Performance parameters of large-scale MEC (Heidrich et al., 2014) 22
2.3 Scenario descriptions 25
2.4 20-year net present value, target current densities, and target OLR for MECs for eight scenarios 28

3.1 Statistical description of substrate degradation rates 45
3.2 Statistical description of measured acetate concentrations 46
3.3 Statistical description of data-set for maximum current densities 48
3.4 Statistical description of data-set for current degradation rates 54
3.5 Statistical description of data-set for coulombic efficiencies 55

4.1 Calibration process 73
4.2 Empirical observations used for calibration and input optimisation 75
4.3 Initial input permutations 76

A.1 technology search terms used for literature review. Search format: '"*technology*" wastewater' 126

B.1 Voltage drift of reference electrodes and subsequent voltage corrections 127
B.2 Placement of salt bridge tip in anode compartment 128
B.3 Measured resistance across cell to determine accuracy of current readings 128
B.4 pH drift after 3 weeks of operation with mean concentration of 37.4mg/l 129

Acronyms

AD	Anaerobic digestion
AS	Activated sludge
ATP	Adenosine triphosphate
BES	Bio-electrochemical systems
BOD	Biological oxygen demand
BVM	Butler-Volmer-Monod
CFD	Computational fluid dynamics
COD	Chemical oxygen demand
CPU	Central processing unit
CV	Coefficient of variation
GHG	Greenhouse gas emissions
MEC	Microbial electrolysis cell
MFC	Microbial fuel cell
NPV	Net present value
OLR	Organic loading rate
RE	Reference electrode
SD	Standard deviation
SS	Suspended solids
UK	United Kingdom
VFA	Volatile fatty acid
WWTP	Wastewater treatment plant
3ES	Three-electrode system
2ES	Two-electrode system

Chapter 1. Introduction

1.1 The need for sustainable wastewater treatment

Reducing the energy used in wastewater treatment is one of the most important challenges the water industry faces. Energy use for wastewater treatment accounts for 1-3% of the total electricity used in developed countries (Curtis, 2010, US EPA, 2006). A value, which places energy as the second highest cost to water and wastewater utilities, after personnel (Olsson, 2012). This is particularly incongruous because wastewater contains a mean energy content of 16.1kJ/g-COD (Dai et al., 2019), approximately 10 times more energy than is currently used to treat it.

Biological wastewater treatments can remove up to 90% of organic matter. The two most common conventional biological wastewater treatments are attached growth processes and suspended growth processes (US EPA, 2014). Predominantly, heterotrophic bacteria in both types of treatment use the organic matter as an electron donor and oxygen (O_2) as an electron acceptor. In attached growth processes microbial growth occurs on a surface such as rock or plastic, as seen in trickling filters. Whilst, in suspended growth processes microbial growth is suspended within a tank by aeration. Here, the aerobic bacteria can work more efficiently as they have increased access to oxygen, and our constantly buffered by passing gas thus increasing mass transport.

Activated sludge (AS), the first suspended growth process, (Arden and Lockett, 1914) is the most prevalent biological wastewater treatments globally (by volume treated) (Malovanyy et al., 2016). AS, arguably, instigated the single largest improvement to environmental protections and public health in the post-industrial western world. However, AS is energetically costly. Aeration lanes in AS tanks require 40-60% of the energy used in wastewater treatment (Shi, 2011). In these aerobic conditions large amounts of sludge is produced, which requires transport and disposal. To regain some of this energy, investment in the anaerobic digestion (AD) of sludge from the AS process (CH_4) is becoming more widespread, especially in the UK (Green Investment Back, 2015, Shi, 2011). However, even with the use of AD, wastewater treatment plants (WWTP) are net consumers of energy (Dobrzyńska and Bernat, 2004).

Approximately 80% of global wastewater is still released into the environment without adequate treatment (WWAP, 2017). And 27% of the global population still lack basic sanitation services (Guterres, 2019). Improving the extent of wastewater treatment, globally, will be essential to im-

proving human health and satisfaction in developing regions, whilst simultaneously reducing industrial economies impact on the environment. However, in regions that rely upon fossil fuels as their primary energy source, increasing wastewater treatment will indirectly increase global carbon emissions, contributing to climate change. There is therefore a need for sustainable wastewater treatments both in developed and developing countries.

Wastewater treatment is currently an energy intensive process, yet wastewater has been estimated to contain ten times the energy required to treat it (Heidrich et al., 2011). Bio-electrochemical systems (BES) could address the misalignment of energy in WWTP. BES make use of electroactive bacteria, which degrade organic matter. An electrogenic biofilm is grown on an anode in an electrochemical cell (Rozendal et al., 2008). The organic matter is the electron donor, and the electrode is the electron acceptor (Logan and Rabaey, 2012). One type of BES, microbial duel cells (MFC) can directly recover the electricity produced by the electrogenic biofilm, whilst other forms of BES use a supplementary voltage to recover value-added products at the cathode.

The advantages of BES over AS and AD as a treatment technology include: low energy input; sustainable energy recovery (Baeza et al., 2017, Gil-Carrera et al., 2013); and proven function at low temperatures with dilute domestic wastewater (Cotterill et al., 2017, Heidrich et al., 2014). This is important as heating wastewater is a costly endeavour due to its high thermal capacity (Metcalf & Eddy et al., 2003). Importantly MEC could be, at least partially, retrofitted into existing infrastructure. Wastewater treatment facilities are typically built for 20–50 year service lives (Patricia et al., 2011), yet the biological contents of these tanks could be changed in a matter of weeks or months (Kumar et al., 2017).

1.2 Bio-electrochemical systems

1.2.1 Thermodynamics

Gibbs free energy is used to determine whether a chemical process occurs spontaneously or requires additional energy. When Gibbs free energy is negative the process will proceed spontaneously (exergonic). Alternatively, when Gibbs free energy is positive the reaction requires additional energy input (endergonic). The change in Gibbs free energy is the change in total heat content of a system (enthalpy, H) minus the product of the absolute temperature (T) and the change in heat content unavailable for work (entropy, S) (1.1). In this context, work and heat are thought of as flows of energy across system boundaries.

$$\Delta G = \Delta H - T\Delta S \tag{1.1}$$

In electrochemical cells it is useful to consider the electromotive force (emf). The emf in a electrochemical cell is determined by the differences in the potentials of the electrodes (1.2)

$$E_{emf} = E_{cathode} - E_{anode} \tag{1.2}$$

The emf can be used to determine the change in Gibbs free energy (ΔG), from the amount of electrons (n) involved in the reaction and Faraday's constant (F = 96,485C/mol) (1.3)

$$E_{emf} = -\frac{\Delta G}{nF} \tag{1.3}$$

1.2.2 Microbial fuel cells

In MFC anodic chambers the electrogenic biofilm oxidises organic matter. Typically, acetate is directly oxidised by the electrogenic organisms (1.4), though metabolic pathways are only partially understood (Ishii et al., 2015, Zhao, 2018). At neutral pH (7), with low concentrations of acetate (5mM) and bicarbonate (5mM) the potential of this oxidation reaction is -0.28V (Lim et al., 2018). In the cathode chamber, oxygen is supplied. The oxygen and protons in the solution are reduced to water at +0.84V (Rabaey and Verstraete, 2005) (1.4). This creates a charge gradient between the electrodes. As the emf is positive c.+1.1V, and the Gibbs free energy negative the reaction occurs spontaneously and electrical current flows from the anode to the cathode (Logan et al., 2006). The electrical current can the be used to charge external devices or be fed into the grid.

Anode

$$C_2H_2O_2 + 4H_2O \rightarrow 2CO_2 + 2HCO^{3-} + 9H^+ + 8e^- \tag{1.4}$$

Cathode

$$2O_2 + 8H^+ + 8e^- \rightarrow 4H_2O \tag{1.5}$$

MFC need the electron acceptor: oxygen, to be present at the cathode. This requires the use of either: large-scale air-cathodes, which are difficult to engineer, or aeration of the cathode chamber, which is energetically expensive. Electricity must be used directly or stored in external batteries. Furthermore, MFC have been known to undergo voltage reversal, which damages the bioanode, and would incur a high replacement cost. This is prevented in a Microbial Electrolysis Cell (MEC) where voltage is applied (Li et al., 2017). Moreover, due to the cheap nature of electricity, MFC have been shown to have little commercial value (Christgen et al., 2015, Rozendal et al., 2008). Other value-added products may be needed to make BES technology a financially feasible technology for the treatment of domestic wastewater (Cusick et al., 2010, Rozendal et al., 2008).

1.2.3 Microbial electrolysis cells

In MEC, higher value products such as hydrogen gas, or other value-added chemicals, can be recovered at an anaerobic cathode by supplementing the potential difference between electrodes (Rabaey and Verstraete, 2005, Rozendal et al., 2008). Hydrogen production is of particular interest as an application of MEC technology. Hydrogen is a storable source of sustainable energy, a feature missing from other sustainable energy sources such as solar and wind. This also allows hydrogen to be used as fuel in vehicles. Compared to other electrolytic products, hydrogen requires only two electrons from the electrochemical process and protons are sufficiently available in water and wastewater.

In an MEC, the anode reaction occurs in the same manner as an MFC. The cathode reaction however, must occur in an anaerobic environment. The reduction of protons to hydrogen gas occurs at a theoretical potential of -420mV (Rabaey and Verstraete, 2005). The emf is thus -0.12V and the process is therefore endergonic. The theoretical potential difference required to produce hydrogen in an MEC (0.12V) are much lower than conventional electrolytic technologies (1.23V) (Rozendal et al., 2008). Though, in reality, high overpotentials in an MEC increase the minimum potential difference to c.0.6V (Fornero et al., 2010).

Anode

$$C_2H_2O_2 + 4H_2O \rightarrow 2CO_2 + 2HCO_3^- + 9H^+ + 8e^- \tag{1.6}$$

Cathode

$$8H^+ + 8e^- \rightarrow 4H_2 \tag{1.7}$$

These systems could be retrofitted into existing infrastructure and have been demonstrated at pilot scale (Baeza et al., 2017, Cotterill et al., 2017, Cusick et al., 2011, Gil-Carrera et al., 2013, Heidrich et al., 2014). Previous estimates for hydrogen production costs in MEC were \$4.51/kg-H_2 for winery wastewater and \$3.01/kg-H_2 for domestic wastewater, less than the estimated merchant value of hydrogen (\$6/kg-H_2) (Cusick et al., 2010), which shows greater promise commercially than MFC.

In further credit to MEC, previous research has shown that the applied potential can effect the microbial community (Hasany et al., 2015). This could, hypothetically, allow a 'tuning' for oxidation of specific wastes and compounds. High anode potentials have also been shown to increase the activity of the electrogenic biofilm and reduce start-up times (Kumar et al., 2017). Most importantly, electrogenic organisms have been observed to outcompete aerobic heterotrophs in substrate removal rates when under the control of a potentiostat (Ren et al., 2014), which could reduce reactor size and cost.

Due to these benefits the scope of this thesis will focus predominantly on MEC. However, some of the performance aspects of MEC are somewhat interchangeable with MFC as the electrical generation in both systems is driven by a community of anode-respiring electrogenic organisms that require organic matter for microbial growth and electron generation.

1.3 Managing microbial electrolysis cell performance

Managing and improving MEC performance requires an understanding of the driving forces behind the thermodynamic reactions. The rates at which different reactions occur is important, as is the sequence of events. Organic matter is oxidised by microorganisms in the anode chamber. These microbes exploit the energy and chemicals released in biochemical reactions for their own growth and maintenance. Microorganisms, which are electrogenic and which are attached to the electrode in a sufficiently conductive manner, release electrons into the electrochemical cell producing current. The current is driven by the rate at which organic matter is oxidised by the electrogenic biofilm. Electrons reach the cathode and are converted into hydrogen gas. The production of hydrogen is, in turn, driven by the current. Therefore the most significant factors affecting MEC performance is the rate at which organic matter is oxidised, as well as the proportion of oxidation that is conducted by the electrogenic biofilm.

1.3.1 Key reaction rates

Organic matter oxidation

The rate at which the oxidation of organic matter ($\frac{dC_s}{dt}$) occurs in the anode compartment, depends primarily upon microbial kinetics, which can be approximated by Monod kinetics at a macro level (1.8). Substrate degradation rates (q_s) tend towards the maximum substrate uptake rate ($q_{s,max}$) as the concentration of the chemical species (C_s) increases. Moreover, increases in degradation rates increase in proportion to the concentration of biomass (C_x). The half saturation constant (K_s) dictates at what concentration the substrate degradation rate is half that of the maximum substrate uptake rate and is usually determined experimentally in each specific circumstance. Monod kinetics is dependent upon on the microbial species, the chemical species and the environmental conditions. Determining rates for each microbial reaction becomes impractical in a complex chemical environment such as wastewater.

$$\frac{dC_s}{dt} = q_s = -q_{s,max} C_x \frac{C_s}{K_s + C_s} \tag{1.8}$$

Chemical oxygen demand

Chemical oxygen demand (COD) is often used in the wastewater industry to quickly indicate the quantity of organic matter. A strong oxidising agent is used to oxidise the organic matter under acidic conditions and the resulting change in colour is measured with a spectrophotometer (APHA, 2017). COD is an assessment of a complex chemical reality and approximates the concentration of oxygen consumed during the oxidation reaction. Not all of the COD is readily biodegradable (Fornero et al., 2010, Henze and Comeau, 2008).

Current production

The current (I) produced by the biofilm depends upon the rate of oxidation by electrogenic species in electrical contact with the anode (Equation 2.1) (Logan, 2008). Current is found by converting the moles of electrons released per second into current, using Faraday's constant (F = 96,486C/mol), and multiplying by the coulombic efficiency (C_e). Coulombic efficiency describes the proportion of electrons from substrate removed that is passed into the circuit. The number of electrons released in the reaction depends upon the volume of the anode chamber (V), the time over which the reaction takes place (t) and the measurable changes in COD. Moles of electrons released per gram of COD (n = 8mol-e^-/g-COD) derives from the molecular weight of oxygen (32 g/mol) and the moles of electrons released per mole of oxygen (4mol-e^-/mol-O_2).

$$I = \frac{C_e \cdot F \cdot V}{n} \frac{dCOD}{dt} \tag{1.9}$$

Hydrogen production

The rate at which hydrogen is produced follows Faraday's law of electrolysis (1.10). The change in concentration of hydrogen gas (m_{H_2}) is proportional to the current (I). Faraday's constant is used to find the moles of electrons arriving at the cathode each second (F = 96,485C/mol). The proportion of electrons converted into hydrogen gas is accounted for by the cathodic efficiency (C_{ce}). The mass of hydrogen gas is found from the molecular weight of hydrogen (M_{H_2} = 2.016g/mol) and the valency of hydrogen gas (z = 2).

$$\frac{dm_{H_2}}{dt} = \frac{C_{ce} \cdot M_H}{F \cdot z} I \tag{1.10}$$

1.3.2 Biochemical performance and microbiology

As oxidation of organic matter is the first reaction in the MEC reaction sequence, high biochemical oxidation rates are essential for high current and hydrogen production. Moreover, wastewater utilities' primary objective is to treat the organic matter in waste streams so that it can be safely released into the environment. In the EU, failing to meet this objective can lead to heavy fines. Furthermore, retrofitting MEC into existing aeration basins will require MEC to have organic loading rates (OLR) greater than AS, otherwise further civil works will be required adding to cost. Therefore improving the oxidation of organic matter in the anode chamber is a high priority.

Known electrogenic species are dependent upon the oxidation of volatile fatty acids for growth and maintenance. Electrogens possess the ability to transfer electrons from outside of their cell into a chemical or material that is not the immediate electron acceptor. BES use this process to drive a circuit in an electrochemical system by growing exoelectrogens on an anode surface and the cathode is the eventual electron acceptor. Acetate provides the highest current densities when used as a single food source (Speers and Reguera, 2012, Zhao, 2018). Wastewater fed BES have typically suffered from limited current densities (Figure 1.2). Typically, the concentration of volatile fatty acids (VFAs) in domestic wastewater is low (Henze and Comeau, 2008, Shi, 2011, Xin et al., 2018). In consequence the biodegradability of soluble organics and fermentation rates of particulate matter in wastewater have been shown as limiting factors (Dhar and Lee, 2014, Velasquez-orta and Yu, 2011). Whilst the microbial networks that support high performing biofilms is still not understood (Ishii et al., 2015). Pre-treatment technologies can be used to increase the concentration of VFAs through biodegradation of more complex organic matter. Hydrolytic up-flow reactors have previously been used to increase acetate concentrations in domestic wastewater (Ligero et al., 2001) and dark fermentation significantly increased acetate and other VFAs from food waste (Cardeña et al., 2018).

Electrogens are predominantly anaerobic (Rabaey and Verstraete, 2005). Anaerobes, typically, only make 2 ATP molecules (adenosine triphosphate) per glucose, whilst aerobic organisms can make 38 ATP molecules per glucose (Kolmos, 2012) and so have a competitive advantage in terms of growth and maintenance. This slows anaerobic populations response to changes in substrate concentrations. In temperate climates, domestic wastewaters have constantly varying chemical concentrations due primarily to variations in temperature and rainfall. Anaerobic treatments are therefore at a disadvantage as their microbial populations cannot grow grow as quickly as aerobic treatments. However, under certain circumstances, electrogenic organisms have been observed to outcompete aerobes in their environment in terms of removal rates (Ren et al., 2014) and MEC have been proven to work at low temperatures (Heidrich et al., 2014), which typically limit microbial activity. These are important observations however, MEC energy extraction requires electrogenic

organisms to colonise a surface and are thus performance is limited by the colonisable surface area of the electrode

Exoelectrogenic species are still being discovered. Previous MFC and MEC have predominantly contained *Shewanella spp.* and *Geobacter spp.* (Logan, 2008). In nature, *Geobacter* gain energy from the coupled oxidation of acetate and reduction of a secondary chemical (Reguera and Kashefi, 2019). *Geobacter spp.* rely upon electrogenic electron transport for ATP production (Mahadevan et al., 2006). The first *Geobacter sp.* to be discovered was *Geobacter metallireducens* (Lovley and Phillips, 1988). This organism reduces iron oxide minerals. The second *Geobacter* discovered was *Geobacter sulfurreducens* (Caccavo et al., 1994), which reduce sulphur into hydrogen sulphide. The genus *Shewanella* contains over 50 known species, which have more diversified microbial interactions (Satomi, 2014). Like *G. sulfurreducens* some species have been observed to reduce sulphur and In BES *Shewanella oneidensis* have been observed to transfer electrons through the oxidation of lactate to acetate, using the anode as the electron acceptor (Kim et al., 2002). More recently Logan et al. (2019) reviewed the literature and found mention of multiple electrogenic species from a variety of Genus across 36 MFC. Species found in MFC with the highest power densities ($>$3W/m^2) were: *Esherichia coli DH5*α, *Geobacter Sulfurreducens KN400*, *Shewanella Oneidensis MR-1*, *Shewanella Putrefaciens*. A mixed culture grown in an MFC with a single chamber and an air-cathode was found to have similar power densities but the predominant species were not mentioned.

1.3.3 Electrode surface area

Electrode surface area is referred to in two different contexts, which each have their own impact on biochemical performance. The projected surface area is the 2D projection of the electrode's shape onto a surface. Typically, this is rectangular and can be measured very simply.

The specific surface area of the electrode however, refers to the total area within the 3D volume of the electrode. The surface roughness of an anode creates micro peaks and valleys on the surface increasing the total surface area and thus the area that the biofilm can colonise. Increases in current densities have been observed on 'rough' surfaces (Champigneux et al., 2018). Porous electrodes that are '3D' create huge surface areas relative to their size due to their pores, however gaps less than 0.5mm in diameter may limit mass transport (Chong et al., 2019) reducing their effectiveness. Furthermore, clogging from colloids could frequently occur when applying MEC to domestic wastewater (Aelterman et al., 2008), though pre-treating streams with screens could mitigate this problem.

The more important question however, regards the surface area to volume ratio. Anodes must be close to cathodes to reduce ohmic losses (Logan et al., 2006), which are already in high in

domestic wastewaters (Henze and Comeau, 2008). Moreover, increasing the quantity of material in a reactor increases the total colonisable area for electrogenic species and reduces the time it takes for substrate to diffuse towards the biofilm. However, increasing the quantity of material drastically increases the capital costs, which are already high (Rozendal et al., 2008). A 'real-world' comparison of this can be seen between Heidrich et al. (2013) and Cotterill et al. (2017), which used the same MEC 'cassette' -style MEC design, the same electrode materials and were operated within the same climactic region. Heidrich et al. (2013) designed and operated the first 'cassette'-style MEC design (Table 1.1). Cotterill et al. (2017) used the same design but placed the cassettes and thus the anodes closer to one another. This increased the ORR but also increased the electrode packing area (Table 1.1). As anodes were made of the same carbon felt, the cost-performance of the reactor was worse overall.

1.3.4 Electron losses

Electron losses can occur both before and after the oxidation of organic matter by an anode-respiring organism. Losses occurring before anode-respiration have a larger impact on current and hydrogen production due to the driving effect of substrate concentration and biofilm concentration on electrogenic oxidation rates.

Before electrogenic anode-respiration

Incompatible chemical species with electrogenic metabolisms mean that electrons present in biodegradable organic matter will be used for maintenance and growth by other organisms and may not reach the anode (Zhao, 2018). Hydrolysis of long-chain particles, which are electrogenic non-preferred products, into electrogenic preferred products is orders of magnitude slower than anode oxidation rates (Velasquez-orta and Yu, 2011). This means that either retention time and thus reactor size will be determined by hydrolysis rates or substrate removal rates will be low. The use of amylase, which hydrolyses organic matter, has shown that soluble COD can be increased significantly when dosed into wastewater (Xin et al., 2018), however this is incredible costly. Cost-effective pre-treatments that facilitate the growth of hydrolytic organisms such as in hydrolytic upflow digesters could be a viable solution (Ligero et al., 2001).

Microbial competition reduces the substrate available for electrogenic uptake (Cotterill et al., 2017). Competition can occur both on and off the anode. As electrogenic organisms require a colonisable surface, substrate presiding in the bulk liquid can be consumed by other microbial species before it reaches the biofilm. Competition for space can also occur on anode (Kim et al., 2005). Active inoculation, which uses the harvest and consecutive use of an already established anode biofilm has improved performance in MEC (Baudler et al., 2014, Kumar et al., 2017). This

may work as immigration into an established biofilm is low (Vignola et al., 2018). Alternatively, high anode potentials have shown to select for anode-respiring communities (Commault et al., 2013, Karthikeyan et al., 2015).

Concentration losses occur when the rate of mass transport of a chemical species to or from the electrode limits current production (Logan et al., 2006). Mass transport of chemical species to and from the electrodes is governed primarily by diffusion from the 'bulk liquid' (Sherwood et al., 1975). The rate of diffusion depends upon concentrations at the electrode and in the 'bulk solution' as well as the distance required for chemical species to travel. Mass transport can be improved by convective forces, such as 'stirring'.

After electrogenic anode-respiration

Activation losses which occur due to the activation energy required for redox reactions at the electrodes, either at the bacterial surface or at the cathode (Logan et al., 2006). These are often proportionally high at low currents, and steadily increase with current density (Logan et al., 2006). In the cathode these can be reduced by increasing the electrode surface area, improving electrode catalysis through material selection (Ribot-Llobet et al., 2013). At the anode these can be improved through material selection and the establishment of an enriched electrode respiring biofilm that has good electrical conductivity (Commault et al., 2015)

Bacterial metabolic losses occur due to metabolic processes within the bacteria (Logan et al., 2006). The anode final electron acceptor and its potential influence the energy gain for the bacteria and electrochemical cell. The higher the difference between the redox potential of the substrate and the anode potential, the greater the gain for the bacteria for processes such as growth and maintenance and the less gain for the MEC (Logan et al., 2006). These can be very low, as coulombic efficiencies as high as 96% have been observed in the laboratory with acetate (Sleutels et al., 2011).

pH inhibition can reduce biofilm concentrations. Following oxidation at the anode, protons are released by the biofilm. Increases in proton concentration decreases local pH. If pH is reduced too drastically microbial activity can be inhibited. This is a larger issue when substrate concentrations are high or biofilms are situated in small spaces (Chong et al., 2019). Most microorganisms have a growth range of 2–3 pH units (Kolmos, 2012) and have been shown to perform best when controlled at 7.50pH (Ruiz et al., 2015). At the cathode, build up of hydroxides can also limit performance (Ye and Logan, 2018). Exchange of ions between anode and cathode compartments can be improved by increasing ionic conductivity.

Ohmic losses occur due to electrical resistance to both the electrons in the electrochemical circuit

and ions travelling between the electrodes (Logan et al., 2006). Resistance in this sense is made up of the electrical resistance in the electrodes and the ohmic resistance in the solution. Ohmic losses directly impact current and hydrogen generation and high ohmic losses require extra power input to meet the thermodynamic demands of the system. There may be a small impact of degradation rates due to ineffective ion transport (Ye and Logan, 2018), but adding external resistance in MEC had little affect on degradation rates (Katuri et al., 2011).

Electrical resistance is primarily determined by the electrode materials. Typically, the anode is made from carbon (Logan, 2008). Baudler et al. (2015) used metal anodes to reduce the electronic resistance with significant improvements to current density when tested with acetate, however compounds such as sulphur present in domestic wastewater reduce electrochemical stability (Aiken et al., 2018). Cathodes, typically, already have very low resistances as they are often made of metal (Kundu et al., 2013). Although some biocathodes containing carbon have been used, which will reduce electronic resistance (Zhen et al., 2015).

Ionic resistance is determined by the concentration of ions in the solutions and the ohmic loss is dependent upon current density (Rozendal et al., 2008). Typical electrolysis cells have very high ion concentrations and either high or low pH (Schalenbach et al., 2016). Domestic wastewater however, has very low ion concentrations and somewhat neutral pH (Henze and Comeau, 2008). Increasing conductivity will affect the profile of the microbial community and would be an expensive endeavour, though some countries use sea-water flushing. MEC developed in these region benefit from the increased conductivity (Leung et al., 2012). The best method to reduce ionic resistance is therefore to place electrodes as close together as possible without short-circuiting the cell (Rozendal et al., 2008).

1.4 State of affairs: bio-electrochemical research

Bio-electro phenomenon were observed as early as 1910 in microorganisms (Potter, 1910, 1911). This phenomenon was combined with electrochemical systems to produce usable electricity as far back as 1978 (Suzuki et al., 1978). In this form, organic matter present in wastewater, was fermented to produce hydrogen. Hydrogen was then utilised by electrogenic organisms in an MFC. In recent years MFC have been further investigated for their use in domestic wastewater (Rabaey and Verstraete, 2005, Rozendal et al., 2008).

As of 23rd October 2020, there were 1,660 results in ScienceDirect for the search terms '"microbial electrolysis cell" wastewater' and 5,891 results for the terms '"microbial fuel cell" wastewater'; yet no commercially viable design has so far been developed for the treatment of domestic wastewater. The gap between the number of research-hours in this field and the lack of a commercially viable

design in the 'real-world' is significant but not necessarily damning for MEC. Of all the research published on MEC in the last 23 years, over 50% has been published since 2016 (Figure 1.1). Furthermore MFC have shown an above average increase of 11.9% per year in the last 23 years, whilst the number of MEC publications has had an annual increase of 19.5%, four times the average field (4-5% each year (Ware and Mabe, 2015))

Moreover, other treatment technologies typically have considerably more research hours dedicated to them. Undertaking a search on ScienceDirect (23rd October 2020) for 87 different wastewater treatment technologies (Table A.1), in the format: '"*technology*" wastewater', showed that the most researched treatment technology "Clarifier" had 824,739 results (100 times the results for MFC and MEC combined). Whilst the tenth most research technology: "thermal hydrolysis" had 140,415 results (20 times the results for MEC and MFC combined) (Figure 1.1).

The majority of papers regarding MFC and MEC in this literature search have been conducted with acetate rather than wastewater (Figure 1.2). Acetate is a known direct food source of electrogenic species (Speers and Reguera, 2012). Using acetate as the primary carbon source in electrogenic experiments allows researchers to study microbial kinetics. Compared with wastewater, reported maximum current densities were much higher when using acetate (Figure 1.2). The highest projected current density reported (33.3A/m^2), at the highest power density after 15 days of operation was reported in an MFC with a brush anode fed with acetate (Nam et al., 2011). These current densities were achieved with a brush anode, which had a high, accessible surface area 8000m^2/m^3, and a high anode potential (+200mV), which may increase electron capture (Logan et al., 2006). Meanwhile, the highest reported current density with domestic wastewater was 2.8A/m^2 (Mathuriya, 2013), which was fed with tannery wastewater - COD concentrations were very high (2839mg/l). Using domestic wastewater, the highest current density reported was 1.1A/m^2 (Hays et al., 2011), as with Nam et al. (2011), a brush anode was used with a high, easily-accessible, surface area. The highest current density achieved in a pilot scale reactor operated with domestic wastewater was 0.79A/m^2, which Cotterill et al. (2017) observed in one cassette for a very short period of time, however mean current densities were 0.29A/m^2. Other pilot-scale MEC have achieved similar current densities: 0.37A/m^2 (Baeza et al., 2017), 0.36A/m^2 (Escapa et al., 2015), 0.30A/m^2 (Heidrich et al., 2013), 0.22A/m^2 (Gil-Carrera et al., 2013). Pilot-scale reactors, in general, achieved marginally lower current densities to their lab counterparts fed with domestic wastewater. The larger size of the electrodes may increase ohmic losses, but the effect appears to be small (Figure 1.2). The larger difference in observed current densities is between wastewater fed reactors and acetate fed reactors.

The difference between performances in acetate-fed reactors and wastewater fed reactors can be explained by electrogenic species preferred food sources. To date, hydrogen, acetate and formate

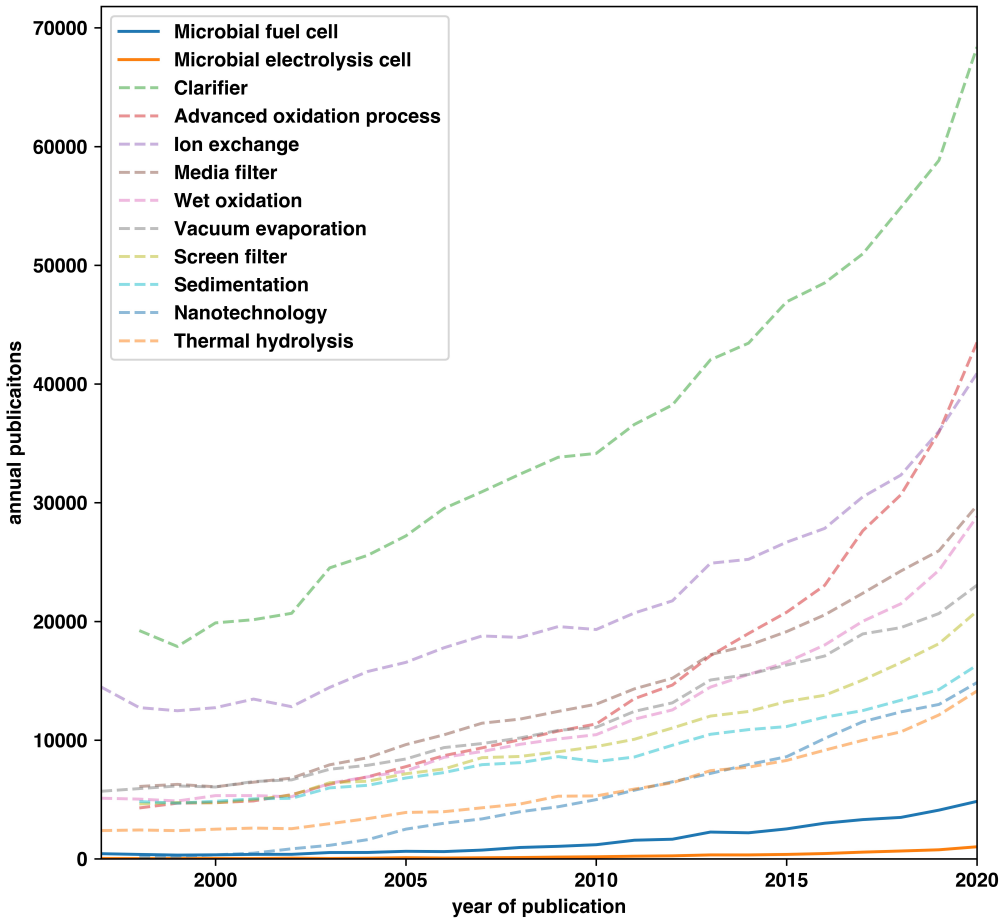

Figure 1.1: Number of results for search terms in ScienceDirect, 23^{rd} October 2020

have all been identified as being directly degraded by electrogenic species (Speers and Reguera, 2012, Zhao, 2018). Acetate concentrations in domestic wastewater are typically low, of the order 10mg/l (Huang et al., 2010). Previous research has shown that hydrolysis rates are also low in MFC, which limits the rate at which larger substrates are broken down into simpler substrates (Velasquez-orta and Yu, 2011). This reduces the biofilms access to food and therefore the rate of oxidation of organic matter at the anode. The addition of amylase to wastewater has shown large increases in the quantities of soluble COD (Xin et al., 2018). Pre-treatments such as hydrolytic upflow reactors could drastically improve wastewater fed reactors by improving the supply of acetate (Ligero et al., 2001). Dark fermentation has previously been successfully used with food waste to produce comparably high current densities of 34.0A/m^2 (Cardeña et al., 2018). COD concentra-

Pilot Reactor Paper	Design	Maximum current density (A/m^2)	Applied potental (V)	Coulombic effi-ciency	Anode volume (L)	Anode packing area (m^2/m^3)	HRT (hours)	ORR ($kg/m^3/day$)
(Cusick et al., 2011)	MEC Brush Cassette	0.41	0.9	173%	910	18.1	24	0.47
(Heidrich et al., 2013)	MEC Felt Cassette	0.3	1.1	13%	88	8.2	24	0.14
(Gil-Carrera et al., 2013)	MEC Felt Tubular	0.22	1.0	31%	4	24.0	10	0.23
(Escapa et al., 2015)	MEC Felt Cassette	0.36	0.7	186%	3	73.3	20	0.14
(Baeza et al., 2017)	MEC Felt Cassette	0.37	1.0	28%	93	12.6	24	0.13
(Cotterill et al., 2017)	MEC Felt Cassette	0.79	0.9	28%	30	192.0	5	0.94

Table 1.1: Pilot reactor performances

tions were exceptionally high in this study at 13,050mg/l, as were acetate (2,627mg/l) and lactate (2,979mg/l). Despite the improvements to current density that are achievable in MEC with high acetate concentrations, current densities are still very low in acetate reactors compared to typical electrolysis, which are on the order of magnitude of $10{,}000A/m^2$ (Schalenbach et al., 2016). As such, MEC will be required to provide additional cost-benefits to offset the high capital costs and allow for hydrogen prices to be competitive.

1.4.1 Modelling

Numerical models can be used to investigate the mechanistic reactions within a typical 'black box' environment. It is typically more cost-effective and time-efficient than physical investigations. Although useful, numerical models are an imperfect reflection of reality (Box, 1976). Models exist on a spectrum of simple to complex. More complex models capture more of reality but can be

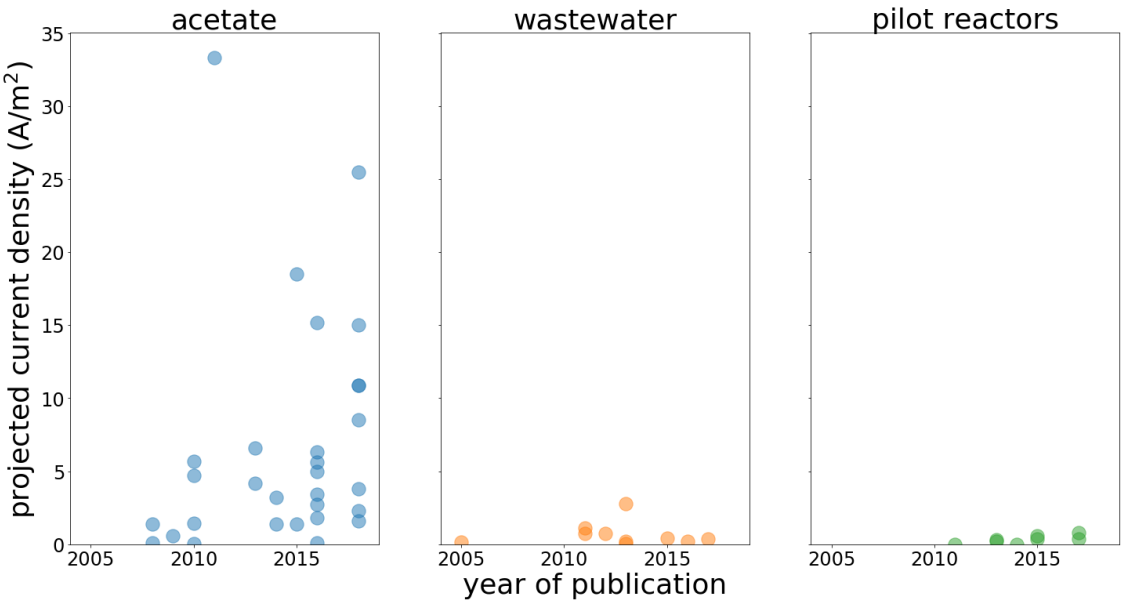

Figure 1.2: Reported current densities in literature fed with acetate and wastewater (Bibliography for current density literature study)

less useful as they require fine tuning to specific circumstances. Moreover, accurate models require calibration and validation to ensure that their predictions are in-line with reality.

Previous modelling of BES has produced a range of model-types. Xia et al. (2018) highlights the use of both mechanism-based models and application-based models. Within mechanism-based models bulk-liquid, electrochemical and biofilm models have been used. Whilst application-based models consist of electrical models and learning and controlling models. As BES require the improvement to macro phenomena such as ORR and current density, models that consider their parameters will be the most useful in achieving MEC commercial viability.

Previous macro models conducted on BES have consisted of 'Monod'-type models (Xia et al., 2018). However, none have taken into account the effect of anode packing density and acetate concentrations on cost-performance, nor sought to provide a guide towards commercial viability. Several of these studies have considered two competing organisms before in simpler 1D models. Pinto et al. (2010) first modelled two competing organisms in an MFC to determine power production from varying acetate concentrations and external resistances. Pinto et al. (2012) further investigated the effect of current control on Hydrogen product generation in an MEC using similar methods to before. Li and He (2016) used Pinto et al. (2010)'s base model to consider the effect of cross flow on a membrane bioelectrochemical reactor (MBER), which first introduced water flux (J) into the model. (Recio-Garrido et al., 2016) also used these methods to evaluate the impact of charge storage on microbial fuel cell (MFC) performance. Further, nonlinear dynamics of MFCs

were considered by merging mass and electron balances with equations describing an equivalent electrical circuit.

Other bulk models have modified Monod kinetics to consider electrochemical phenomenon (Xia et al., 2018). The Butler-Volmer-Monod (BVM) model (Hamelers et al., 2011) and the double-limited Monod-Nernst model (Torres et al., 2007) are both presented as robust models as they consider electrochemical impacts on performance. Both of which take into account the influence of potential on substrate uptake rate. And both of which extend logistic expression curves, such as found in the Monod equation, to electrochemical parameters.

1.5 Key challenges facing MEC development

The high capital costs and modest performance of the technology under 'real-conditions' (Rozendal et al., 2008), are barriers to the commercial adoption of MEC. Early estimates by Rozendal et al. (2008) of MEC costs were 10 times that of AD (Rabaey and Verstraete, 2005), but material costs have reduced in recent years especially with the use of cheap membranes and stainless-steel cathodes (Pant et al., 2011).

Furthermore, COD removal and hydrogen production have both proven to be highly variable in pilot reactors (Baeza et al., 2017, Cotterill et al., 2017, Cusick et al., 2011, Escapa et al., 2012, Heidrich et al., 2014), a property that is not tolerable in an industrial setting. With mounting economic pressure (OFWAT, 2019) to reduce emissions and costs for customers: industry leaders are interested in knowing whether this technology is worthy of investment.

Slow progress in scale-up may be due to the fact that most research has been conducted in laboratories with simple substrates, controlled conditions and expensive materials. Additionally, the lack of consistency in reporting MEC data, such as material cost, energy efficiency, scale and temperature, makes the process of assessing performance and predicting commercial potential very difficult.

Pilot reactors also have their problems (1.1). The slow start-up which occurs in pilot-reactors operated under 'real conditions', especially in temperate conditions is time-costly as biofilms take weeks to months to grow (Cotterill et al., 2017, Heidrich et al., 2014). Furthermore, any changes to the flowrate or concentration in the reactors requires further biofilm incubation periods before noticeable changes can be observed. This is further obfuscated when temperatures, pH and chemical constituency of the influent are constantly in flux. Pilot-scale studies thus take months to years to complete.

The three major challenges facing MEC development are limited organic removal rates (ORR) as

compared to conventional treatments, low energy recovery in domestic wastewater and suitable material selection that is both cheap, electrically conductive, biologically compatible and electrochemically stable (Kadier et al., 2014). This thesis seeks to quantify both the allowable material costs and thus guide material selection, and to predict removal rates under a wide range of potential environments and MEC designs. To achieve this aim we seek to address the trade-off in cost-performance that occurs in densely packed anode chambers, which increase ORR but also incur higher material demands and thus cost (Table 1.1, Cotterill et al. (2017), Heidrich et al. (2013)).

1.6 Aims, Objectives and Research Questions

Aim	To investigate the commercial viability of Microbial Electrolysis Cells (MEC) as a sustainable treatment for domestic wastewater and to quantify key parameters to be used in any commercially viable design or application.
Objective 1	Assess the financial viability of MEC against activated sludge (AS)
Objective 2	Understand key parameters affecting MEC performance
Objective 3	Quantify the impact of key parameters on the cost and performance of MEC
Objective 4	Provide feedback on the feasibility of MEC's commercial viability and direction to future research

Research questions	**Chapter**
What costs and organic loading rates (OLR) are required in a financially competitive MEC?	Chapter 2
What affect does low acetate concentration have on MEC performance with low conductivity solutions in temperate climates	Chapter 3
How cost-effective are potentiostats in "real-world" MEC?	Chapter 3
How accurately can MEC performance be predicted using computational techniques?	Chapter 4
What effect does high acetate concentration have on the cost-performance of MEC?	Chapter 4
What effect does the distance between anode surfaces have on the cost-performance of MEC ?	Chapter 4
What conditions and design parameters are required to achieve a commercially viable MEC?	Chapter 4
Under what conditions can MEC become net energy positive?	Chapter 4
What impact will MEC have on greenhouse gas emissions if deployed?	Chapter 4

Chapter 2. Avenues to the financial viability of microbial electrolysis cells (MEC) for domestic wastewater treatment and hydrogen production

2.1 Introduction

The high capital costs and modest performance of the technology under 'real-conditions' are barriers to the commercial adoption of MECs (Rabaey and Verstraete, 2005). Early estimates by Rozendal et al. (2008) of MEC costs were 10 times that of AD. Nevertheless, material costs have reduced in recent years especially with the use of cheap membranes and stainless-steel cathodes (Sleutels et al., 2012); thus more recent analyses on economics are needed. Rozendal et al. (2008) propose necessary current densities (10A/m^2) to break-even, however current density can be increased by means other than removal of organic matter. This therefore requires supplementary targets better suited for the application of wastewater treatment, such as organic loading rates (OLR).

Zhang and Angelidaki (2016) highlight the lack of data available in the literature on capital costs, and the non-standardised reporting methods of capital costs normalised to the performances posed as barriers to commercial adoption. Operating costs and revenue also need to be considered as MECs must be financially competitive with existing technologies. Additionally, using metrics found in the normalised-costs for other treatments, for example OLR (Shi, 2011), would allow for cross-technological cost-performance comparisons with conventional wastewater treatment technologies.

Previously, Sleutels et al. (2012) estimated the cost of COD removal at varying current densities for MECs. This study provides an insight into the potential applicability of MECs, however: costs for electricity are low (€0.06/kWh, [c.£0.05/kWh (2018)]); cathodic efficiencies are high (90%); material costs are low (£100/m^2); and the current densities considered are very high (0-50A/m^2). High efficiencies and high current densities are unlikely to occur for MECs fed with domestic wastewater and built with low-cost materials. Therefore, empirical data is needed for a more accurate estimation.

Escapa et al. (2012) estimated the financial feasibility of MECs using empirically derived data and concluded that MECs could be viable at loading rates of 2kg/m^3. However, the study was based on an OLR observed at a very small scale ($<$100ml), and at a very warm temperature ($30^{\circ}C$). In reality the acceptable loading rate will be a function of temperature. Most treatments plants, even in the

tropics, operate at substantially less than $30°C$. Consequently, there is a need to complement these studies with an economic evaluation of MECs based on "real world" performances using domestic wastewater in a temperate climate.

The material investment costs; operational energy costs; and revenue of a large-scale MEC are considered in this financial evaluation. Performances and costs based on a pilot-scale reactor (Heidrich et al., 2014), built with low cost materials and fed with 'real' domestic wastewaters, at ambient temperatures in a temperate climate ($55°N$). Cost-performance ratios are compared against AS, for the equivalent OLRs, using net present value (NPV). NPV is a tool to assess the profitability of a future project in comparison to its initial investment cost by considering the depreciating real value of money over time, due to inflation and missed investment opportunities. A discounted compound interest rate is applied (Hillier et al., 2013), typically 3.5% per anum (OECD, 2006).

The NPV of AS and MEC after 20 years were compared for eight potential scenarios to assess MEC's financial competitiveness for domestic wastewater treatment. The impact of each scenario on the financial viability of the MEC design is identified. The analysis can be used to guide the conceptual design of large-scale commercial MEC systems; and focus research on those features of an MEC that must be improved to make the technology financially viable.

2.2 Methodology

2.2.1 Case study

Heidrich et al.'s design (2014) incorporated low-cost materials and treated "real" domestic wastewater; it is used as the basis of the material and performance projections. The pilot MEC had a total working volume of 88 L, larger than most laboratory scale studies, and operated for 12 months in air temperatures ranging from $1°C$ to $22°C$. The hydrogen gas produced was of high quality (98%-99%). The reactor had a 'cassette' style design that could, in principle, be retrofitted into aeration lanes, provided retention times are sufficiently low. Costs for the essential components used in the construction of the electrochemical cells were inputted into the model (Table 2.1). Stainless-steel wire wool was used as the cathode, which greatly reduces cost compared to original estimates (Rozendal et al., 2008) by up to 97% (Ribot-Llobet et al., 2013). The membrane was Rhinhode (£1.50/m2) (Entek, UK), which costs much less than Nafion (€400/m2 [c.£350/m2] (Rozendal et al., 2008)). Carbon felt anodes (£285.90/m2) (Olmec, UK) were combined with stainless-steel current collecting frames (£30.80/m2) (Unkammen Supplies, UK). The anode and current collecting frames combined, constituted the highest proportion of the cost, and therefore the most important element to cost correctly. The costs for hydrogen capture and storage are also incorporated (Table 2.1).

Component	Material	Price	Normalised Cost (£/(g-COD/d)	Source
Cassette	PVC Sheets	£0.536/kg	< 0.01	(Shandong Jintiancheng Plastic Products Co., China)
Anode	Carbon Felt	£285.90/m2	£15.22	(Olmec Advanced Materials Ltd, UK)
Cathode	Stainless Steel Wire Wool	£35.40/kg	£0.73	(Merlin, UK)
Membrane	Rhinohide© Battery Separator	£1.50/m^2	£0.09	(Entek Ltd, UK)
Current Collector	Stainless Steel Mesh	£30.80/m^2	£3.87	(Tiantai Global Screen Mesh Co.)
	Stainless Steel Wire	£0.67/m	-	(UnkamenSupplies, UK)
Gas Pipes	ID PVC tubing	£3.00/m	£0.14	(VWR Jencons, UK)
Hydrogen Tank	Hydrogen Compression Tank	£362.23/unit (80m^3/unit)	£0.28	(Materials Sci.& Tech. Co.)

Table 2.1: List of components, material, price and source

2.2.2 Material investment costs

The fundamental relationship between COD removal (ΔCOD) and current production (I), presented by Logan (2008) (2.1), forms the basis for understanding of the MECs function:

$$I = \frac{C_e \cdot F \cdot Q \cdot \Delta COD}{n} \tag{2.1}$$

Coulombic efficiency (C_e) describes the proportion of electrons from the degraded substrate that is passed into the circuit; flowrate (Q) governs the size of the treatment process; the COD removed is

divided by the number of electrons released by a gram of COD (n = 8mol-e^-/g-COD) and Faraday's constant (F) is used to convert the rate change in moles of electrons into current (I).

Current density (I_d) is equal to electrical current (I) divided by the anodal surface area (SA). This was rearranged to make the anode surface area (SA) the subject (2.2). Current density in this instance is used as a performance indicator for the rate of substrate uptake per area per time by electrogens in the system.

$$SA = \frac{C_e \cdot F \cdot Q \cdot \Delta COD}{n \cdot I_d} \tag{2.2}$$

Based upon the surface area of the anode (2.2), the developer software 'Visual Basic for Applications' (VBA) within Microsoft Excel was used to estimate the quantity of materials required for a large-scale MEC. Performance parameters are known from empirical data (Table 2.2). Population and flow rate, for the hypothetical large-scale reactor, were assumed to be 100,000p.e. and 15,000m3/day (150 L/p.e (Metcalf & Eddy et al., 2003)), and dimensions of cells were assumed to be 4m x 6m (typical AS lane dimensions) (Metcalf & Eddy et al., 2003). Material costs were extrapolated from the unit costs in the case study (Heidrich et al., 2014) (Table 2.1). The model assumes that dimensions of components scale in proportion to anode size, there are no new infrastructure or land purchase costs and staff can be retrained at minimal cost to the water companies. These are likely to give conservative estimates as economies of scale may reduce unit prices, albeit modestly.

Parameter	**Symbol**	**Value**
Coulombic efficiency	C_e	13.3%
Faraday's constant	F	96,485 J
Influent	Q	15,000 m^3/day
COD removed	ΔCOD	140 g/m^3
Current density	I_d	0.3 A/m^2
Anode surface to volume ratio	S_v	0.72 m^2/m^3
Population	Pop.	100,000 p.e.

Table 2.2: Performance parameters of large-scale MEC (Heidrich et al., 2014)

2.2.3 Energy costs and revenue

The price of electricity was assumed to be homogeneous across the model (whether buying or selling), at £0.10/kWh, typical of business rates in the United Kingdom (UK) (Business Electricity Prices, 2016). Input power to the MEC was based on an input voltage of 1.1V and was multiplied by the current density (0.3A/m^2) (Heidrich et al., 2014) to give power ratings and therefore electricity costs.

2.2.4 Hydrogen production

Hydrogen production was assumed to have a comparable yield (15L-H_2/m^3-influent/day) to the pilot-scale reactor (Heidrich et al., 2014). Annual hydrogen production was calculated based on reported yields and a hydrogen density of 0.09g/L. Cathodic efficiency was approximately 50% (around half of the electrical current was recovered as hydrogen - possibly due to scavenging and leaks). Prices for hydrogen are expected to decrease in the future as more of the gas is produced to meet with the demand for hydrogen powered vehicles (ITM Power, 2013). The European target price for hydrogen is €4.00/kg (£3.55/kg) by 2020, and €3.00/kg (£2.66/kg) by 2030 (Europa, 2008). By 2030 hydrogen is expected to be fully competitive with other fuels. The model assumes a 2020 target price for hydrogen. In addition to calculating annual cash flow, required hydrogen yields to break-even were calculated based on these targets.

2.2.5 Activated sludge comparison

There are numerous estimates in the literature for the cost of activated sludge (AS), and costs vary between treatment works. Aeration typically costs 40-60% of the total energy of a wastewater treatment plant (WWTP) (Shi, 2011). This may depend upon the strength of the wastewater and the size of the WWTP (Metcalf & Eddy et al., 2003). Pant et al. (2011) estimate an energy cost of 0.7 to 2 kWh/kg-COD removed in AS. Using this as a comparative estimate for the savings made if concentrations are reduced by 140g-COD/m^3 by an MEC treating 15,000m^3/d, this equates to an annual saving between £53,000 and £153,000. Averaging this gives an annual average saving of about £103,000. Shi (2011) provide a detailed break-down of energy costs in a real-world WWTP. Electricity use for aeration was assumed to scale linearly with flow rate and was scaled down from 10MGD to 15,000m^3/d. This equated to an annual aeration cost of £105,000, similar to the average given by Pant et al. (2011). A linear assumption is appropriate for aeration, however a linear assumption would not be suitable for the overall treatment works as electricity costs for pumping constitute a higher proportion of electricity usage for smaller sites (Metcalf & Eddy et al., 2003).

Estimated costs of air pipes and diffusers (FLI Water Ltd., UK, personal communication) were

based on quotes from a WWTP currently under refurbishment (Seaham, UK). Pipe and diffuser requirements were linearly scaled up from 11,000m^3/d to 15,000m^3/d. Sizes and prices for blowers were also taken from quotes and specifications (APG-Neuros, UK, personal communication). The replacement rate for pipes and diffusers was assumed to be 5 years, blowers were assumed to last for at least 20 years, which is consistent with current industrial practice. The cost of sludge treatment was purposefully omitted, as although MECs produce less sludge than AS, and therefore incur less sludge disposal costs, the quantities are not yet clear (Heidrich et al., 2011). If electrogenic biofilm yields are lower than AS, then less sludge will be produced.

2.2.6 NPV calculation comparison

NPV was used to compare costs (C_i) for MECs and AS over an assumed twenty-year operational period (n) with an assumed one-year construction for both (2.3). This is speculative as the construction period for MECs is unknown, as is their operational life span. The rate of return (r) was assumed to be equal to that of the UK government discount rate, at 3.5% (OECD, 2006). As NPV is a measure of economic value, and wastewater treatment does not produce profitable products, all NPV discussed will be negative. An increase (toward positive values) in NPV for MECs is therefore beneficial for the technology, and a decrease detrimental. The opposite is true for costs, increases in costs are detrimental and decreases in costs are beneficial.

$$NPV = \sum_{i}^{n} \frac{C_i}{(1+r)^i} \tag{2.3}$$

2.2.7 MEC scenarios

Seven scenarios (Table 2.3) were considered in addition to the base MEC model (Scenario 0). These include changes in energy input, output and energy prices; return on assets after the investment period, and maintenance such as staff costs and replacement costs. Scenario 1 modelled a doubling of hydrogen yield, a common goal in research. This may be addressed by reducing hydrogen leakage and scavenging. Scenario 2 modelled a reduction in power requirements by decreasing the applied voltage to 0.6V, considered to be close to a lower limit (Fornero et al., 2010). Scenario 3 considers an energy price increase of 33%, predicted by 2030 (Gummer et al., 2017) and a hydrogen price decrease to 2.66/kg to assess the impact of future markets (Europa, 2008). Scenario 4 modelled a return on anode and current collectors, at the same value as purchased (assumed re-use) after 20 years of operation; elsewhere it has been noted that if uncorroded, stainless steel in MECs can be an asset at the end of its lifespan (Brown et al., 2017). The length of operation of the anode is unknown; performance is dependent on self-replicating microorganisms and can been sustained for at

least 12-months (Heidrich et al., 2014). Scenario 5 took into account the annual replacement of the membrane, scenario 6 modelled annual replacement of both the membrane and cathode; it is likely that these components will not last 20 years, an annual replacement was chosen as a conservative estimate. Scenario 7 considers costs if an additional member of staff is required, with an annual salary of £30,000, this could be feasible given that MECs require careful monitoring as compared to AS. In reality many of these scenarios may occur simultaneously, however this exercise serves to demonstrate the impact and importance of each on cost and performance.

Scenario Number	Description
Scenario 0	Baseline MEC model
Scenario 1	Double hydrogen yield
Scenario 2	Applied voltage reduced to 0.6V
Scenario 3	Energy price changes expected in 2030
Scenario 4	Anode and current collector value returned after 20 years
Scenario 5	Membrane replaced annually
Scenario 6	Membrane and cathode replaced annually
Scenario 7	Additional staff member (£30,000/anum)

Table 2.3: Scenario descriptions

2.2.8 Target Finder

OLR (mass flux of g-COD removed per metre cubed per day) and current densities are used as performance indicators to address the amount of substrate that was taken up by electrogenic species per area per time. OLR and current density correspond with one another (2.4); based, in this case, upon a coulombic efficiency of 13% (Heidrich et al., 2014). The model (Target Finder) was run at incrementing OLRs for each of the scenarios until the NPV after 20-years of operation was less than that of AS. The 'target' OLR and current density, meaning the OLR and equivalent current density that would be required to achieve financial viability against AS, for a given scenario, was calculated. This was "outputted" to a worksheet along with; the increase in performance required from the pilot; the NPV for the scenario at current performances; the NPV of the scenario at 'target' performances, and any profit margin (Table 2.3). In tandem, a sensitivity analysis was conducted to determine the "target" OLRs required for reductions in capital costs (at incrementing steps of 10%) for each of the scenarios (Figure 2.3). The model assumes all other parameters remain constant, such as hydrogen yield. In reality, increasing OLR and thus current may also increase potential losses (Rozendal et al., 2008) and thus decrease coulombic efficiency, If conductivity remains constant.

However, if the increase in OLR is caused by an increase in acetate concentration, conductivities will increase - and so too may coulombic efficiency. Moreover, biodegradability of organic compounds has been shown as the primary current-limiting factor (Dhar and Lee, 2014, Velasquez-orta and Yu, 2011), and is therefore more consequential. Sensitivity analyses for maintenance scenarios (5, 6) assume that material cost savings are made to components other than the membrane and cathode. This is a legitimate assumption as membrane and cathode costs have already been reduced drastically and are a small percentage of the overall material costs (Figure 2.2).

$$OLR = \frac{8 \cdot I_d \cdot SA}{C_e \cdot F \cdot V} \tag{2.4}$$

2.3 Results and Discussion

2.3.1 Current state of financial feasibility

The capital investment costs for MECs is currently substantially higher than that of AS. For an influent flowrate of 15,000m^3/day, material costs for MECs were predicted to be £42,700,000. This is comparable to the material cost of Ge and He's small-scale MEC (2016): scaling up linearly with flowrate, material costs are approximately £45,000,000. The material costs for AS for the same flowrate were estimated to be £172,000, two orders of magnitude less.

This disparity in the initial investment could be a deterrent to commercial adoption. However, MECs have the potential to be energy neutral, if not positive, whereas AS consumes about 0.2kWh/m^3, for aeration alone, throughout the entirety of its life (Shi, 2011). Annual energy costs were £106,000 for AS and £11,000 for MECs. Annuals costs in MECs are a factor of 10 less than AS. However, current NPV at 20 years was -£42,900,000 for MECs whereas NPV was -£2,000,000 for AS. At present loading rates of 140g-COD/m^3/day (0.3A/m^2) the NPV comparison is clearly unfavourable. To make MECs a competitive technology under this baseline scenario (0) the OLR would need to increase to 4,450g-COD/m^3/d equivalent to a current density 10.1A/m^2; a 34x increase from the pilot's performance (Figure 2.1, Table 2.4).

These costs are based on the differences between MEC and AS, and so naturally neglect the costs they have in common. Any minor discrepancies in these costs will be negligible in comparison to the order of magnitude in differences found.

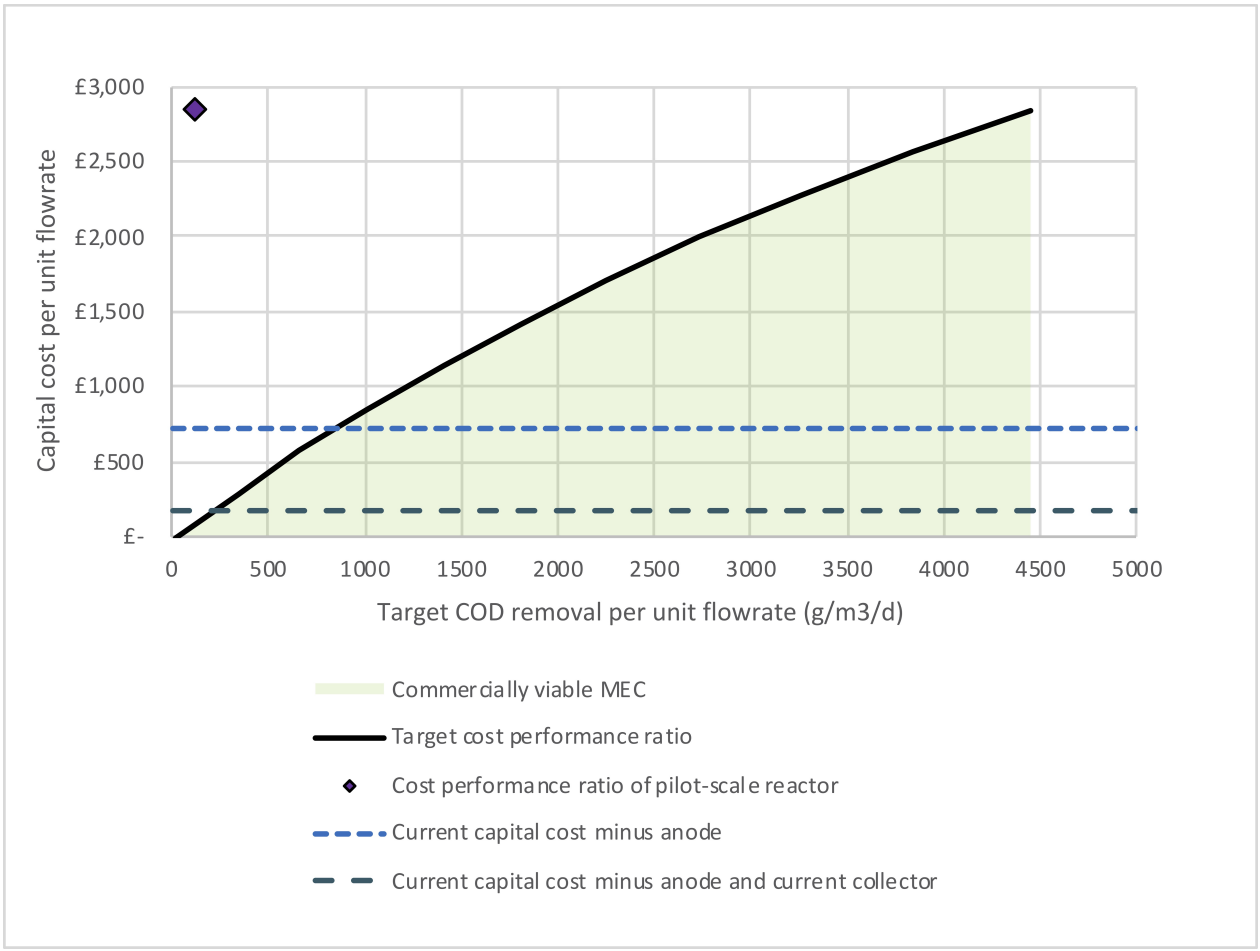

Figure 2.1: Target cost-performance ratios for financially competitive MECs treating domestic wastewater

2.3.2 Material costs

The material costs accounted for 99% of NPV. Of this, the anode constitutes the greatest proportion of material costs (75%) and the current collector the second greatest (19%). Together these features account for 94% of total costs (Figure 2.2). This contrasts Rozendal et al. (2008), where the cathode constituted the greatest proportion of the capital investment (Figure 2.2). This change is due to the use of cheaper cathode and membrane materials (Table 2.1). Significantly, the membrane was less than 1% of total costs, contradicting the impact on economics that membrane-less systems are hypothesised to make (Christgen et al., 2015).

2.3.3 Hydrogen production

Under scenario 1 (a doubling of current yields to 30L/m^3) the positive cash flows generated at 2020 prices (£15,000 /year) (Table 2.4, Figure 2.3) had a negligible impact on NPV because of the cost

Scenario*	NPV at present (4sf)	Target current density (A/m^2)	Target OLR ($g/m^3/d$)	Performance increase required
Pilot MEC (Heidrich et al., 2014)	-	0.3	140	-
Scenario 0	£ (42,850,000)	10.1	4,451	34
Scenario 1	£ (42,480,000)	7.8	3,437	26
Scenario 2	£ (42,610,000)	8.5	3,746	28
Scenario 3	£ (43,120,000)	8.6	3,790	29
Scenario 4	£ (26,790,000)	6.3	2,776	21
Scenario 5	£ (45,430,000)	10.7	4,715	36
Scenario 6	£ (65,750,000)	15.6	6,875	52
Scenario 7	£ (43,280,000)	15.2	6,699	51
Scenario 0 (50% cost reduction)	£ (21,510,000)	4.1	1,806	14
AS (Metcalf & Eddy et al., 2003)	£ (2,009,000)	-	500 – 2,000	-

Table 2.4: 20-year net present value, target current densities, and target OLR for MECs for eight scenarios

** Scenario 0: baseline MEC model; Scenario 1 - Double hydrogen yield; Scenario 2 – Applied voltage reduced to 0.6V; Scenario 3 – Energy price changes; Scenario 4 - Anode and current collector value returned after 20 years. Scenario 5 - Membrane replaced annually; Scenario 6 - Membrane and cathode replaced annually; Scenario 7 - Additional staff member required*

of materials (assuming current performances). It is therefore unlikely hydrogen production alone will account for MEC capital costs.

To break-even under the baseline scenario (0), either hydrogen would need to be priced at £5.09/kg (more than the EU's target of £3.55 by 2020, and £2.66 by 2030) or yields will need to increase from 15L/m^3 to 21.5L/m^3 by 2020 and 28.7L/m^3 by 2030 (an increase of 43% and 91%, respectively). Cathodic efficiencies are relatively high and therefore to increase yields, coulombic efficiencies and OLR will need to increase. Nevertheless, even if hydrogen is sold at a loss in order to be competitive with other sources of hydrogen, electricity costs in MECs are minimal compared to AS.

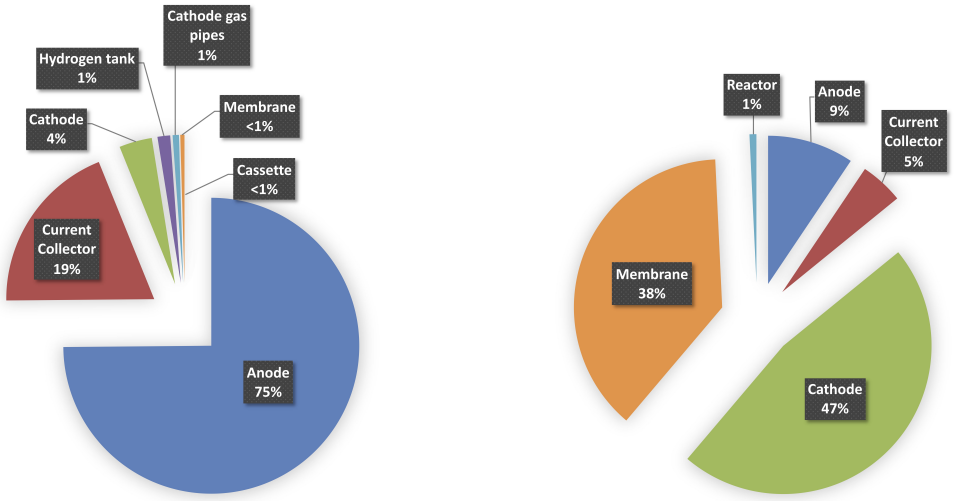

(a) This study

(b) Rozendal et al. (2008)

Figure 2.2: Percentage of components costs compared to total material costs (left) compared to early estimates (Rozendal et al., 2008) (right)

2.3.4 Applied voltage

Reducing the applied voltage to 0.6V, whilst maintaining yields (scenario 2), likewise provided positive cash flows by reducing energy input. Current density targets were reduced to 8.5A/m^2 (3,750g-COD/m^3/d) (reftable:NPV,Figure 2.3), however as applied voltage directly impacts hydrogen production this may not be technically achievable.

2.3.5 Future energy prices

Energy and hydrogen prices are expected to change in the future (scenario 3). Predicted changes had modest impacts on NPVs for both AS and MECs. 20-year net loss for AS increased by 8% (NPV:-£2,160,000), whilst MEC net loss increase was negligible, at less than 1%. This shows MECs are currently less sensitive to price rises due to their high material costs. However, a modest change in target performances was observed 3,790g-COD/m^3/d (8.6A/m^2). This means should the price of electricity increase in the future, as predicted, MECs will become more competitive.

2.3.6 Asset recovery

Recovering the current collector and anode materials value after 20 years (scenario 4) had the largest effect on NPV, which improved to -£27,000,000. Target current densities were reduced to 6.3A/m^2 (2,780g-COD/m^3/d) (Table 2.4, Figure 2.3). It may also be possible to recover value from other components to further increase MECs value such as the cathode, however this only accounts

for 4% of the material costs. Reusing assets and reducing capital costs would make MECs more competitive, however corrosion and fouling will need to be prevented.

2.3.7 Maintenance: Replacement costs

Replacing the membrane annually (scenario 5) was detrimental to NPV by about -£3,000,000. Current densities would need to be 10.7A/m^2 (4,720g-COD/m^3/d) (Table 2.4, Figure 2.3) to pay for the replacement: a small increase from baseline targets (10.1A/m^2). Thus, fears about the use of membranes at full scale (Christgen et al., 2015) are probably misplaced as the membrane is 1% of the cost.

However, annual replacement of the cathode and membrane (scenario 6) decreased NPV by -£23,000,000 and target current densities increased to 15.6A/m^2 (6,880g-COD/m^3/d, 54% increase from baseline) (Table 2.4, Figure 2.3). It will therefore be necessary to protect the cathode from fouling if performances are to be sustained and annual costs kept to a minimum. Fouling of the cathode is more likely to happen when operating with 'real' wastewater due to the complex microbial and chemical environments (Stott and Abdullahi, 2018).

2.3.8 Maintenance: Personnel

Increasing the number of staff by one member, on a £30,000 salary, had a negligible impact on NPV (-£43,000,000), however performance targets were increased significantly at these capital costs (15.2 A/m^2, 6,700g-COD/m^3/d) (Table 2.4). It would therefore be beneficial for MECs to be easy to operate, and staff easily and readily retrained. Staff will require basic working knowledge of electrical, electrochemical and computer systems and be able to operate safely on a wastewater treatment plant. Care should be taken to ensure that staff are able to safely handle toxic gases, biohazards, carcinogenic COD tests and electrical malfunction. Preferable skills would include plumbing. There is a discrepancy between higher target OLRs at high capital costs and lower target OLRs at lower capital costs. This is because salaries do not change with respect to OLR. Therefore, a greater OLR (which increases hydrogen production and revenue) is required to induce a positive cash flow and mitigate the effects of a high capital cost; whereas at lower capital costs less mitigation is required - although OLRs are still higher than baseline (Figure 2.3).

2.3.9 Space

At presently achieved OLRs MECs would be too large to simply retrofit most existing AS aeration basins. Therefore, more space and civil works (which were not costed in this paper) would be required. However, due to the order of magnitude in differences found in material costs, it will be necessary to reduce OLRs for material costs to be comparable. In scenarios where target OLRs for

MECs are higher than AS (Table 2.4), the new technology could be refitted within existing facilities and therefore the cost of supplying extra space for MECs with a low OLR is moot. Moreover, increased performances have been observed in MECs that were pre-treated using fermentative reactors, which require the retention of sediment to operate correctly (Cardeña et al., 2018). Combining these two novel technologies may reduce the need for large sedimentation tanks, "freeing-up" more space. Secondary sedimentation facilities could be retained as humus tanks to further improve effluent quality, though if they could be decommissioned, further cost savings could be made.

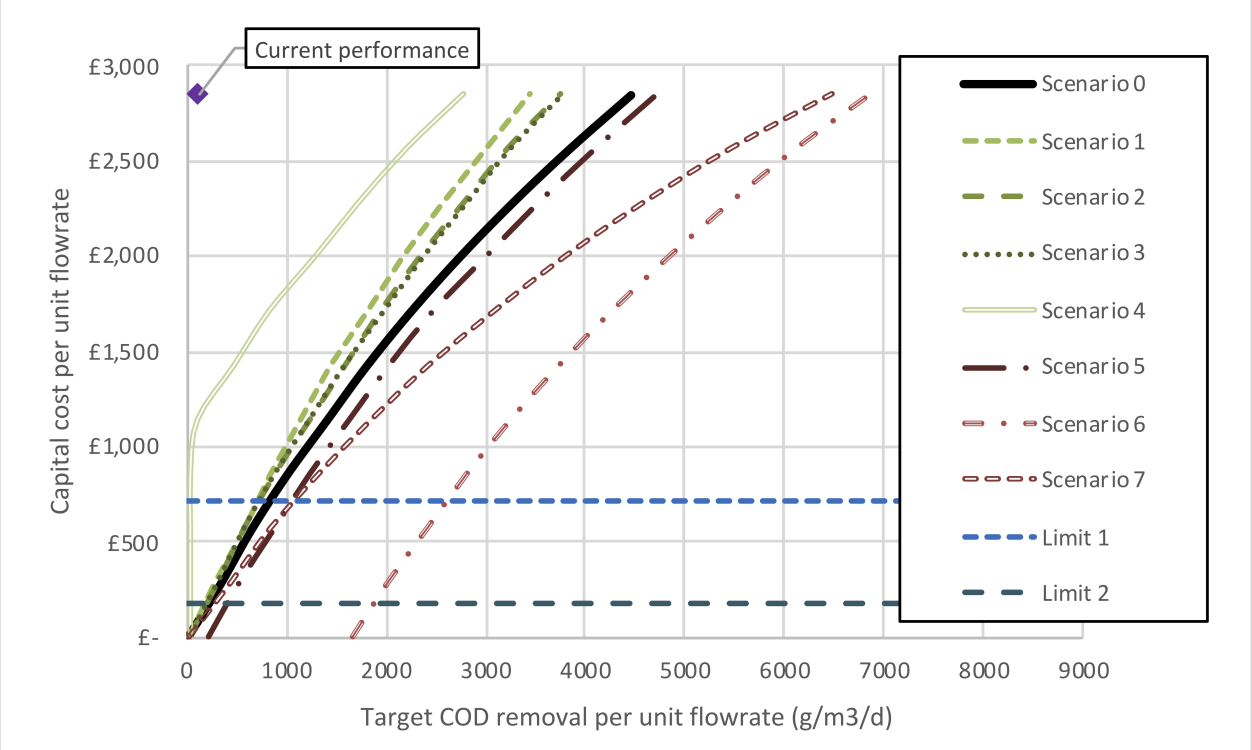

Figure 2.3: Cost-performance ratio curves for eight scenarios of a financially competitive MEC** ** *Scenario 0: baseline MEC model; Scenario 1 - Double hydrogen yield; Scenario 2 – Applied voltage reduced to 0.6V; Scenario 3 – Energy price changes; Scenario 4 - Anode and current collector value returned after 20 years. Scenario 5 - Membrane replaced annually; Scenario 6 - Membrane and cathode replaced annually; Scenario 7 - Additional staff member required; Limit 1 – Capital cost of reactor minus the anode; Limit 2 – Capital costs of reactor minus the anode and current collector*

2.3.10 Making financially viable MECs

A reduction in the cost of the anode and current collector by 90% (a reduction in total material costs of 84%) had a large impact on NPV. OLRs required to break-even for most scenarios (0-3, 5, 7) are reduced to 800 - 1,400g-COD/m^3/d (Figure 2.3): an order of magnitude higher than

presently achievable (140-g-COD/m^3/d) (Heidrich et al., 2014), but much less than baseline targets (4,450g-COD/m^3/d), and within the 'middle range' of AS removal rates (500-2000 g-COD/m^3/d) (Metcalf & Eddy et al., 2003). This therefore seems feasible given that electrogenic organisms have been observed to out-compete aerobes, in terms of removal rates, given the correct conditions (Ren et al., 2014). Subsequently, target current densities at these costs (2-3A/m^2), are much less than baseline targets (10.1A/m^2) and early predictions (10A/m^2) by (Rozendal et al., 2008). Reusing (or reselling) the anode and current collecting materials after 20-years could lead to large improvements in cost-performance ratios (Figure 2.3). Under this scenario (4) MECs could be financially competitive at current performances (140-g-COD/m^3/d [0.3A/m^2]); if anode and current collecting material costs were reduced by around 80% (and assuming sufficient space was available).

2.4 Conclusion

At the present cost of MEC design, target OLRs are more than an order of magnitude higher than pilot-scale performances achieved under "real" conditions (140g-COD/m^3/d). Although a range of cost-performance targets are demonstrated, I propose that viable targets presuppose a 90% reduction in anode and current collector cost, and an increase in OLR to between 800 – 1,400g-COD/m^3/d (equivalent to 2-3A/m^2). This goal seems more achievable in reality than some of the higher OLR targets. Neither annual membrane replacement, nor additional staff members would preclude a commercially viable MEC; as both costs are modest compared to the expense of other materials. Regular replacement of the cathodes would be highly detrimental to MEC competitiveness. Contrary, recovering the value of the anodes significantly reduces target OLRs, and could be another avenue to achieving financial viability. The strategic targets for MEC costs and performances identified in this paper are presented as a guide for researchers in this field to deliver a commercially competitive technology.

Chapter 3. Limitations of acetate concentration on electrogenic biofilm activity

3.1 Introduction

Microbial electrolysis cells (MEC) require two orders of magnitude increase in their cost-performance ratio to be financially competitive with activated sludge (AS), over a 20-year period. This could be achieved with a 90% decrease in current material costs and a 10-15x increase in organic loading rate (OLR), depending on operational parameters (Aiken et al., 2019). Organic removal rates (ORR) would need to be approximately 90% of OLR to achieve effluent standards. Previously, pilot MEC have had lower ORR (140-210g-COD/m^3/d) (Baeza et al., 2017, Cotterill, 2017, Heidrich et al., 2014) than activated sludge (AS) (450-1,425g-BOD/m^3/d) (Stanbury et al., 2017). But, MEC ORR upper limits are currently unknown. In previous large-scale reactors it has been difficult to determine, until after decommissioning, exactly where the current-producing biofilm is active (Cotterill et al., 2017). It is likely that in previous reactors most of the anode was under colonised, increasing cost. Design criteria could allow for researchers and engineers to predict performance and thus optimise design and reduce costs.

Changing reactor designs and operational parameters to improve outputs is a costly and time intensive endeavour. Electrodes are expensive and biofilm development can take weeks to months to manifest (Kumar et al., 2017). The benefit of using computational methods allows for the cost and time effective investigation of processes that were previously a 'black box'. Useful models accurately predict reality. Empirical observations are needed to calibrate and validate models. This chapter seeks to address the need for calibration. OLR was used as a performance indicator in Chapter 2. This allowed for cross-technological comparison between MEC and AS (Shi, 2011). However, OLR is a measure of a complex chemical reality. Domestic wastewater contains a plethora of both biodegradable and inorganic chemical compounds. And COD, a measure of organic compounds, is fractionated into inert, readily biodegradable and slowly biodegradable compounds. Electrogenic species can only degrade specific biodegradable substrates. Known electrogenic food sources are acetate, formate and hydrogen (Speers and Reguera, 2012, Zhao, 2018). As such, measuring the removal rates of these compounds by electrogenic species can give a mechanistic understanding of MEC performance and investigate limits. Moreover, understanding the expected removal rate and current reponse achievable with a given substrate concentration can

better inform engineers to the design of pre-treatment technologies. Technologies, which can increase VFA concentrations (Ligero et al., 2001, Rezaei et al., 2008, Xin et al., 2018), and thus MEC performance, include hydrolysis and (Ligero et al., 2001) and dark fermentation (Cardeña et al., 2018). Moreover, upflow-hydrolysis can reduce the concentration of suspended solids in the influent, reducing fouling and blockages (Aelterman et al., 2008).

Acetate is of particular interest as a substrate as acetate-fed MECs produce the highest current densities (Zhao, 2018). Acetate has been studied many times before in BES experiments, however the literature has shown that, often, experiments are conducted under unrealistic conditions when compared to domestic wastewater: either temperature is high (Cusick et al., 2011, Escapa et al., 2012, Nam et al., 2011), conductivity is high (Madani et al., 2015, Nam et al., 2011, Rozendal et al., 2008), volatile fatty acid (VFA) concentrations are unrealistic (Dhar and Lee, 2014, Zhao, 2018) or any combination of the three. This gives an unrealistic measure of performance. Furthermore, electrochemical cells often use platinum cathodes, which has a very low overpotential (Ribot-Llobet et al., 2013) but is also prohibitively expensive (Aiken et al., 2019).

The aim of this chapter is to investigate acetate degradation rates and the subsequent current response with cheap materials, in controlled conditions, that although idealistic were analogous with the 'real-world'. We chose acetate as it is a known direct electrogenic substrate and MEC and MFC fed with acetate produce the highest current densities (Speers and Reguera, 2012, Zhao, 2018). Concentrations, conductivity, temperature and pH were therefore carefully controlled to reflect realistic values for temperature ($10\pm0.5^{\circ}$, conductivity ($770\pm15\mu$/S), and pH (7.50 ± 0.5). Acetate concentrations were increased from 10mg-COD/l up to 50mg-COD/l. Furthermore, cathodes and membranes had good cost-performance ratios (Ribot-Llobet et al., 2013) and could be expected to be electrochemically stable under MEC conditions (Christensen and Hamnet, 1994, Janicek et al., 2015). Further simplifications were however made for control purposes. Stainless-steel cathodes were made to be large so that the cathodic surface area was not limiting (Dewan et al., 2008). Graphite plates were used as an anode to create a 'flat' surface for biofilm attachment where substrate could diffuse towards the biofilm in a consistent manner. Reactor chambers were 3D printed to ensure consistency between reactor dimensions.

Furthermore, we investigated current degradation rates for the first time. In a batch reactor, current production can be thought of as a dose-response relationship. Current increases in response to the introduction of substrate and slowly degrades as the microorganisms in the reactor compete and collaborate for food. Current degradation rate: rate of change of current over time, following feeding, can be used to quantify electrogenic activity. Current degradation rate is a precise measurement of the rate of change in the end product of electrogenic anode respiration. Current degradation rate is therefore a function of electrogenic activity. This is contrary to the substrate

degradation rate, which measures the rate of change in the reactant of all microbial interactions in the reactor. Substrate degradation rate is therefore a function of all microbial activity. By investigating and comparing both rates of change, electrogenic kinetics can later be differentiated from microbial kinetics (Chapter 4). We used an exponential decay curve as this best fit empirical observations.

The secondary aim of this chapter will investigate whether setting a high, stable anode potential (+300mV) can improve MEC cost-performance beyond that of setting the voltage, in the given environmental conditions. Potentiostats are classically used in electrochemical systems to finely control redox reactions, though they are expensive. Logan et al. (2006) has suggested that higher anode potentials may allow for more efficient capture of electrons from the biofilm. Acetate oxidation occurs at -0.28V (vs.H^+/H^2), and thus higher anode potentials, create a stronger attraction due to the increased potential difference. Furthermore, setting the potential may also improve electrogenic selection (Commault et al., 2015, Liu et al., 2008). There are suggested links between removal rates of MEC and the anode potential (Commault et al., 2013, Cucu et al., 2013, Nam et al., 2011). Nam et al. (2011) had one of the highest reported current densities (33.3A/m^2) and applied a higher anode potential. However, overall evidence is mixed on whether anode potential can effect substrate degradation and current generation (Kim et al., 2005, Nam et al., 2011, Sultana et al., 2016). Other studies have shown that increasing the potential difference is enough to improve current density and Hydrogen production (Heidrich, 2012, Nam et al., 2011) and is much cheaper to install. Controlling potential is a simple procedure, and is therefore an enticing possibility to increase MEC performance. To investigate whether controlling potential was beneficial over allowing anode potential to vary, we split reactors into two electrode systems (2ES) and three electrode systems (3ES) and assessed cost effectiveness. The 3ES set the anode potential in relation to a known reference electrode (RE), whilst 2ES set the cell potential difference (voltage) between the anode and the cathode. We determined a safe, stable, positive anode potential (+300mV) using linear sweep voltammetry. Whilst the 2ES system's anode potential was free to vary - potentially influencing MEC performance.

3.2 Methodology

3.2.1 Set-up

Reactor chambers

Reactors were designed in four parts using AutoCAD 2016 (Autodesk, USA): anode and cathode compartments and two 'doors' (Figure B.1). Components were manufactured by Amtech, UK. Electrode compartments were 3D printed using SLA Ultra Resin (Water Clear Ultra Resin 10122,

DSM Somos, Newcastle-upon-Tyne, UK) with a clear lacquer finish. The 'doors' were machined from transparent acrylic to facilitate better viewing of electrodes. Anode compartments contained a rectangular slot 2.5mm thick and 50mm wide to insert the anode, and the cathode compartment contained a smaller rectangular slot 2.5mm thick and 10mm wide to allow the cathode to extrude. This allowed for the electrodes to be inserted into the reactors yet have parts exposed for electrical connections without the need to solder additional wires. A groove was manufactured on the bottom of the anode chamber to allow the anode to be 'slotted' into it and kept firmly in place. Anode compartments also contained three circular slots on the top of the compartment (14.5mm diameter) and one of the side: these were for the RE, gas collection and for sampling, emptying and allowing pressure to be released during filling. The cathode compartment contained two circular slots on the top and one on the side, as a slot for the RE was not required. Compartments were 'fitted' together using threaded bars, wing nuts and washers. Internal compartments for both electrodes were: 40mm deep, 60mm wide and 50mm in height. Chambers were tested for leaks, first by filling with DI and then further tested by filling with DI and pressuring with Nitrogen gas. Components were sealed into their respective slots using a combination of hot glue (Beeway, UK), tape (Shurtape, USA) and superglue (Wilkinson, UK). Inlets and outlets were sealed with rubber bungs (SLS, UK).

Electrochemical components

Anodes were smooth graphite plates, to provide a 2D surface (GPE Scientific UK, machined by Erodex, UK). Stainless steel mesh (SS316L) (The Mesh Company, UK) was used as a cathode. The mesh was cut and folded into a concertina from 1m length to be approximately 50mm wide and inserted into the cathode chamber. Specific surface area was approximately 20 times greater than that of the anode. The membrane was cut from a large sheet of Rhinohide (Entek, UK) and glued with epoxy (Wilkinson, UK) between two 1.5mm thick neoprene (Thorne, UK) 'frames' for a watertight seal. Holes were 'punched' out to allow for the insertion of threaded bars (Screwfix, UK).

RE were Ag/AgCl (Cole Parmer, UK). RE were inserted into salt bridges to protect them from the anolyte. Salt bridges were created using a 1.5%(w/v) agar (no 1) and 1M of KCl, which was the same concentration of KCl found in the RE. The gel was formed by heating the stirred mixture to 200°C. Heat was removed once bubbles formed and the clear solution was pipetted into an autoclaved 10ml pipette tip. Pipette tips were then placed into a solution of 1M KCl, RE were inserted and left to cool. Voltage drifts were measured against a master RE (Table B.1). Finally, RE-salt bridges were inserted and sealed into the reactor chambers using the same adhesives as before. Distances between RE and anode were measured to ensure voltage losses were minimal (Table B.2).

Two four-channel 'Quad' Potentiostats (Whistonbrook, UK) were used to control the potential and measure electrical current. Accuracy was assessed by measuring current flowing across a 1kohm and a 2kohm resistor. Variations were negligible (Table B.3). In 2ES, potential differences across the cells were set to 0.6V (close to a lower limit (Fornero et al., 2010). Voltage differences between the anode and the RE were measured using a pico-logger (Pico Technology, UK) to determine relative potentials of the cells electrodes. Linear sweep voltammetry (LSV) was conducted to determine stable anode potential ranges and corresponding cathode potentials, to prevent corrosion in the cathode chamber (Figure B.7). Consequently, anode potentials in 3ES were set to +300mV (vs. Ag/AgCl). In 3ES voltage differences between the anode and cathode were measured using a picologger. Recorded potentials and voltages were adjusted for voltage drifts in RE (Table B.1).

Electrolyte

Catholyte was a sodium phosphate buffer (PB) that was specifically made to have a pH of 7.50$\pm$0.05 and a conductivity of 770μS/cm$\pm$15μS/cm, which were reflective of local primary effluent (Chester-le-Street). 1L of PB contained deionised water (DI), 1.5mM of NaH_2PO_4 and 3.5mM Na_2HPO_4. pH was measured using a DrDAQ pH probe (Pico Technology, UK), calibrated at pH 4.00, 7.00 and 10.00. Conductivity was measured by removing 25ml of solution and inserting the conductivity probe from a HQd/IntelliCAL™ Rugged Field Kit (Hach, UK). Solutions were sparged with nitrogen gas for 30 minutes to reduce oxygen.

Anolyte contained a mixture of sodium acetate, ammonium chloride, sodium phosphate buffer and trace element and vitamin solutions. Initial acetate concentrations were 10mg-COD-equiv/l. Following the same motif, ammonium chloride concentrations were 20mg-NH_4-equiv/l, reflective of mean levels found on a treatment works (Chester-le-Street, UK). Vitamin and trace element solutions were also included at concentrations of 10mg-COD/l each (formulas below). Again, PB was added so that the pH was 7.50$\pm$0.05 and conductivity was 770μS/cm$\pm$15μS/cm at room temperature. PB contained 1mM NaH_2PO_4 and 2.5mM Na_2HPO_4, less than the catholyte to account for the increase in conductivity from the sodium acetate, ammonium chloride, vitamin and trace elements solutions. The mixed solutions were sparged with nitrogen for 30 minutes to reduce oxygen.

The trace element solution was based on an adaption of Wolfe's trace element solution. A 1x stock solution was comprised of EDTA (0.5 g/l), $MgSO_4$. $7H_2O$ (3.0 g/l), $MnSO_4$. H_2O, (0.5 g/l), NaCl (1.0 g/l), $FeSO_4$. $7H_2O$ (0.1 g/l), $Co(NO_3)_2$. $6H_2O$ (0.1 g/l), $CaCl_2$ (anhydrous) (0.1 g/l), $ZnSO_4$. $7H_2O$ (0.1 g/l), $CuSO_4$. $5H_2O$ (0.010 g/l), $AlK(SO_4)_2$ (anhydrous) (0.010 g/l), H_3BO_3 (0.010 g/l), Na_2MoO_4 . $2H_2O$ (0.010 g/l), Na_2SeO_3 (anhydrous) (0.001 g/l), Na_2WO_4 . $2H_2O$ (0.010 g/l) and $NiCl_2$. $6H_2O$ (0.020 g/l). The vitamin solution used Wolfe's vitamin formula. A 1x stock solutions

contained folic acid (2.0 mg/l), pyridoxine hydrochloride (10.0 mg/l), riboflavin (5.0 mg/l), biotin (2.0 mg/l), thiamine (5.0 mg/l), nicotinic acid (5.0 mg/l), calcium pantothenate (5.0 mg/l), vitamin B12 (0.1 mg/l), p-aminobenzoic acid (5.0 mg/l), thioctic acid (5.0 mg/l), monopotassium phosphate (900.0 mg/l).

3.2.2 Operation

Start-up

Reactors were inoculated with sparged settled wastewater taken from a local wastewater treatment works (Chester-le-Street, UK). For inoculation the anode chamber was filled with 50% anolyte and 50% settled sewage. Reactors were placed in an incubator (Samsung, UK) and temperature was set to 10°C - the median temperature for wastewater in the region (North East, UK). Initial feeding periods occured every seven days but current failed to grow.

Successive re-inoculations failed to produce any current. The time between feeding was reduced to four to five days, and after four weeks three out of eight reactors started up with an acetate concentration of 10mg-COD/l. I further reduced the feeding to 48 hours and after eight weeks all 8 reactors were producing current with an acetate concentration of 10mg-COD/l. Vitamin solution was removed for two weeks after it was found to influence current using an exclusion test. Current dropped in all eight of the reactors. Randomised testing was conducted to ascertain which of the vitamins was contributing to the current increase. No vitamin was found to influence current, but the vitamin solution contained some lactic acid. Acetate concentrations were then increased to 16mg-COD/l and a new vitamin solution was administered.

Main experiment

Acetate concentrations were increased at an approximate rate of 1.5x the previous concentration and measurements were taken once current had stabilised. Three main concentration stages were investigated: 16mg-COD/l (runs A & B), 24mg-COD/l (runs C & D) and 36mg-COD/l (runs E &F). However, actual acetate concentration in the reactor varied. At 24mg-COD-equiv/l projected mean change in maximum current densities was -0.131mA/m^2/day, and at 36mg-COD/l, -0.085 mA/m^2/day. A sodium acetate solution was pipetted into the anode chamber with a 1ml pipette at feeding times. Concentration of this solution was based on pipetting a 1ml solution into a 112ml chamber (accounting for anode volume) to give desired overall concentration. Upon feeding, the current responded almost immediately, with current readings showing increases after 1 minute (measurements were taken once per minute).

Reactors were fed approximately every 48$\pm$2 hours. Media was refreshed once every two weeks

to prevent excessive pH changes. The sparged anolyte and catholyte were pipetted into the chambers using 110ml syringes and drawn out with another syringe. This was to reduce oxygen in the chamber as much as possible. pH was measured at the end of this period and was found to vary by a maximum of 7.50$\pm$0.33pH (Table B.4). During the refresh period it took approximately 24 hours for the solution to cool to 10°C

Substrate samples were taken using 1ml syringes. Approximately, 0.5ml was removed and filtered through 0.22μm filter to remove biological material. Samples were then flash frozen in liquid nitrogen to prevent any further degradation and stored at -80°C. Upon thawing, samples were spun through 10kDa centrifuge filters at 4°C for 10 minutes to remove any proteins from the sample. Gel electrophoresis imaging (agarose gel (1%w/v)) found no proteins present in one set of samples (Figure B.2). Acetate concentrations were measured using Acetate Colorimetric Kits (MAK086-1KT, Sigma Aldrich, UK). Standard curves were created for each of the runs. This was achieved by using concentrations of acetate (S) at 0-8nM/L in incremental steps of 2nM/l. Ultimately, an average of the standards was used to reduce variations in standards and reaction mix (Figure B.3).

Blank were taken away from the main data-sets to remove reaction mix interference. Absorbance spectra at 450nm was determined using SpectraMax M3 (Molecular Devices, UK). To determine degradation of acetate directly, acetate concentrations were measured four times over a 6 hour period: 5 minutes, 1 hour, 3 hours and 6 hours after feeding. Acetate concentrations were converted into equivalent COD.

3.2.3 Analysis

All reactors took weeks to months to before current was produced and a further four weeks (approximately) before a stable current profile was observed. Stable current profile was said to be achieved when maximum current densities were similar between consecutive runs. Once the stability in the current profile was achieved, the degradation of current followed an approximate exponential decay, which was not observed during the 'growth phase'. The feeding runs used in the analysis were taken once the majority of reactors had stable current profiles. Projected mean changes in maximum current density, which occurred 5-10 minutes after feeding, was -0.727mA/m^2/day. Analysis was predominantly conducted using Python in Spyder3 (Anaconda, USA). Data from the potentiostats was converted into a csv format, combined and separated into 'runs', with each 'run' corresponding to the 48 hours following feeding.

Four out of the 48 runs had very low current production and a poor fit to the exponential decay function (due to a lack of measurable current). One of the four runs occurred in the first feeding run and three of the four in the second, when acetate concentrations were low. As all 8 reactors had previously started, it is possible that the low concentrations were unable to stably sustain the

biofilms. This problem did not occur when concentrations were higher. The primary aim of the experiment was to determine the current production and substrate degradation of anode biofilms. As these four runs did not represent a developed electrogenic biofilm, they were excluded from analysis. However, it is worth noting that MEC reactors did not all start at the same time and this risk should be taken into account when designing commercial systems.

Current

Outliers in electrical current due to connection and disconnection of wires were removed (<-100μA, >1000μA). For current degradation and maximum current density analysis, peaks in current caused by pressure changes due to sampling were corrected. Peaks were identified from rapid increases in current followed by rapid decreases. Maximum current density (surface) was equal to the maximum current, between feeding times, divided by the area of two sides of the graphite electrode. Maximum current density was plotted against COD concentration and a linear curve was fitted. Often the literature reports current density as the projected current density. In this study, the projected current density is equal to the maximum current divided by one side of the graphite felt, and was double the surface current density. Surface current density is later referred to simply as 'current density'. The degradation of the current following peak currents was observed to very closely approximate exponential decay once current had stabilised (Figure B.8, Equation 4.17). The exponential decay function was adapted for current (Equation 4.17), with the scalar being equal to the maximum current (I_{max}). Functions were fitted to the curve using SciPy and the exponent (λ) and constant (c) were outputted, along with the coefficient of determination (Equation 3.2). Mean cycle lifetimes (τ), current half lives ($t_{\frac{1}{2}}$) and time until 90% reduction in current ($t_{0.9}$) were also outputted (Equation 3.3).

$$I = I_{max} e^{-\lambda . t} + c \tag{3.1}$$

$$R^2 = 1 - \frac{\sum_i (I_i - I_{mean})^2}{\sum_i (I_i - I_{i,pred})^2} \tag{3.2}$$

$$\tau = \frac{1}{\lambda} = ln(2).t_{\frac{1}{2}} = ln(10).t_{0.9} \tag{3.3}$$

Time until peak

Current production occurred within 5 minutes of the reactors being fed, during the 'plateau phase'. Approximate feeding times ($\pm$5min) were found by measuring the gradient of the growth in current

between 25% and 75% of maximum current and back calculating to give a precise measurement. The time until peak was then measured between the 'feeding time' and the time at which maximum current occurred.

Coulombic efficiency

Coulombic efficiency (C_e) directly calculates the proportion of charges recovered compared to the total charge stored chemically. The equation for coulombic efficiency was adapted from Logan (2008)'s (page 49) equation, to easily fit the recorded current (I) data (Equation 3.4). Time-step (Δt) between recordings was 1 minute. Volume (V) was 112mL. Faraday's constant (F) was 96,485C/M. The change in COD (ΔCOD) was equivalent to the total COD as all COD was assumed to be removed. The conversion factor (n = 8mol-e^-/g-COD) was equal to the molecular weight of dioxygen (32g/mol) divided by the total number of electrons exchanged per mole of oxygen (4mol-e^-/mol-O_2). All measured acetate concentrations were assumed to be removed in the 48 hour runtime and current was summed from the feeding time of the run until the following feed.

$$C_e = \frac{n}{V \cdot F} \sum_{t=t_{feed,run}}^{t=t_{feed,run+1}} \frac{I_t \Delta t}{\Delta COD} \tag{3.4}$$

Acetate degradation

Mean substrate degradation rates ($q_{mean,t}$) were measured over the 6 hour sampling period (t). Linear approximations were found using the python module SciPy (Figure 3.5) and are approximately equal to the change in concentration (S_t-S_0) over time (t) (Equation 4.15). Mean measured starting acetate concentration were compared between runs and reactors were compared to assess sources of error. Starting concentrations were assessed against degradation rates to test for concentration removal prior to reading.

$$q_{mean,t} \approx \frac{S_t - S_0}{t} \tag{3.5}$$

Monod functions (Equation 3.6) were fitted to the substrate degradation rate (q) plots to find the maximum degradation rates (q_{max}) and the half-saturation constant (K_s).

$$q = q_{max} \cdot \frac{S}{K_s + S} \tag{3.6}$$

Voltage, resistance and power

Maximum voltages and potentials were used for each of the runs. Resistances in the salt bridges were assumed to be negligible due to the very high conductivity. Total cell resistances and power were estimated based upon maximum voltage and current, using ohm's law (Equation 3.7, Equation 3.8).

$$R_{cell} = \frac{V_{max}}{I_{max}} \tag{3.7}$$

$$P_{max} = V_{max} \cdot I_{max} \tag{3.8}$$

Confidence intervals

Two-tailed confidence intervals (Equation 3.9) were calculated for 2ES and 3ES at a 95% confidence interval for each of the feeding run groups. Feed runs with stable maximum currents and similar acetate concentrations were grouped together: A&B, C&D and E&F. Parameters analysed were current degradation, max current density, coulombic efficiency and substrate degradation.

$$Limits(P = 95\%) = \mu \pm 1.96\frac{\sigma}{\sqrt{N}} \tag{3.9}$$

Microbial analysis

Microbial samples of the bulk liquid were taken and stored prior to feeding in the same manner as concentration samples. Biofilm samples were not taken so as not to disturb the biofilm during operation. DNA extraction was conducted using FastDNA® SPIN Kit for Soil (MP Biomedicals, USA). Methods were adapted for liquid samples: 250μL of sample, 978μL of Sodium Phosphate Buffer and 122μL of MT Buffer were added a Lysing Matrix E tube before centrifuging at 14,000g for 5 minutes. Supernatant was transferred to a 2mL micro-centrifuge tube with 250μL protein precipitation solution and mixed by hand. Tubes were centrifuged again at 14,000g for 5 minutes. Binding matrix was resuspended and added with 800μL of supernatant to a 2mL tube. Tubes were inverted for 5 minutes to allow binding of DNA before removing 500μL supernatant was removed. Binding matrix was resuspended and 500μL was added to the SPIN® filter and centrifuged at 14,000g for 1 minute. Next 500μL SEWS-M was added, and the pellet was gently resuspended using a pipette. The solution was centrifuged at 14,000g for 1 minute, the catch tube was emptied and the solution centrifuged for another 2 minutes. The catch tube was disposed and a clean catch tube was inserted. The remaining binding matrix was air dried for 5 minutes. Binding matrix was finally resuspended with 70μL of DNase Pyrogen Free-Water and centrifuged for another minute at 14,000g. The catch

tube containing the DNA was stored at -20°C. Illumina MISeq sequencing was conducted on the DNA extraction and blanks (Nuomics DNA sequencing research facility, Northumbrian University, UK). Primers were removed during the demultiplexing process. Consequent analysis was conducted using the DADA2 pipeline in R (Callahan1 et al., 2016). Quality profiles were high, all reads had the first 10 bases removed, forward reads had a length of 240 bases and reverse reads had a length of 220 bases (Figure B.10, Figure B.11). Reads were also filtered so only models that had 2 expected errors remained. Error rates were determined via a parametric error model and sample interference was removed (Figure B.12, Figure B.13). The forward and reverse pair reads were merged, chimeras removed and sequence tables constructed. Taxa were assigned using the silva taxonomic database for 16s rRNA (Glöckner et al., 2017). The differences in source communities, feeding runs and electrical systems was investigated, as well as the relationship between observed taxa in the bulk liquid and coulombic efficiency. Non-metric multidimensional scaling (NMDS) analysis was conducted to observe the differences between runs and inoculate. Finally a Simpson's index of diversity analysis (Equation 3.10) was conducted to compare richness and evenness in 2ES and 3ES. The Simpson's index of diversity takes into account the observed number of a particular species (n) and the total number of observations (N). Results were conducted and presented with phyloseq (McMurdie and Holmes, 2013)

$$1 - D = 1 - \frac{\sum n^2}{N^2} \tag{3.10}$$

3.3 Results and Discussion

3.3.1 Acetate degradation

Acetate degradation rates were predominantly described by Monod kinetics. Degradation rate means for each of the feeding runs had a very good fit with Monod kinetics (R^2 = 93%), whilst individual degradation rates had a moderately good fit (R^2 = 59%). Maximum substrate degradation of 9.2$\pm$5.0mg-COD/l/h and a half-saturation coefficient of 52.9$\pm$18.0mg/l were predicted to fit the data ($\pm$2SD). Although acetate concentrations fed to reactors were lower than the half-saturation constant, which is not ideal for determining this parameter, the curve was fit to 6 concentrations, reducing its degrees of freedom and coefficients of variation for the half-saturation parameter were 17%. Though ideally, the reactors could have been fed with higher concentrations to confirm this parameter.

Moreover, similar maximum degradation rates (10mg-COD/l/h) have been observed with *Geobacter spp.* fed with higher acetate concentrations (500mg-COD/l) and grown in warmer conditions (23-25°C). Some MFC and MEC have been shown to have high substrate removal rates as low as

4°C (Larrosa-Guerrero et al., 2010, Lu et al., 2012). Typically, enzyme activity is a function of temperature (Kolmos, 2012), however 10°C appears to be suitable for electrogenic communities. These observations add weight to the suitability for BES to operate in temperate regions without additional heating (and cost). However, reactors took 3 weeks to start-up. Reactors fed at higher temperatures typically start-up much quicker (Kumar et al., 2017), but can incur more methanogenic competition (Lu et al., 2012). Hypothetically, some limited heating may be useful during start-up, though this may lead to poorly adapted microbial communities when heat is removed.

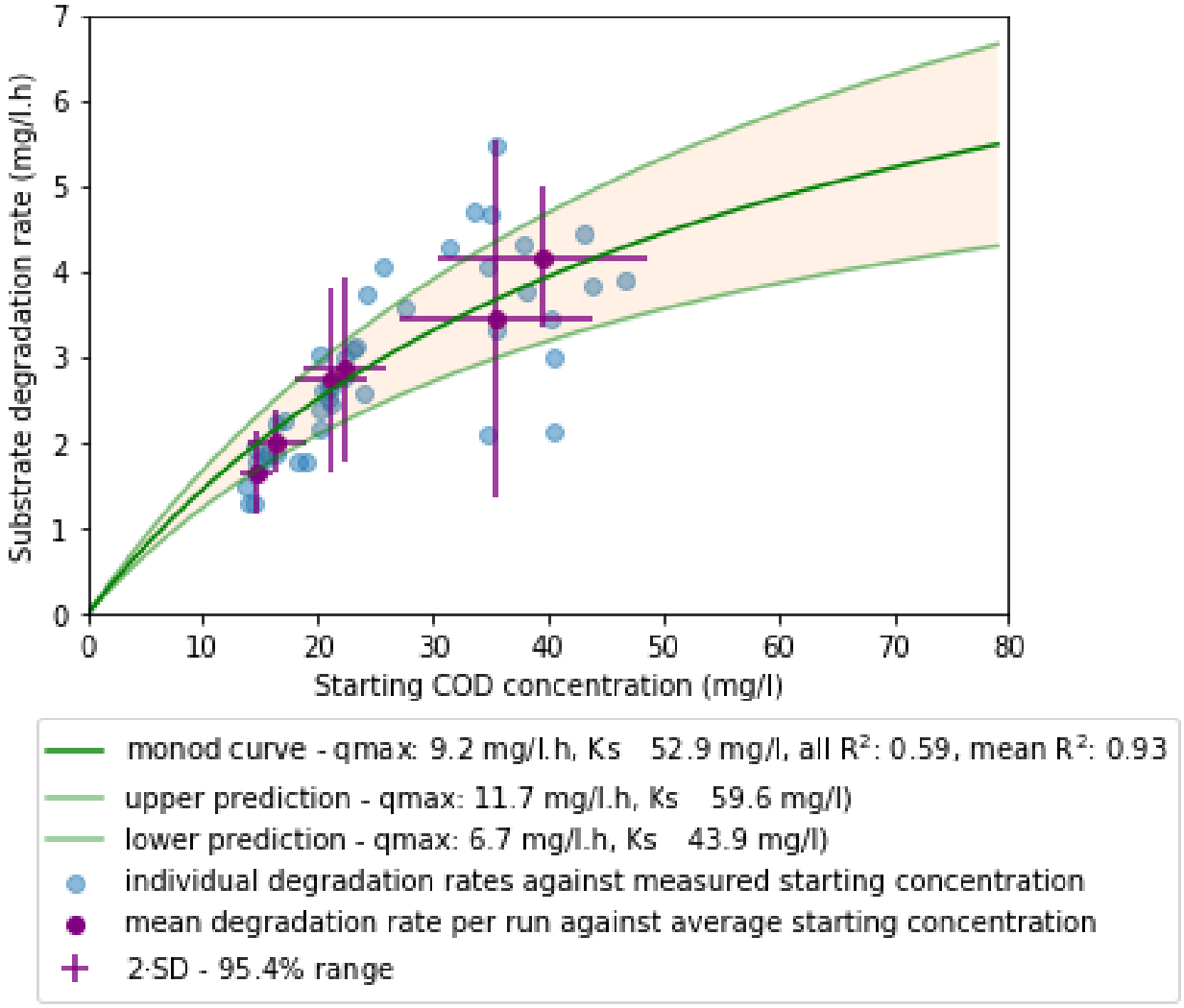

Figure 3.1: Monod substrate degradation rate distribution against COD concentration

Degradation rates were well approximated by a normal distribution for each of the concentration groups. However, runs C&D had a moderately positive skew (0.62) and a moderately positive effective kurtosis (0.4). Coefficient of variation (CV) marginally increased with acetate concentration (16.1-22.8%, Table 3.1). As pH, temperature, conductivity, surface area, concentration and

chemical species were all carefully controlled. This change in CV is likely due to differences in microbial community and development. In the 'real-world' variation will be higher as biofilm development will be affected further by the chemical species present in the wastewater (Kadier et al., 2014, Zhao, 2018), pH, temperature (Roger et al., 2008), prior microbial communities (Ishii et al., 2015), and shear forces (Fink et al., 2016). Biofilm will also be affected by their access to substrate and will likely undergo a growth and and death cycle (Cotterill et al., 2017, Judd, 2013). Baudler et al. (2014) showed that inoculation of systems with pre-grown electrogenic communities can help improve electrogenic activity; but as mixed systems are necessary for the degradation of complex substrates in treatment works (Fornero et al., 2010), the usefulness of inoculation will be dependent upon the concentration of readily digestible electrogenic food and thus some variability in performance is to be expected.

In a continuous system, biofilm development will vary along the length of the anode. Degradation rates and concentration will thus diminish in-line with the direction of flow as opposed to diminishing over time in these batch systems. Supposedly, biofilm concentrations will be higher closer to the influent where acetate concentrations are higher. The optimal length (and viable removal capacity) of the reactor will be a function of the concentration and consistency of acetate and the subsequent biofilm response.

Runs	**A&B** (15.4±1.3mg/l)	**C&D** (21.8±1.8mg/l)	**E&F** (37.4±4.8mg/l)	**all** (25.7±9.7mg/l)
Mean	1.8mg/l.h	2.8mg/l.h	3.8mg/l.h	2.9mg/l.h
SD	0.29mg/l.h	0.55mg/l.h	0.87mg/l.h	1mg/l.h
CV	16.1%	19.5%	22.8%	35.4%
Maximum	2.3mg/l.h	4.1mg/l.h	5.5mg/l.h	5.5mg/l.h
Minimum	1.3mg/l.h	1.8mg/l.h	2.1mg/l.h	1.3mg/l.h
Skew	-0.28	0.62	-0.41	0.48
Kurtosis	-0.62	0.4	-0.12	-0.65

Table 3.1: Statistical description of substrate degradation rates

Acetate concentrations

Mean COD concentration for the same runs were 15.4mg/l, 21.8mg/l and 37.4mg/l. The largest difference was in runs E&F. As feeding concentration was higher in these runs, and current did not completely return to baseline in some reactors after 48 hours, it is possible that some acetate was left from the previous feeding run, thus marginally increasing the concentration. Reactor concen-

Runs	A&B	C&D	E&F	all
Mean	15.4mg/l	21.8mg/l	37.4mg/l	25.7mg/l
SD	1.3mg/l	1.77mg/l	4.78mg/l	9.71mg/l
CV	8.5%	8.1%	12.8%	37.7%
Maximum	18.3mg/l	25.6mg/l	46.8mg/l	46.8mg/l
Minimum	13.8mg/l	18.9mg/l	27.5mg/l	13.8mg/l
Skew	0.653	0.476	0.0224	0.573
Kurtosis	-0.38	-0.69	-0.352	-1.01

Table 3.2: Statistical description of measured acetate concentrations

trations had up to ±30% variation from the mean (c.60%). Runs A&B, C&D and E&F had COD concentration ranges of 13.8-18.3mg/l, 18.9-25.6mg/l and 27.5-46.8mg/l, respectively. Acetate concentrations were generally normally distributed about means, although concentrations in A&B had a moderate positive skew (0.653, Table 3.2). Comparing run means and reactor means showed that (2/3 of variation) was random and 1/3 of variation was observed between runs (Figure B.4). Generally differences in concentration for each run were likely due to differences in pipetting and colorimetric laser measurements, although some variation may due to acetate assay kits, standards and in weighing initial concentrations. Pipetting occurred during feeding, sampling, filtering and plating.

3.3.2 Maximum current density

Maximum current density were reasonably approximated by a linear fit (mean R^2 = 95%, all R^2 = 56%, Figure 3.2) and were normally distributed about the mean (Table 3.3). The highest current densities (0.10-0.12A/m^2-surface, 0.20-0.27A/m^2-projected, Table 3.3) were found in three out of the eight reactors (runs E&F, Figure 3.2). This is comparable to the highest projected current densities found in pilot studies using 'real' wastewater (0.22-0.37A/m^2-projected) (Baeza et al., 2017, Escapa et al., 2015, Gil-Carrera et al., 2013, Heidrich et al., 2013). Acetate concentrations in domestic wastewater are typically around 10mg-COD/l (Henze and Comeau, 2008, Huang et al., 2010, Shi, 2011). Although acetate concentrations were higher for these runs (37.4±4.8mg/l), reactors were run in batch with a smooth graphite surface, not in continuous mode with a porous carbon anode and total COD was much lower than in domestic wastewater. As current densities are within the same order of magnitude, the use of low acetate concentrations to mimic wastewater was therefore at least a somewhat accurate simplification, at least where maximum current densities are concerned.

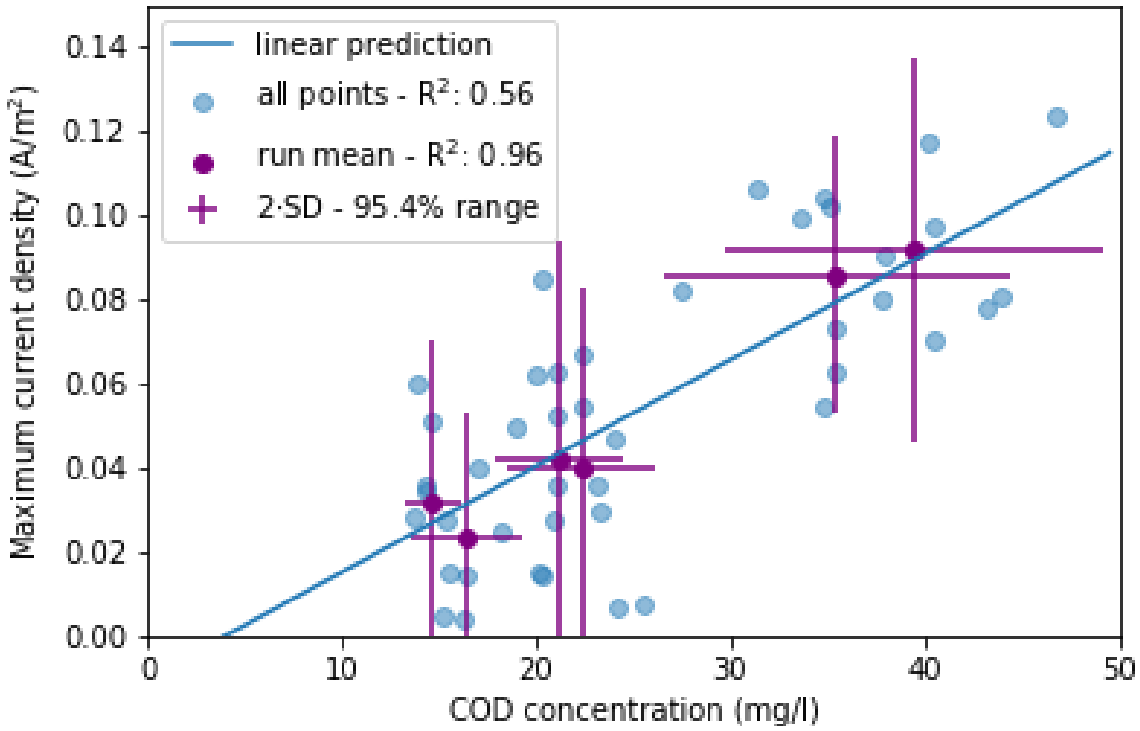

Figure 3.2: Maximum current density with respect to concentration

Mean maximum current density was predicted to be intercept the x-axis at 3.98mg/l/ (Figure 3.2). This suggests that at low concentrations some proportion of reactors will not have sufficient electrogenic activity to produce current and may be why some reactors started sooner than others when initial concentrations were low (c.10-16mg/l). Cotterill et al. (2017) also found that some MEC cells failed to start when fed with domestic wastewater where acetate concentrations are typically c.10mg-COD/l (Henze and Comeau, 2008, Huang et al., 2010, Shi, 2011). Furthermore, SD was similar at all concentrations (0.017-0.022A/m^2, Table 3.3) and as such CV decreased as concentration increased. Presumably, increasing acetate concentrations in wastewater would improve MEC reliability. Although MEC performance will also likely be effected by the chemical species present in the wastewater (Kadier et al., 2014, Zhao, 2018), prior microbial communities (Ishii et al., 2015), pH, temperature (Roger et al., 2008) and shear forces (Fink et al., 2016).

3.3.3 Time until maximum current

Following feeding, reactors took on average 2h05 to reach maximum current density, however the distribution was heavily positively skewed (+2.61). The median time taken to reach maximum current density was 1h37 and the most frequent 15 minute interval was 1h to 1h15 (Figure 3.3).

Runs	**A&B** (15.4±1.3mg/l)	**C&D** (21.8±1.8mg/l)	**E&F** (37.4±4.8mg/l)	**all** (25.7±9.7mg/l)
Mean	0.028A/m^2	0.041A/m^2	0.089A/m^2	0.055A/m^2
SD	0.017A/m^2	0.022A/m^2	0.019A/m^2	0.033A/m^2
CV	58.7%	54.5%	21.2%	59.6%
Maximum	0.060A/m^2	0.085A/m^2	0.123A/m^2	0.123A/m^2
Minimum	0.004A/m^2	0.007A/m^2	0.055A/m^2	0.004A/m^2
Skew	0.245	0.085	0.047	0.240
Kurtosis	-0.723	-0.897	-0.843	-0.937

Table 3.3: Statistical description of data-set for maximum current densities

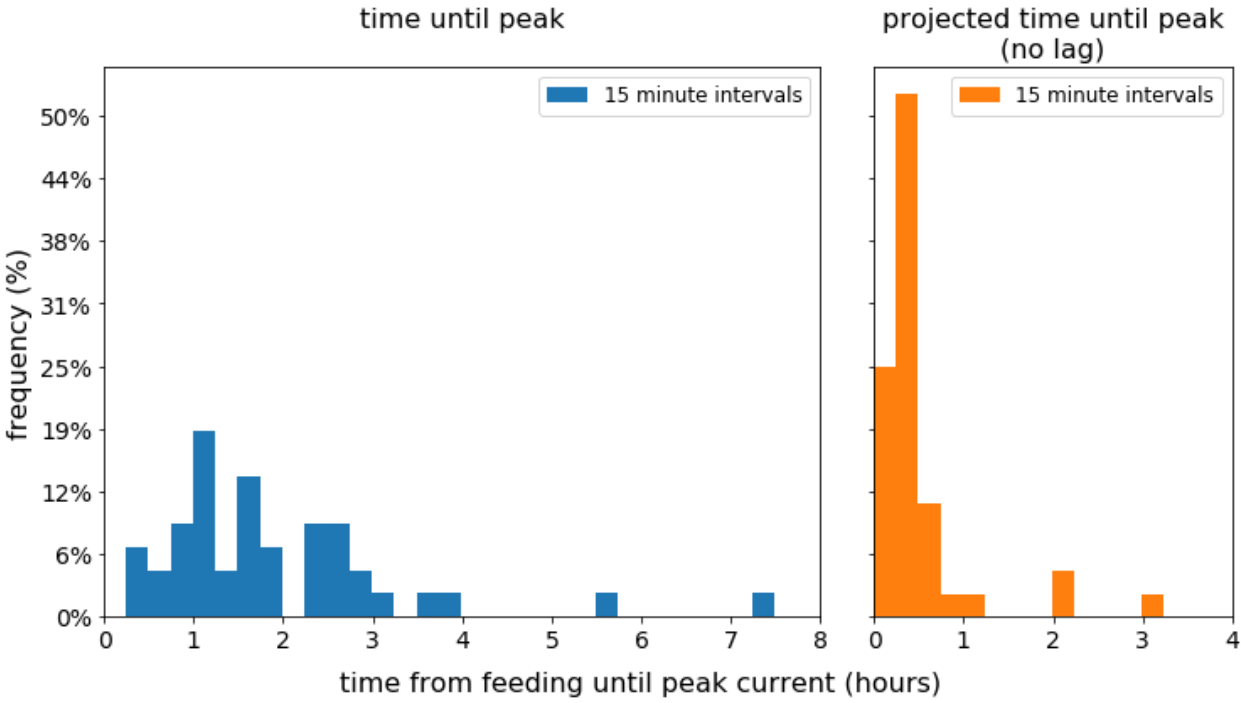

Figure 3.3: Time taken from feeding to reach maximum current density

Current typically increased quickly following feeding to more than 90% of the maximum current and then there was a small lag whilst current increased slowly up until the peak. This lag was more apparent when maximum current densities were still growing between feeding runs. Supposedly this represents the growth of new biofilm following feeding. The two longest times until feeding took place in one reactor, which took 9.91h (not shown) in run E and 7.27h in run F (Figure B.9). Maximum current densities were the lowest in its feeding run and a significant amount of 'slow growth' occurred following a rapid peak suggesting that the biofilm had not finished growing.

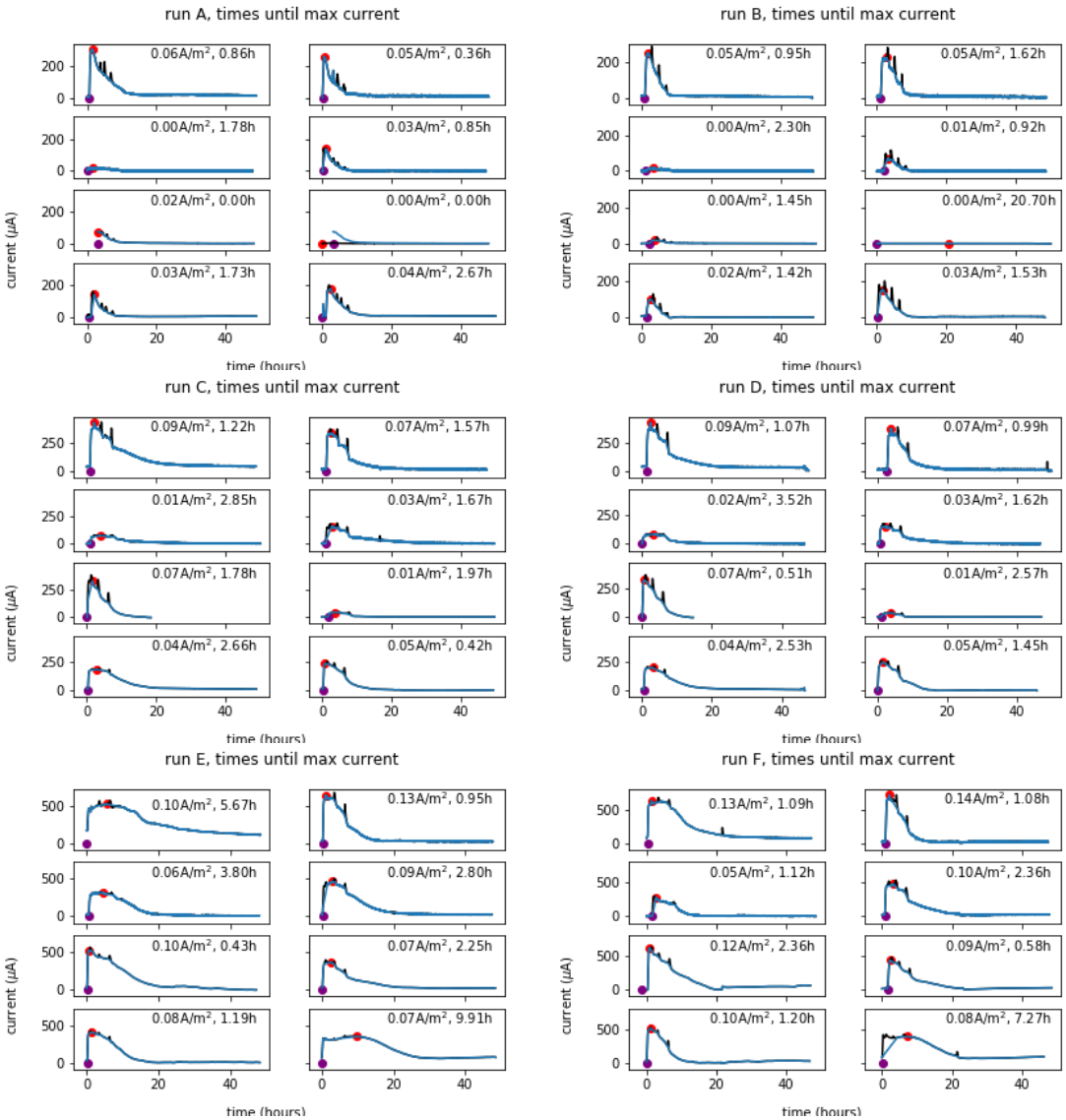

Figure 3.4: Calculated feed times for each reactor over each run

For runs A&B, when acetate concentrations were low (c.16mg-COD/l), most of the acetate was removed in most of the reactors within the 6 hour sampling window (Figure 3.5). Maximum current density therefore occurred when around a third of the acetate had been removed. As acetate concentrations increased so too did the time of acetate removal. Runs C&D had approximately a quarter of the acetate left after 6 hours. Whilst run D and run E had about one half and one third left, respectively. As run D occurred earlier in the experiment, took longer to reach maximum current density and had slower degradation rates, the biofilm may have still been growing. If acetate concentrations were reduced linearly then all of the acetate will have been removed within the first 24 hour period. It is more likely, that acetate was degraded in an approximately exponential manner. In most of the feeding runs, the acetate measured shortly after feeding was approximately equal to

the intended acetate concentration and therefore all acetate was removed after 48 hours. Except in run D, which had much higher acetate concentrations.

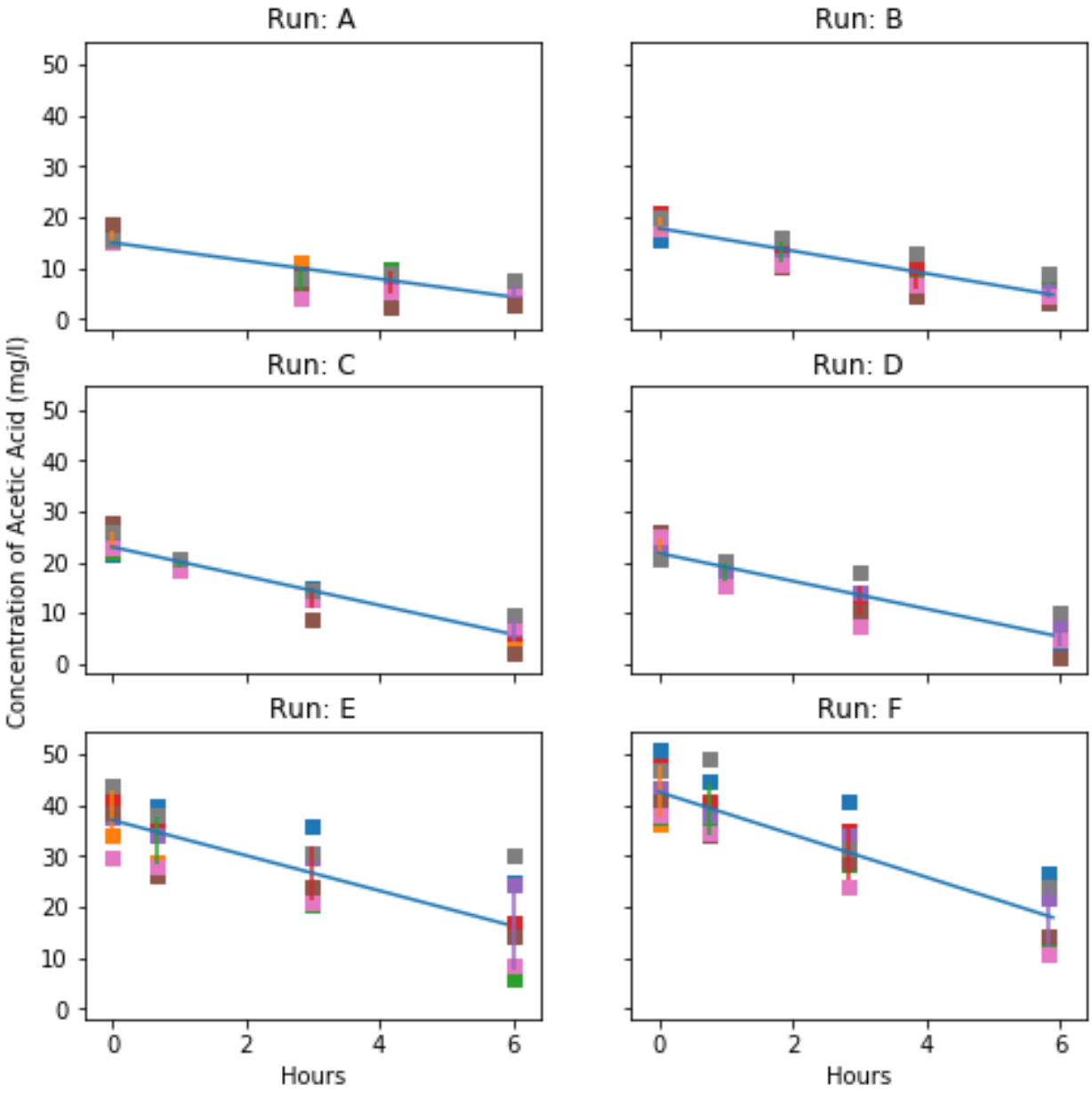

Figure 3.5: Acetate concentrations during feeding runs

Hypothetically, the time until maximum current density should be related to the mass transport of substrate and the mass of the biofilm. In continuous reactors this may not be present as biofilms will be continually supplied with substrate. Though other factors such as biofilm metabolism may play a roll (Mortia et al., 2011). If the lag phase had not occurred time until maximum current would have been reduced. Extrapolating the maximum growth in current from 25% peak current

to 75% peak current showed that maximum current would have been reached within 15 minutes 25% of the time, within 30 minutes 77% of the time and within 45 minutes 88% of the time (Figure 3.3). In a continuous system this spike in current should not be apparent as substrate should (in perfect conditions) be present continuously. Current densities (and biofilm biomass) would likely vary along the anode with the highest current occurring close to the inlet and the lowest biomass concentrations and current close to the outlet. In a porous material this may also occur perpendicularly, with the highest current being produce from the front of the anode close to the bulk liquid and the weakest at the back. If the biomass close to the inlet experiences no famine periods, then current densities may be much higher in his portion of the anode.

3.3.4 Current degradation rate

Degradation of current following maximum current density was well approximated by a first-order decay function in reactors whose maximum current had plateaued Figure B.8. Out of the 44 runs used in the final analysis, 39 had a very good fit ($R^2 > 90\%$) and the remaining data-points had a good fit ($R^2 > 70\%$). This preliminarily suggests that an exponential decay function may be a good description of current decay for an MEC with a well developed anode-respiring microbial community. Contrarily, current degradation rates following feeding in reactors during the 'growth phase' exhibited a general logistical curve.

Degradation of current was not normally distributed and had a moderately negative skew during runs A&B and a high positive skew in runs C-D. Effective kurtosis was also high during these runs. Current degradation rates thus had shallow distributions and tended towards lower values as concentrations increased with a smaller number of higher degradation rates. Current degradation rates reduced with respect to concentration approximately exponentially (mean $R^2 = 77\%$) (Figure 3.7). As concentration increased above 30mg-COD/l, current remained higher for longer and degraded similarly over time, with more consistency between reactors. Mean substrate degradation for runs E&F were 0.15/h, with the lowest substrate degradation of 0.077/h in run E (Table 3.4).

A sustained high current is beneficial for cathodic reactions and the subsequent production of cathodic products - due to Faraday's law of electrolysis. However, sustaining higher current stably presents a limit for biofilm removal and thus retention times. At 0.15/h, half-life in the reactor is approximately 4h37, meaning that 90% reduction in current should be achieved in 15h21. Higher current degradation rates would facilitate lower cycle times, allowing for smaller, cheaper and faster reactors. As acetate concentrations were sampled during these runs with a pipette, pressure was exerted in the chambers creating convective currents and current production spiked and quickly fell soon after. It is possible that current degradation rates may be higher than would have occurred had this not taken place.

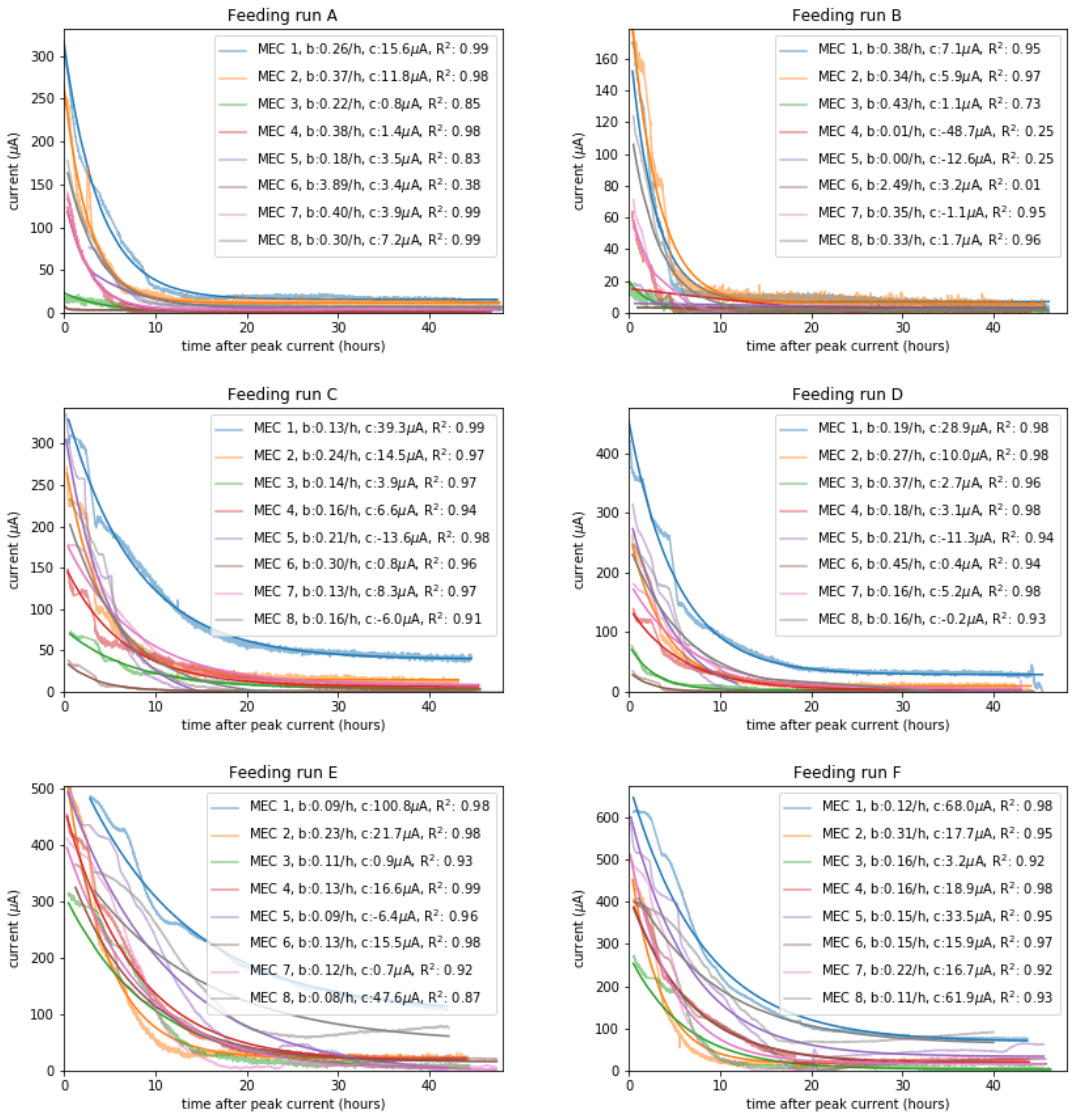

Figure 3.6: Smoothed current dose-responses following feeding for all 6 runs and fit to exponential decay curves

In the present configuration, acetate takes a significant amount of time to diffuse through the bulk liquid towards the biofilm, as per Fick's Law. As the substrate spends more time in the bulk liquid, more substrate is likely consumed by microbial species that are not in electrical contact with the anode. This likely limits biofilm development, and lower coulombic efficiencies would be observed. Diffusion may be an inherent issue in MEC as biofilms require a support surface and electrochemical cells require two electrodes to be adjacent and in close proximity to one another to reduce to ionic resistances (Rozendal et al., 2008). Porous, 3D anodes would reduce the diffusion time and increase surface area and access to substrate. Use of thin, porous anodes could ensure that ionic resistance is not heavily reduced. Pores would have to be large enough to prevent

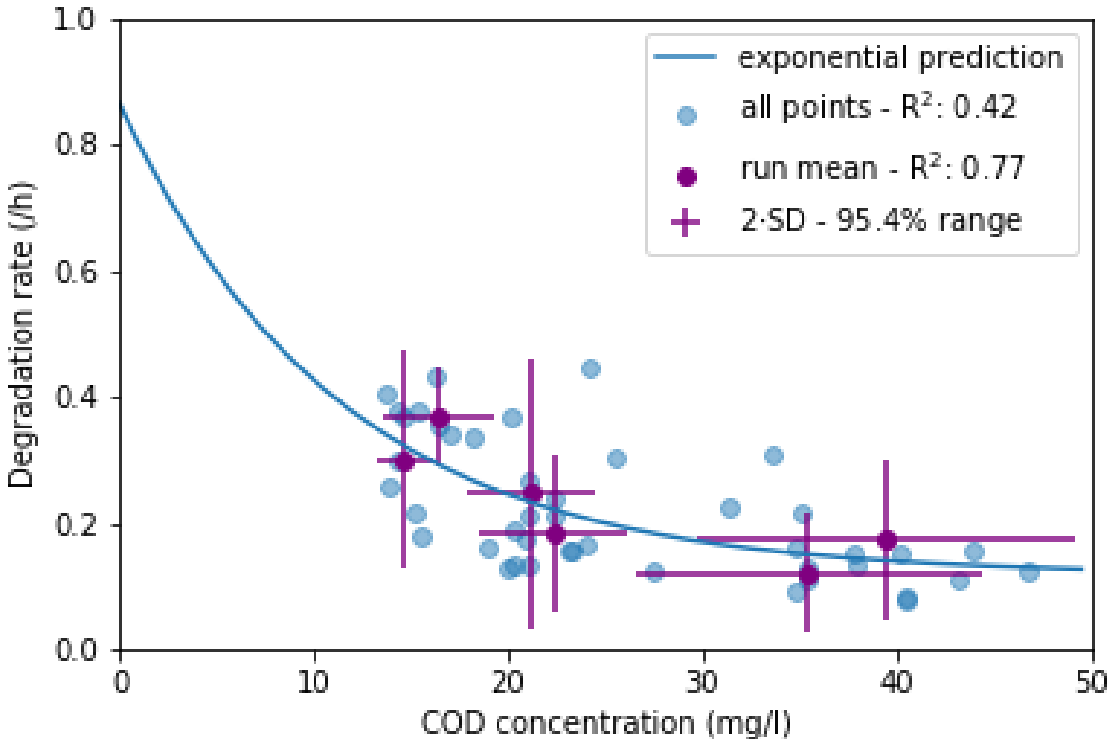

Figure 3.7: Substrate degradation rate against COD concentration

clogging (Aelterman et al., 2008) and small enough to support sufficient biofilm and mass transfer. Alternatively, increasing convection through rotation of the anodes or stirring of the liquid (Liao et al., 2015, Wang et al., 2015) has also been shown to increase access to substrate. However, this requires the input of electrical energy in a system that generates modest amounts. Charged particles could theoretically be attracted to electrodes with polarised electrodes. However, the impact of magnetic fields on particle velocity in a typical electrolysis cell, which had higher current densities, has shown only modest improvements (König et al., 2011). Differences in set potential in this experiment showed statistically no difference in current degradation rates (Section 3.3.6), though other studies have shown decreases in cycle time (Nam et al., 2011). Regardless, pilot reactor designs will likely have to take diffusion into account, unless a cost-effective approach to increasing convection can be achieved.

3.3.5 Coulombic efficiency

Coulombic efficiency is a measure of the proportion of the electrons in the substrate being converted into current. Coulombic efficiencies had an approximately linear relationship with concentration (R^2 = 29%), with coulombic efficiency means better fitting a linear approximation (R^2 = 78%,

Runs	A&B (15.4±1.3mg/l)	C&D (21.8±1.8mg/l)	E&F (37.4±4.8mg/l)	all (25.7±9.7mg/l)
Mean	0.328/h	0.216/h	0.147/h	0.221/h
SD	0.073/h	0.087/h	0.058/h	0.103/h
CV	22.3%	40.3%	39.5%	46.4%
Maximum	0.431/h	0.445/h	0.307/h	0.445/h
Minimum	0.177/h	0.131/h	0.077/h	0.077/h
Skew	-0.696	1.317	1.297	0.610
Kurtosis	-0.540	0.871	1.289	-0.862

Table 3.4: Statistical description of data-set for current degradation rates

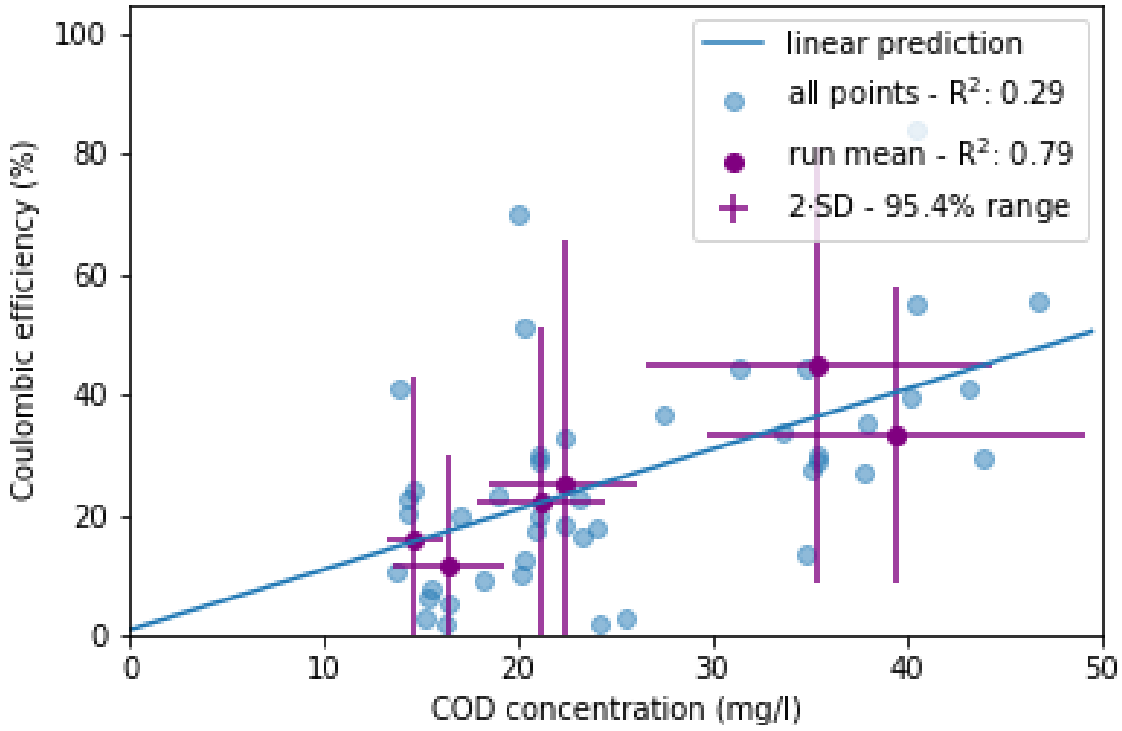

Figure 3.8: Coulombic efficiency against COD concentration

Figure 4.15). Coulombic efficiency increased at a rate of 1.00%/mg.l. The highest coulombic efficiency was for reactor 1 at 84% in run E. Other studies with acetate have also shown high coulombic efficiency up to 96% (Sleutels et al., 2011), close to a theoretical maximum of 100%. This suggests that in this reactor, the vast majority of the microbial community were both electrogenic and

situated on the surface of the anode. The mean for runs E&F were 45% and 33%, respectively. Interestingly, coulombic efficiency reduced between these two runs despite maximum current increasing. The proportion of bulk community uptake may have increased despite an increase in biofilm activity soon after feeding.

Zhao (2018) showed that at much higher acetate concentrations (500mg-COD/l) reactors inoculated with mixed communities became predominantly electrogenic. Electrogens have been observed to outcompete aerobic organisms in terms of substrate uptake rates under certain circumstances (Ren et al., 2014). Assuming no energy loss, 100% coulombic efficiency is predicted at 99mg-COD/l based on a linear extrapolation, however in reality, some electrons will always be lost. Moreover, a logistical relationship may be more likely as electrogens tend towards their carrying capacity, their growth rate will decrease and the subsequent response in coulombic efficiency may show, however this is impossible to fit accurately fit with only 3 data points and with CE means $< 50\%$.

Runs	**A&B** (15.4±1.3mg/l)	**C&D** (21.8±1.8mg/l)	**E&F** (37.4±4.8mg/l)	**all** (25.7±9.7mg/l)
Mean	14.3%	23.5%	39.1%	26.7%
SD	11.0%	16.6%	15.6%	18.0%
CV	76.6%	70.6%	39.8%	67.3%
Maximum	40.9%	70.1%	84.1%	84.1%
Minimum	2.0%	2.1%	13.7%	2.0%
Skew	1.0	1.4	1.3	1.0
Kurtosis	0.3	1.7	2.0	1.1

Table 3.5: Statistical description of data-set for coulombic efficiencies

3.3.6 Two-electrode and three-electrode systems

The secondary aim of this experiment was to determine if potentiostats could provide cost-effective boosts in substrate degradation and current generation within temperate conditions. In this study, with low temperatures, conductivities and cheap electrode materials,

Substrate degradation rate

In five out of the six feeding runs there was no statistically significant difference between acetate degradation rates in 2ES and 3ES. 3ES had a better fit to Monod kinetics (mean R^2 = 96%, all

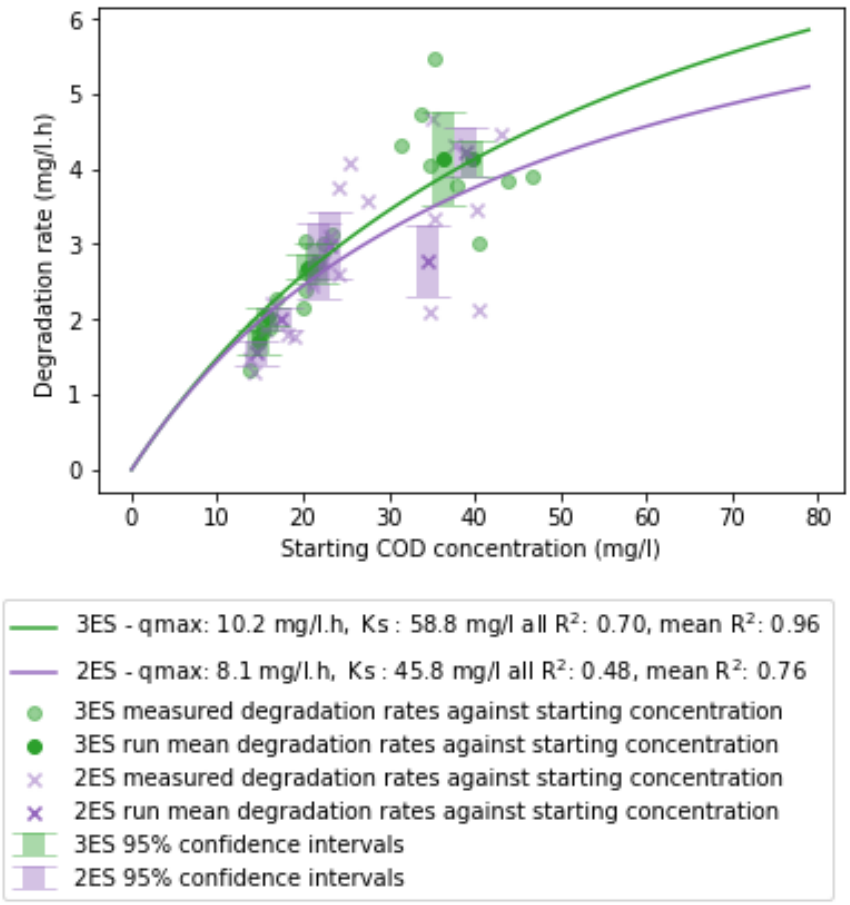

Figure 3.9: Substrate degradation rates against COD concentration in 2ES and 3ES

R^2 = 70%) and predicted a maximum substrate uptake rate of 10.2mg-COD/l/h and a Michaelis constant of 58.8mg/l (Figure 3.9). The 2ES predicted a lower uptake rate of 8.1mg-COD/l/h and a Michaelis constant of 45.8mg/l, however the fit to Monod kinetics was poorer (mean R^2 = 76%, all R^2 = 48%) and was likely caused by run E, which was statistically significantly lower than 3ES. Furthermore the two lowest degradation rates in run E 2ES also had the lowest fit to the original data (R^2 < 90%). This was either due to erroneous measurements, or substrate degradation rates were had not yet increased due to poorer biomass growth. Had these points been discarded then 2ES would have had a maximum degradation rates of around 10mg-COD/l/h. It therefore seems likely that setting the potential (3ES) and setting the voltage (2ES) ultimately has no effect on the upper limits of acetate degradation rates in MEC under the given conditions. This is significant as the majority of the financial benefits of MEC is from reduced aeration costs in treating organic matter (Aiken et al., 2019), and potentiostats are expensive, particularly when currents are high (personal communication, Whistonbrook, UK).

Current production

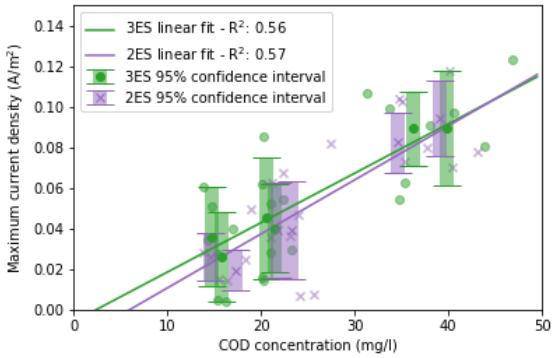

(a) Maximum surface current densities

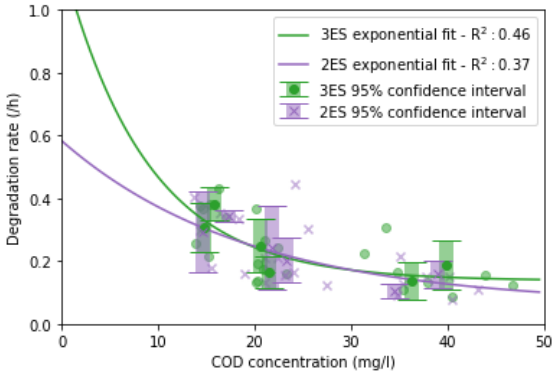

(b) Current degradation rates

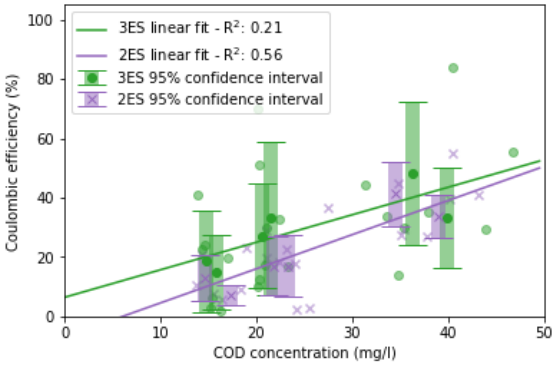

(c) Coulombic efficiencies

Figure 3.10: Current densities, current degradation rates and coulombic efficiencies for 2ES and 3ES

Higher current densities and coulombic efficiencies were observed when anode potentials were set to +300mV (vs.H^+/H^2) more so at lower concentrations. However, means were not significantly statistically different for current density, coulombic efficiency or current degradation rate (Figure 3.10a). Nevertheless, x-intercepts were different between 3ES and 2ES for current density but more so for coulombic efficiency. Maximum current density intercepted the x-axis at 6.0mg-COD/l and 2.4mg-COD/l for the 2ES and 3ES, respectively. Whilst coulombic efficiency intercepted the x-axis at 6.1mg-COD/l and -6.9mg-COD/l for the 2ES and 3ES, respectively. In 2ES both x-intercepts were remarkable similar (6.0mg/l vs. 6.1mg/l), whilst greater variation was seen in 3ES (2.4mg/l vs. -6.9mg/l).

The 3ES typically had a higher charge passing through the circuit across the entire feeding period. Anode potentials were much lower in 2ES as compared to 3ES, which had a consistent potential of +300mV. The higher anode potential may have acted as a stronger attractor for electrons (Logan et al., 2006) in some reactors, increasing efficiency and thus increasing means and SD. This

did not occur in all systems and optimum potential may be community dependent (Kumar et al., 2017). Alternatively, some 3ES reactors may have selected for a higher proportion of electrogenic species and thus increased coulombic efficiency. Moreover, the 3ES coulombic efficiency had a weak linear fit (R^2 = 21%) as opposed to 2ES (R^2 = 56%) and thus extrapolations are somewhat inaccurate.

Concentrations of 6mg-COD/l may represent the minimum concentration at which electrogenic biofilms can form in mixed cultures under 2ES conditions. Substrate may have been lost to acetate oxidisers. If the chamber been saturated with oxygen due to leaks (11.2mg-O_2/l) then around 54% of this loss could be accounted for by acetate oxidation (Equation 3.11). Reactors operated with 3ES may circumnavigate this problem by selecting against acetate oxidisers as the x-intercept for for 3ES reactors was close to zero but correlations with concentration were weak (R^2=0.21). Moreover, less diversity was observed in 3ES systems when concentrations were high (Figure 3.13). This may explain why coulombic efficiencies were low (Figure 3.10c). And, why some reactors failed to start in both the lab and in prior pilot reactors (Cotterill et al., 2017) where acetate concentrations are low (Henze and Comeau, 2008). Alternatively, mass transport to the anode was limited by diffusion. If substrate concentrations are low then most substrate may be consumed by organisms presiding in the bulk liquid before the substrate reaches the anode and a biofilm can form and remain stable.

$$C_2H_2O_2 + 2O_2 + H^+ -> 2CO_2 + 2H_2O + 8e^- \tag{3.11}$$

Voltages and potentials

Acetate is oxidised at -280mV (vs.H^+/H^2) whilst the reduction of protons to Hydrogen occurs at -420mV (vs.H^+/H^2) (Rabaey and Verstraete, 2005). Therefore, MEC therefore require atleast an additional 140mV plus voltage losses from the ohmic and electrical resistances and from the electrical double layer (Sawyer et al., 1995). Cell voltage was held at a constant 0.6V in 2ES, and anode potential decreased to 0.22V, typical of MEC anode potentials (Lim et al., 2018). This suggests that only 60mV was lost between the biofilm and the anode. After stabilising, mean measured maximum voltage for 3ES in runs A&B was approximately 1.1V, and increased linearly with respect to current density up to 1.4V (R2 = 95%), much higher than in 2ES (Figure 3.11). Despite the significantly higher cell voltages, current density was only marginally higher. Power requirements were much higher in 3ES (Figure 3.12) to sustain the higher anode potential (+300mV) above acetate oxidation (-280mV). As a result, resistances between the two systems were much greater, possibly due to increased electrical insulation from ions close to the surface of the electrodes.

The minimum measured cathode potential decreased linearly to -1.1V in both 3ES and 2ES. Cathode potential at the electrode was calculated to be lower than the pH-potential boundary at which

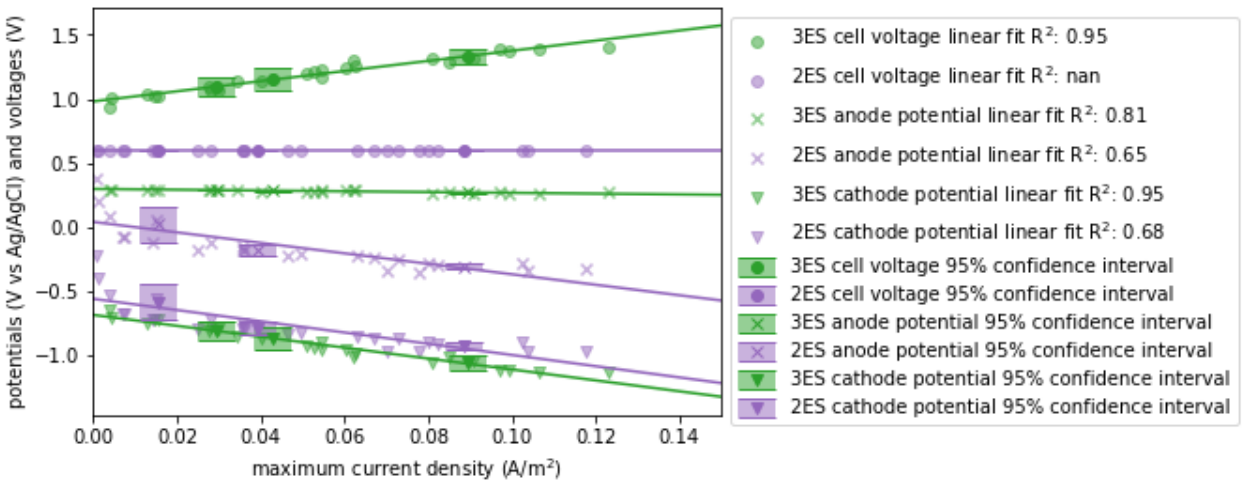

Figure 3.11: Cell voltages and anode potentials in 2ES and 3ES versus current density

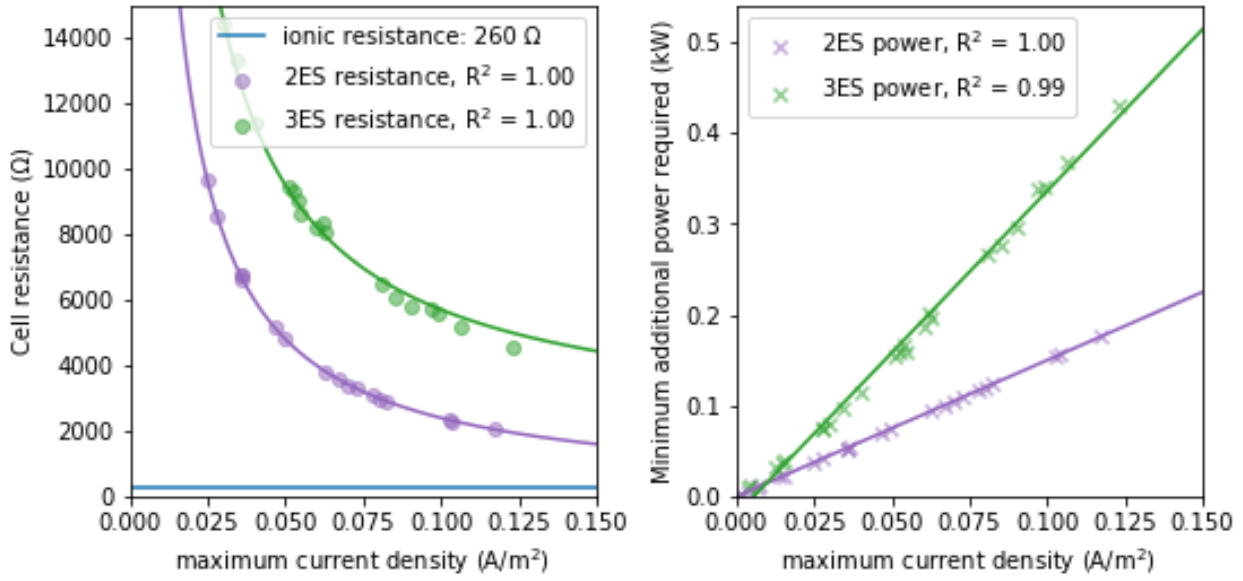

Figure 3.12: Power and resistances in 2ES and 3ES versus current density

iron (the most electrochemically unstable element in SS316L) is electrochemically stable when current densities were >0.01A/m2 (Lothongkum et al., 2006). Due to the enforced potential difference between electrodes, the cathode must be more negatively charged than the anode. Compared to MFC, this has a protective effect (Li et al., 2017). Hydrogen reduction occurs at -420mV (vs.H^+/H^2) (Rabaey and Verstraete, 2005), which suggests that Hydrogen should have been produced. However, insufficient gas was collected for analysis and solution potentials close to the cathode could not be accurately determined due to the affects of low ion concentration. Previously, potentials have been corrected for ionic conductivity (Logan et al., 2018). However, voltage

losses in the Helmholtz layer, an electrically insulating layer composed of attracting counterions at the surface of the electrode and an opposing layer of coions, are greater than in the diffuse layer, which is composed of free-flowing ions somewhat attracted to the surface charge. This is further compounded in this studies experimental conditions as low concentrations of ions in the solution greatly affects the voltage losses close to the electrode (Sawyer et al., 1995). Hydrogen production therefore may have been limited by very high voltage losses close to the cathode, although it's also feasible that Hydrogen gas may have been lost through leakage due to its small molecular size.

Microbial analysis

Microbial analysis was conducted on samples of the bulk liquid taken throughout the experiment, as sampling the biofilm would have been destructive. Although not ideal, as biofilm sampling is necessary to determine the electrogenic active species driving the reactor, understanding the activity of the bulk community can give some insight into the selection processes in the reactors and the abundance of competition. By far the most abundant genus present in the bulk liquid was *Rhodocyclaceae*, being typically present in nutrient rich conditions (Chaudhary et al., 2018). Its correlation with increases in concentration then is no surprise. *Pseudomonas*, a known genus of electrogens (Logan et al., 2015), was present in very high abundance in the inoculated reactors, however its presence in the bulk community diminished during current production. Nevertheless, several *Pseudomonas spp.* had higher abundance at higher concentrations despite their lower abundance from inoculum. *Geobacter sp.*, another well known electrogen (Logan et al., 2015), was also found in the bulk community, however it was only ranked 20th most abundant. Electrogenic species must be in high abundance as coulombic efficiencies reached a maximum of 87% in one of the reactors. Low observance in the bulk community likely does not translate to overall low abundance as electrogenic species can create relatively high density biofilms on anode surfaces that are 10-30μm thick (Speers and Reguera, 2012).

Inoculated reactor communities were dispersed between the communities found from the inoculation source (Chester-le-Street) and the negative control, albeit in much higher quantities (Figure 3.13). This suggests that reactors began with a combination of bacteria from both domestic wastewater and from the laboratory. As concentration increased, community profiles began to differ from their original sources. At lower concentrations, communities still retained some of their original background community, namely (*Escherichia coli spp.*), however as concentration increased *Rhodocyclus spp.* began to dominate the bulk community in all reactors. The bulk community profile will likely be different in domestic waster due to the presence of other chemical species. However, if acetate concentrations are increased, hypothetically the community profile of may rep-

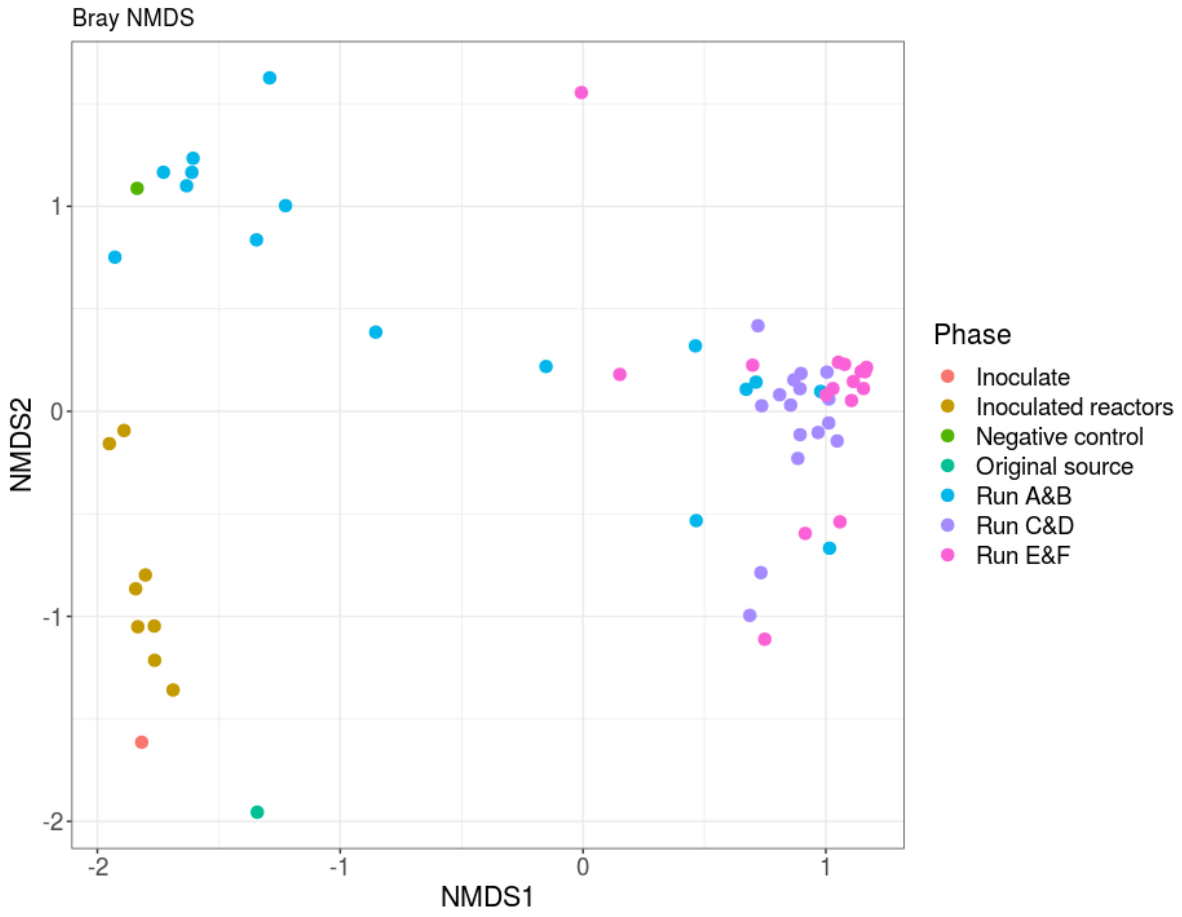

Figure 3.13: Changes in microbial community between runs

resent something similar to observed in this experiment. There was a general tendency towards similar community profiles in all reactors once acetate concentrations were >20mg-COD/l, despite not being connected. Organisms that are dominant in one environment are likely to do well in a similar environment. Furthermore, acetate re-uptake is a relatively fast process (Velasquez-orta and Yu, 2011) and thus organisms that use acetate as a food source are likely to grow faster than species that feed on longer chain molecules. However, community profiles will also be dependent upon prior community structures (Ishii et al., 2015) and the presence of other chemical species can alter microbial metabolisms (Cselovszky et al., 1992). Moreover, pH, temperature (Roger et al., 2008) and availability of substrate will vary and may impact any one species chances of survival.

Less species were observed overall in runs A&B, likely due to the lower total biomass and are thus more likely to fall below detection limits (Figure 3.14). In runs C&D the number of observed species increased in both systems, but more so in 3ES. In runs E&F this trend reversed, less species were observed in 3ES and more in 2ES. This may represent greater selection pressure in 3ES as acetate concentrations increase. Diversity was similarly varied between runs A-D between 3ES and

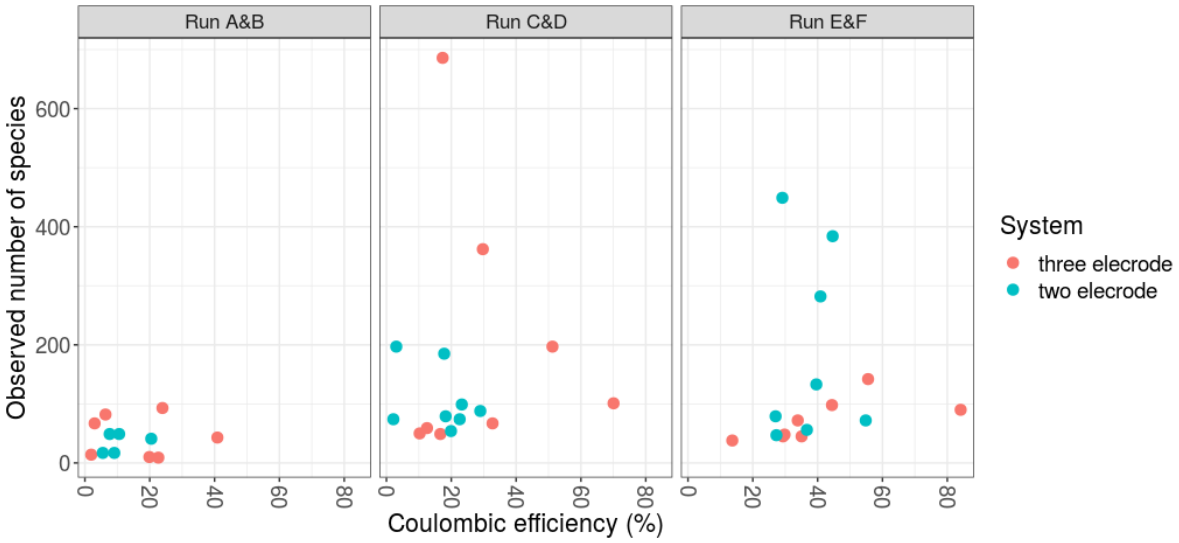

Figure 3.14: Observed species and coulombic efficiency

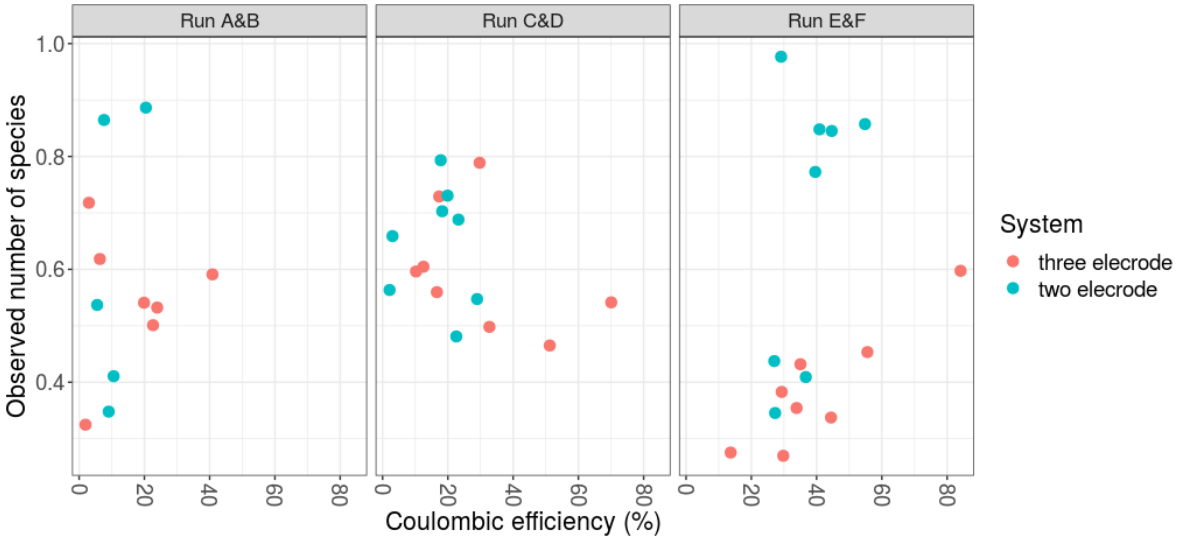

Figure 3.15: Simpson's diversity and coulombic efficiency

2ES. As richness increased in 3ES, but did not effect diversity, evenness must have decreased. In runs E&F, when acetate concentration was the highest (>30mg-COD/l) there was less diversity in 3ES than in 2ES (Figure 3.15). All 3ES reactors had a Simpson diversity measure <0.6, whilst five out of the eight 2ES reactors had Simpson diversity in the range 0.75-1.0, and three out of the eight 2ES reactors also had low diversity (0.3-0.45). Although, this effect was only pronounced when acetate concentrations were higher. Interestingly, the reactors with the highest efficiency in each of the runs had a diversity measured in the range 0.55-0.6 and there was a trend on either side of this range towards lower efficiencies. This effect was more pronounced as acetate (and likely biomass) concentrations increased. This may suggest that there is an optimum amount of competition and

cooperation within a reactor that facilitates high performance biofilms. Moreover, the reduction in competition in 3ES may explain why run E was much lower in 2ES than 3ES, as the biofilm may have had a greater number of species to compete with and thus taken longer to fully develop (as in run F). Further study using higher acetate concentrations would be required to confirm both of these effects as there was a high degree of variability in runs (A-D) when concentrations were low.

Electrode set-up summary

Increasing anode potential appeared to suppress loss of electrons to aerobic activity, however power requirements were significantly higher and thus operational costs would be higher. The commercial reality is that potentiostats are expensive. The systems used in this experiment cost approximately £825 per reactor and could only support up to 10mA. Larger commercial systems would require a better ability to carry current and therefore disperse heat, which greatly adds to the expense (personal communication, Whistonbrook, UK). As Hydrogen production does not yield great returns (Aiken et al., 2019), the minor benefits that may or may not be realised on a large scale are therefore unlikely to pay dividends in a commercial system. Some studies have found differences in microbial community at different potentials (Commault et al., 2013, Cucu et al., 2013, Nam et al., 2011), however selection may not even be ultimately favourable. In real wastewater, it would be more beneficial to have a 'mixed' community capable of digesting a plethora of substrate (Fornero et al., 2010).

3.4 Conclusion

Maximum current densities were similar to those observed in pilot reactors. As such low acetate concentrations ($<$50mg/l) may be used as a proxy for domestic wastewater. Maximum current densities increased approximately linearly with concentration, which supports increasing acetate concentrations in domestic wastewater to improve current output. Biofilms were unstable in some of the reactors when acetate concentrations were low $<$20mg-COD/l. MEC performance has been highly unstable in pilot reactors. Supposedly, increasing acetate concentrations in domestic wastewater may increase stability.

Maximum acetate degradation rates were around 10mg-COD/l at 10°C, similar to values found in literature at higher temperature, but start-up was slow and it took weeks to months for current to stabilise. Setting the anode potential in the three electrode systems showed no statistically significance in substrate degradation rates over setting the potential difference between electrodes. More importantly, setting the anode potential required more power to support the high anode potential

above the redox potential of acetate and given the capital costs of a potentiostats there is insufficient evidence for cost-effective potentiostat use in larger systems.

Current degradation rates were proposed as a measure of biofilm kinetics. Once current production had stabilised between feeding periods, current degradation rates were well described ($R^2 > 90\%$) by exponential decay in 39 out of 48 feeding runs. When acetate concentrations were >30mg-COD/l, the lowest current degradation rate mean was 0.077/h. At this rate of decay biofilm activity is expected to be reduced by 90% after 30h. Current degradation rate was however limited by diffusion in this study and will likely also be dependent upon placement of the electrodes, physical design of the MEC and the flow-regime. Further work will be required to understand these affects on biofilm kinetics.

Mean coulombic efficiencies increased with respect to concentration. One hypothesis is that this is due to the electrogenic biofilm outcompeting its neighbours for resources in proximity to the anode, but being limited by diffusion due to its planar existence on a flat anode and thus having insufficient substrate at low concentrations for biofilms to consistently develop in a mixed community. High coulombic efficiencies may therefore be achievable in mixed communities by increasing acetate concentration, reducing diffusion time through reactor design and allowing sufficient time for biofilms to stabilise.

Chapter 4. Designing a viable microbial electrolysis cell (MEC)

4.1 Introduction

Over 40,000 articles are available on ScienceDirect for the search terms: 'microbial electrolysis cell' and 'microbial fuel cell' - yet no commercially viable bio-electrochemical system (BES) has been developed for the treatment of domestic wastewater. The gap between the number of research-hours in this field and the lack of a commercially viable design in the 'real-world' is significant but not necessarily damning for the technology. Current densities are currently three to four orders of magnitude lower in BES than in conventional electrolysis (Schalenbach et al., 2016). Possible revenue from hydrogen over a twenty-year period is much lower than the current capital costs. Consequently, the majority of cost-benefit attained from implementing the technology will come from reducing aeration costs (Aiken et al., 2019). The largest factors affecting the cost-performance ratio of MEC technology are the organic removal rates (ORR) and the cost of the anode and current-collector, which currently account for 96% of recent pilot reactor costs (Aiken et al., 2019). This study investigates the combined effect of acetate concentration and anode interstices distance, the space between anode surfaces, on ORR, allowable costs to break-even and net energy recovery. All predictions are calibrated against empirical observations conducted in controlled environmental conditions analogous to those found in domestic wastewater (Chapter 3).

Electrogenic biofilm development, associated with current production, is dependent upon sufficient concentrations of readily-digestible substrate close to a colonisable anode surface. Increasing both the anode surface area and the concentration of direct food sources, such as acetate, will therefore increase electrogenic activity. Reactors fed with domestic wastewater have consistently performed worse than reactors fed with acetate (Figure 1.2). Acetate is known to be direct food source of certain electrogenic species and provides the highest current densities when used as a single food source (Speers and Reguera, 2012, Zhao, 2018). The concentration of acetate and other volatile fatty acids (VFAs) in domestic wastewater is low. Consequently, the biodegradability of soluble organics and fermentation rates of particulate matter have been shown as limiting factors in domestic wastewater fed reactors (Dhar and Lee, 2014, Velasquez-orta and Yu, 2011). Therefore, pre-treatment technologies should be used to increase the concentration of VFAs from more complex organic matter. Hydrolytic up-flow reactors have previously been used to increase acetate concentrations in domestic wastewater (Ligero et al., 2001). Moreover, dark fermentation signifi-

cantly increased acetate and other VFAs from food waste (Cardeña et al., 2018).

Increasing the quantity of anode material, although likely to improve performance, will certainly increase cost proportional to its price and quantity. A trade-off between improved performance and the extra cost incurred by increasing the anode density is therefore unavoidable. However, anode areas are under utilised at low concentrations. Biofilm concentrations on anodes surfaces are dependent upon the mass transport of substrate from the bulk liquid to the biofilm. In a stable batch reactor, where convection forces are hypothetically negligible, acetate concentration and biofilm mechanics drives this reaction. No study to date has investigated the combined effect of acetate concentration and anode surface area on both the cost-effectiveness and the performance of a MEC. Understanding what performances and material costs are required to reach cost-performance targets, coupled with a mechanistic understanding between the key determinants (acetate concentration and anode surface area) and cost-performance is the key to designing a commercially viable reactor.

To provide a design guide for MEC technology, computational methods were employed and calibrated against empirical observations to investigate the effects of a wide range of concentration and anode interstices distances. The model developed in this study combined computational fluid dynamics (CFD) with the Monod equation. I originally considered a simple linear 1D mass flow calculation, however this could not solve the partial differential equation required to accurately compute the concentration gradient. Numerical models, in general, are time and resource sensitive and allow for an understanding of the mechanics occurring within a given system. However, numerical models require calibration to an empirical reality, and may over simplify some phenomenon. As such, model outputs need to be demonstrated in future work. Regardless, models are useful tools to quickly and efficiently understand and optimise generalised physical systems. Models can be thought of as existing upon a spectrum - with complex models on one end and simpler models on the other. Complex models take into account more parameters, that are not always easy nor possible to determine (Picioreanu et al., 2007). Simpler models use less parameters and are arguably less precise. Both are useful in certain contexts (Box, 1976). The varying and changeable composition and concentration of the microbial community make more precise models somewhat redundant. This is particularly relevant to MEC, which require improvements in cost-performance on two orders of magnitude. It is therefore more useful to develop a model that can provide a range of solutions to a range of observed outcomes. By calibrating outputs against empirical observations the models robustness could be tested and ranges for macro-microbial parameters could be determined.

CFD was used to capture the effects of mass transport within a volumetric space. CFD models are well-established and can easily capture laminar flows. Moreover CFD schemes allow for the inclu-

sion of scalar terms and are therefore easy to modify for mass-transport and biological schemes. A pseudo-3D model was employed to accurately capture the mean microbial activity within laboratory based MEC reactors. This allowed for modelling of a 2D slice of the laboratory anode chamber (Chapter 3). A 1D model would not have been able to capture fluid flow around the surface of the anode, whilst a 3D simulation would exponentially increase computational complexity due to the extra dimensionality. Previously, 2D models using convection-diffusion equations have been shown to be time-efficient and good approximations of empirical observations (Gardner et al., 2017).

The Monod equation is a mathematical model for the growth of microorganisms within a specific space. The Monod equation was based upon the Michaelis–Menten equation, but differs in that it is used to model mean empirical observations of microorganisms while the latter is based on theoretical enzymatic reactions. The Monod equation fit the objectives of the study, as it allowed for the prediction of the key parameters of acetate concentration and anode interstices distance on macro-scale phenomenon: ORR, allowable material costs and net energy recovery. Xia et al. (2018) review the literature on microbial fuel cell (MFC) models and finds that amongst macro models, Monod-type models dominate. The Butler-Volmer-Monod (BVM) model (Hamelers et al., 2011) and the double-limited Monod-Nernst model (Torres et al., 2007) are both presented as robust models as they consider electrochemical impacts on performance. Both of which take into account the influence of potential on substrate uptake rate. And both of which extend logistic expression curves, such as found in the Monod equation, to electrochemical parameters. However, empirically electrochemical parameters have been found to have little effect on removal rates (Commault et al., 2013, Cucu et al., 2013, Nam et al., 2011). This is not a surprise, as MFC and MEC are typically operated with low conductivity substrates (Rozendal et al., 2008) and thus ion transport is low. As mean removal rates fit a Monod curve with a coefficient of determination of 96% and potential had no affect on the removal rates in the reactors used in calibration (Chapter 3), including these additional metrics in the calibration process would have had little impact on the cost-performance ratio and thus would add unnecessary complexity.

Empirical observations used in the calibration process used cheap materials, in controlled conditions, that although idealistic were analogous with the 'real-world'. Concentrations (10-50mg-COD/l), conductivity (0.77μS/cm), temperature (10°C) and pH (7.50) were carefully controlled and set at environmentally realistic values. Electrochemical components were constructed from elements that had good cost-performance ratios (Ribot-Llobet et al., 2013) and could be expected to be electrochemically stable in a commercial system (Christensen and Hamnet, 1994, Janicek et al., 2015). Four parameters were used in calibration: peak current density, coulombic efficiency, substrate degradation rate and current degradation rate, which has not been previously discussed in

the literature. Current degradation rate is the first order time-derivative to current and the second order time-derivative to coulombs and was essential in describing the current response to substrate and is used here to quantify biofilm kinetics over time. Costs to break-even were determined using previous financial models (Aiken et al., 2019) and took into account the energy cost and revenue from producing hydrogen, and the costs saved from reducing aeration.

4.2 Methods

The numerical methods were developed in three phases. The first phase involved the discretisation of a representation of the experimental anode chamber as well as the development of a macro CFD-biofilm model and the use of 'dummy values'. The second phase developed an evolutionary algorithm to select input variables that would produce output variables with a 'good fit' to the mean empirical observations. Accuracy of outputs were measured, initial inputs were randomly selected between reasonable numerical ranges. Pools of inputs were modified and recombined over 25 'generations'. Models whose outputs were in the bottom 50% of measured accuracies were deselected. This was repeated six times and models with current production and mean accuracies above 90% were selected as 'best fit'. The third phase involved the discretisation of a section of a hypothetical anode chamber with a section of 'flat' anode. Inputs from 'best fit' schemes were transferred and a number of scenarios were run to measure the extrapolations of performance under changing concentrations and anode interstices distances. Projections were then linked with cost-performance targets (Aiken et al., 2019) to ascertain costs. Projections were made and compared with empirical observations and literature for: substrate degradation rates, ORR, times until 90% substrate removal, current densities, coulombic efficiencies, hydrogen production rates, net energy recoveries, anode area requirements and allowable capital costs with varying acetate concentrations and anode interstices distances.

4.2.1 Phase one: CFD-biofilm model and discretisation

OpenFOAM

OpenFOAM was used as the base environment for the models. OpenFOAM is a well-developed, open-source tool for the solution of continuum mechanics, such as computational fluid dynamics (CFD). "Numerical solvers", are used to compute specific numerical equations related to real-world mechanics in a discretised scheme. The 'scalarTransport' solver was modified using C++ to create the basic numerical solver for the model. OpenFOAM uses directories to organise model inputs and outputs. Model inputs and outputs were controlled and read using Python, a higher-order programming language. Manipulating inputs data in this manner allowed for automation of scheme setups, function calls, allowed for the development of an intelligent algorithm to find the optimum

inputs and increased programming efficiency and consistency when running a large number of model permutations.

Finite volume method

Discretisation was performed using the finite volume method (FVM). The advantages of FVM are that it is simple to understand, and thus can be applied to other physical equations relatively easy. It is conservative by construction and all terms have a physical meaning, ideal for engineering challenges. The solution domain was split into a finite number of 'control volumes'. Values were applied at the centroid of the control volume. This reflected bulk phenomena such as concentrations and densities, which are required for the mass transport equations and Monod kinetics. Fluxes between control volumes were interpolated at the boundaries of cells using the "linear schemes" dictionary.

Flux

Initial fluxes (ϕ) through cells were determined using "icoFoam". IcoFoam solves the incompressible laminar Navier-Stokes equations for the velocity (U) and pressure (p) tensors (Equation 4.2) using the PISO algorithm for transient flow. Initial conditions were set so that velocity was 0 in all cells. Boundary walls were set so that the change in velocity and pressure across the boundary walls were 0, as the reactor was contained. The kinematic viscosity of the substrate was set to 1.3 mm^2/s, an estimate for (waste)water at 10°C (Metcalf & Eddy et al., 2003).

$$\nabla \cdot U = 0 \tag{4.1}$$

$$\frac{dU}{dt} + \nabla \cdot (U \oplus U) - \nabla \cdot (\nu \nabla U) = -\nabla p \tag{4.2}$$

CFD-Monod kinetics

The biofilm solver adapted the scalar transport equation, for diffusion and convection, to include Monod kinetics. The numerical solver included the PIMPLE algorithm (a transient solver), which allowed for the inclusion of time derivatives. Substrate concentration (C_s, Equation 4.3) was used in place of temperature (Figure C.3). The solver used the Navier-Stokes equations. Flux (ϕ) was imported from the outputs of 'icoFoam' and the diffusion coefficient for acetate was set at $1.2x10^{-9}$ m/s (Leaist and Lyons, 1984). Substrate removal was introduced as two independent source terms for the bulk biomass (q_{bc}) and biofilm biomass (q_{bf}).

$$\frac{dC_s}{dt} + \nabla \cdot (D_C \nabla C_s) - \nabla \cdot \phi \, Cs = -q_{bf} - q_{bc} \tag{4.3}$$

Additional fields were introduced to compute substrate removal from the the biofilm (q_{bf}, Equation 4.4), substrate removal from the bulk community (q_{bc}, Equation 4.5), biofilm biomass (C_{bf}, Equation 4.6), bulk biomass (C_{bc}, Equation 4.7) and volumetric current density (I_v, Equation 4.8). These were computed within the PIMPLE loop. Monod kinetics was used as the basis for the substrate removal fields. Substrate removal rates were found using maximum degradation rates ($q_{bc,max/bf,max}$) and Monod constant ($K_{bc/bf}$). Substrate removal terms were included into the substrate field, biomass fields and volumetric current field. Changes in biomass' mass (Equation 4.6, Equation 4.7) were determined from degradation rates (q_{bf},q_{bc}), yields ($Y_{bf/bc}$) and death rates ($kd_{bf/bc}$).

$$q_{bf} = q_{bf,max} \, C_{bf} \, \frac{C_s}{Ks_{bf} + C_s} \tag{4.4}$$

$$q_{bc} = q_{bc,max} \, C_{bc} \, \frac{C_s}{Ks_{bc} + C_s} \tag{4.5}$$

$$\frac{dC_{bf}}{dt} = Y_{bf} \, q_{bf} - kd_{bf} \, C_{bf} \tag{4.6}$$

$$\frac{dC_{bc}}{dt} = Y_{bc} \, q_{bc} - kd_{bc} \, C_{bc} \tag{4.7}$$

Volumetric current density was calculated based on an adaption of Logan (2008)'s equation by substituting in Monod removal rates from the biofilm for changes in concentration over time. The substrate removed by the biofilm was converted into volumetric current density (A/m^3) using Faraday's number (96,485C/mol-e$^-$), and the number of electrons released per gram of COD (n = $\frac{32mol_{O_2}/g}{4mol-e^-/M_{O_2}} = 8mol_{e^-}/g$). The portion of coulombic efficiency relating to electrons directly transferred to the electrode and measured in the electrochemical cell (Ce_{bf}) was assumed to be 100%. In reality this percentage will be less than 100% and will be dependent upon microbial growth, maintenance and activation losses (Logan et al., 2006). Nevertheless, total coulombic efficiencies were observed as high as 87% in the calibration data, and higher total coulombic efficiencies have been reported in the literature (96%) (Sleutels et al., 2011). An assumption of 100% is therefore a useful simplification to reduce the degrees of freedom and help avoid the equifinality of microbial parameters during calibration.

$$\frac{I}{V} = I_v = \frac{Ce_{bf}\ F}{n}\ q_{bf} \equiv \frac{F}{n}\ q_{bf} \tag{4.8}$$

Adaptive time-step

To facilitate stability and boundedness an adaptive time step was used. The abstract parameter 'qNum' was developed as an analogue to Courant's number. Courant's number typically determines stability within flow regimes. Fields for 'qC$_b f$' (Equation 4.9) and 'qC$_b c$' (Equation 4.10) were introduced as the product of the degradation rate (q$_{bf,bc}$) and time-step (δt) divided by the substrate concentration field (C$_s$). These fields provided each cell with the proportion of the total substrate that was to be removed for that particular time-step. The parameter 'qNum' was then found to be the highest cell value in either of the two fields (Equation 4.11). A 'qNum' >1 is likely to lead to unstable models and a 'qNum' < 1 allows for stability and bounds the model, as it prevents negative concentrations from being calculated within cells. Unlike Courant's number, a 'qNum' less than one did not affect the end result as Monod parameters were applied as source terms. Initial time-steps were set to 900s (15min) and the time-step was adjusted as necessary to keep 'qNum' within a set range between 0.8 and 0.96, where a 'qNum' closer to one allows for faster computation time (Equation 4.12).

$$qC_{bf} = \begin{cases} \frac{q_{bf}\delta t}{C_s}, & \text{if q}_{bf} > 0 \\ 0, & \text{otherwise} \end{cases} \tag{4.9}$$

$$qC_{bc} = \begin{cases} \frac{q_{bc}\delta t}{C_s}, & \text{if q}_{bc} > 0 \\ 0, & \text{otherwise} \end{cases} \tag{4.10}$$

$$qNum = max(qC_b f.field,\ qC_b c.field) \tag{4.11}$$

$$\delta t_{t+1} = \begin{cases} 1.1\ \delta t, & \text{if } qNum < 0.8 \\ \frac{\delta t}{max(1.2, 1.2\ qNum)}, & \text{if } qNum > 0.96 \\ \delta t, & \text{otherwise} \end{cases} \tag{4.12}$$

BlockMesh

The blockMesh was designed to reflect a horizontal 'cut-out' of the anode chamber. The block consisted of 8 'blocks', which were situated around the 'anode': represented by boundary walls.

The biofilm was contained within adjacent cells and set using 'setFieldsDict'. A pseudo-3D model was used to reduce complexity. Thickness of the biofilm was related to the resolution of the mesh. Mesh resolution was 0.5mm in both the x and y direction and 50mm in the z-direction (Figure C.1). A resolution of 0.5mm is appropriate as the finest resolution for a macro model as biofilms become limited by acidification due to poor mass transport of buffering ionic species when biofilms are situated in pores less than 0.5mm (Chong et al., 2019).

Numerical schemes

Numerical schemes were set within OpenFOAM's fvSchemes. Time schemes used Euler, a transient first-order implicitly bounded scheme. This was to ensure that the time component was included in the solver. Gradient schemes used Gauss linear. The Gauss entry specifies standard FVM discretisation, which interpolates values from cell centres to face centres. Linear specifies linear interpolation of these values. Divergence schemes used Gauss linearUpwind. The upwind component biases solutions in the direction of the velocity but ensures that answers are more bounded, the velocity field was specified as the discretised gradient. The Laplacian scheme for substrate concentration was Gauss linear corrected, this corrected component corrects for non-orthogonal meshes, a redundant measure. Interpolation schemes for velocity to flux were linear by default and all surface normal gradient terms were orthogonal.

Linear solvers

Timed tests were carried out to find the most efficient linear solver for a dummy scheme. Linear solvers do not impact the final result but do impact the speed at which results are processed. Velocity and flux fields used "smoothSolver'. Pressure fields used the preconditioned conjugate gradient and other scalar fields used the pre-conditioned bi-conjugate gradient solver. Tolerances for all fields were 10^{-12} and final relative tolerances were set to be equivalent to the first loop.

setFields

The dictionary "setFields" was used within the OpenFOAM environment to position the biofilm. Starting biofilm concentrations were added to only the cells adjacent to the anode, creating a 'cross-like' pattern. Starting bulk biomass concentration was added to all other cells, and substrate concentration was added to all cells.

4.2.2 Phase two: Calibration

Input optimisation process

An evolutionary algorithm was developed using Python to automatically optimise models inputs to produce models whose outputs had a 'good fit' against empirical observations (Table 4.1). Inputs were selected at random within reasonable ranges (Table 4.3) for 100 model iterations, creating the 'input pool'. Following the completion of all OpenFOAM schemes and analysis of outputs, each model index was ranked based upon the fitness equation (Equation 4.19). The bottom 50% of model indexes were removed from the pool and a new 'mating pool' of inputs was created. Two 'parent' models were selected at random from the 'mating pool' and a random selection of their inputs were combined to produce the inputs for the 'child' model. A total of 100 'child models' was created for the new 'pool' (generation 1). One in six models had one of their inputs 'mutated', where the value assigned to the 'child' model was increased or decreased randomly by ± 0, 1 or 2%. Substrate concentration was randomised for all values between the observed mean concentrations (Table 4.3) so as to ensure that fitness was assessed at each concentration over a large large number of generations. The new 'pool' of inputs was assigned to a new generation of OpenFOAM schemes and the process was repeated for 25 generations. Schemes within each generation were computed in parallel to reduce computation time. The entire process was run 6 times to ascertain whether the starting population would influence the ultimate outcome of input optimisation and accuracy of the 'best fits' (Figure 4.11).

Step 1	Create generational directory
Step 2	If generation = 0, create inputs at random for 100 indices (Table 4.3) If generation > 0, select best fits, breed and mutate inputs, create new pool
Step 3	Parrallelise all indices within this generation
Step 4	Copy dummy scheme and edit OpenFOAM files
Step 5	Run setFields and biofilm solver in new directory
Step 6	Run analysis of supplementary data file
Step 7	Summarise inputs and outputs from parallel processes in csv file
Step 8	Calculate fitness and accuracy, plot charts
Step 9	Repeat for 25 generations

Table 4.1: Calibration process

Calibration parameters

Model outputs were calibrated against mean empirical observations from the laboratory (Table 4.2). As no statistically significant difference was found between the two-electrode systems and the three-electrode systems, mean, maximum and minimum values were taken from the population as

a whole from each of the 6 feeding runs. Substrate degradation rates, maximum current densities and current degradation rates were taken as reported. Coulombic efficiencies and starting acetate concentrations were adjusted to better reflect the starting conditions in the model. The model started two time steps (30min) before maximum observed current. By starting the numerical solver close to the maximum current, the starting biomass concentration could be set close to its maximum. This simplified the calibration process and reduced CPU time. The additional two time steps were included to account for the oversimplifications made when discretising Monod parameters into discrete cells. Starting acetate concentration was adjusted from the mean observed starting acetate concentration for each of the runs to account for the amount of substrate removed by the measured degradation rate over the mean lag time minus the 30 minute offset (Equation 4.13). Coulombic efficiencies were recalculated from the maximum current density until the following feeding time and the adjusted starting concentration (Equation 4.14, Table 4.2).

$$C_{start} = C_{obs,mean} - q_{mean}(t_{lag} - t_{offset}) \tag{4.13}$$

$$C_e = \frac{n}{V \cdot F} \sum_{t=t_{I_{max,run}}}^{t=feed_{run+1}} \frac{I_t \Delta t}{\Delta COD_t} \tag{4.14}$$

Input ranges

Seven inputs were included in the model optimisation for both the bulk community and the biofilm in addition to a randomly chosen starting acetate concentration, for a total of 15 inputs (Table 4.3). Yields (Y_{bf},Y_{bc}) were assessed between 1% and 100%. Growth rates (μ_{bf},μ_{bc}), were assessed between 0.002/h and 0.06/h (Marozava et al., 2014*b*, Velasquez-orta and Yu, 2011). Maximum removal rates ($q_{bf,max}$,$q_{bc,max}$) were calculated as the growth rates divided by the yields. Monod constants for the bulk community Ks_{bc} and the biofilm Ks_{bf} were set between $10 - 1000 g/m^3$. Death rates (kd_{bf},kd_{bc}) were considered to be a proportion of the growth rates (10-100%). As the observations used in calibration occurred once bio-electrical production had plateaued, death rates were thought to be similar to growth rates. Food to mass ratios (F/M_{bf},F/M_{bc}) were considered between 1 and 0.001 and subsequent starting biomass concentrations ($C_{bf,t=0}$,$C_{bc,t=0}$) were found by dividing the starting substrate (C_s) concentration by the relevant food to mass ratio. Total number of possible permutations was 2.51 x 10^{24}.

Feeding run		**A**	**B**	**C**	**D**	**E**	**F**
Substrate degradation rate	max	2.26	1.89	4.08	3.76	5.47	4.72
(mg/l/h)	mean	2.02	1.64	2.86	2.73	3.47	4.18
	min	1.79	1.31	2.16	1.78	2.11	3.47
Observed mean concentration (mg/l)	mean	16.5	14.7	22.4	21.2	35.4	39.4
Time until maximum current (h)	mean	1.1	1.1	1.3	1.3	2.9	1.6
Adjusted concentration (mg/l)	mean	16.4	14.7	22.4	21.2	35.4	39.4
Maximum current density	max	0.04	0.06	0.067	0.085	0.107	0.123
(A/m^2)	mean	0.023	0.032	0.04	0.042	0.086	0.092
	min	0.004	0.004	0.008	0.007	0.063	0.055
Current degradation rate	max	0.43	0.4	0.3	0.45	0.23	0.31
(mg/l/h)	mean	0.37	0.3	0.18	0.25	0.12	0.17
	min	0.33	0.18	0.13	0.16	0.08	0.11
Adjusted coulombic efficiency	max	14.9	39.1	59.8	53.2	62.1	51.7
(%)	mean	7.2	14.6	18.2	16.0	32.6	26.1
	min	1.4	2.4	1.5	0.9	16.7	11.7

Table 4.2: Empirical observations used for calibration and input optimisation

Model analysis

The supplementary data file that was exported from the OpenFOAM solver was recorded in each of the relevant directories. The csv file included the CPU time elapsed, the model time step, the time increment, volume, the sum of substrate concentrations, the sum of the biofilm biomass, the sum of the bulk biomass, the sum of all biomass and the sum of the current. Analysis of this file allowed for the calculation and reporting of the substrate degradation rate (linear approximation), the coulombic efficiency across time, the current density across time, the current degradation rate (exponential approximation), biomass growth, the consistency of the model and the CPU time elapsed (Figure C.2).

Substrate degradation rates ($q_{mean,t}$, Equation 4.15) were found from a linear fit using SciPy to the output data over the first 6 hour period, similar to that conducted in the lab. Maximum current densities ($I_{d,max}$, Equation 4.16) were taken as the highest current from the 3rd time-step onwards ($I_{t_{2+}}$), divided by the area of the anode (A). Current degradation rates were quantified by the exponent

Input	Symbol	Maximum value	Minimum value	Increment	Number of permutations
Yields (%)	Y_{bf}	100	1	1	100
	Y_{bc}	100	1	1	100
Growth rates (/s)	μ_{bf}	1.6x10^{-5}	10^{-8}	10^{-8}	1600
	μ_{bc}	1.6x10^{-5}	10^{-8}	10^{-8}	1600
Specific degradation	$q_{bf,max}$	$\frac{\mu_{bf}}{Y_{bf}}$	-	-	1
rates (/s)	$q_{bc,max}$	$\frac{\mu_{bc}}{Y_{bc}}$	-	-	1
Monod constants	Ks_{bf}	1000	10	1	990
(mg/l)	Ks_{bc}	1000	10	1	990
Death rates (/s)	kd_{bf}	μ_{bf}	$0.1\mu_{bf}$	$0.1\mu_{bf}$	10
	kd_{bc}	μ_{bc}	$0.1\mu_{bc}$	$0.1\mu_{bc}$	10
Food to mass ratios	F/M_{bf}	1	0.001	0.001	1000
	F/M_{bc}	1	0.001	0.001	1000
Biomass (mg/l)	$C_{bf,t=0}$	$\frac{C_s}{F/M_{bf}}$	-	-	1
	$C_{bc,t=0}$	$\frac{C_s}{F/M_{bc}}$	-	-	1

Table 4.3: Initial input permutations

(b), of an exponential function (Equation 4.17) relating current (I) to time (t), from the maximum current density onwards. The exponential decay function was adapted for current (Equation 4.17), with the scalar being equal to the maximum current (I_{max}). Functions were fitted to the curve using SciPy and the exponent (λ) and constant (c) were outputted coulombic efficiency (Equation 4.18) computed the proportion of substrate removed by the biofilm between the second time-step and t=48 hours. Total current (I) was summed and multiplied by the change in timestep (Δt) to give total coulombs. Coulombs were converted to COD from Faraday's constant (96,485C/mol) and the moles of electrons in a gram of COD (n=8). COD converted into current was then divided by the total amount of substrate (C_s) removed over the time period (C_s). In addition to mean observations, maximum and minimum observed values were used to assess whether model outputs were within empirical ranges.

$$q_{mean,t} \approx \frac{S_{t=6h} - S_{t_2}}{t} \tag{4.15}$$

$$I_{d,max} = max(\frac{I_{t_{2+}}}{A}) \tag{4.16}$$

$$I = I_{max} e^{-\lambda.t} + c \tag{4.17}$$

$$C_{e,tot} = \frac{n}{V \cdot F} \sum_{t=t_2}^{t=48h} \frac{I_t \Delta t}{\Delta C_{s,t}} \tag{4.18}$$

Fitness

The fitness function (Equation 4.19) was created to select models whose outputs were most similar to the substrate degradation rates, maximum current densities, current degradation rates and coulombic efficiencies observed at the three concentrations from the experimental set-up (Table 4.2). Two additional parameters were included to ensure that the biomass was similar at the start and end of the 48 hour period for each of the microbial communities. These two parameters each related to the proportion of biofilm concentration and bulk concentration at the end of the simulation in relation to the beginning of the simulation. This gave a total of six parameters (n=6). The stability of the bulk community was also computed but not included in the fitness function. The ratios of the output to the target were used as the basis for the fitness function. Values greater than one were inverted to give accuracies (Equation 4.19) and divided by the maximum 'accuracy' for that generation. This ensured that the algorithm would select for models that fit all six parameters equally and prevented overfitting. The summed ratios were then divided by the total number of ratios to standardise the fitness function.

$$f_{fit} = \frac{\sum^{n=6}(\frac{x}{max(x)})}{n},\ x = \begin{cases} \frac{output}{target}, & \text{if } \frac{output}{target} < 1 \\ \frac{target}{output}, & \text{if } \frac{output}{target} > 1 \end{cases} \tag{4.19}$$

After calculating base fitness, 'fitnesses' were ranked in ascending order in groups of the three concentrations, with a high rank representing a better fit. The ascending rank was then divided by the total number of iterations (100) and added to the original fitness equation (Equation 4.20). This ensured that model pools would tend towards solutions that would be accurate for each of the feeding runs, whilst maintaining computational efficiency. Additionally, mean accuracy was computed for the mean of the four empirical observations: substrate degradation rates, maximum current densities, current degradation rates and coulombic efficiencies (n=4) (Equation 4.21).

$$f_{fit,Cs} = f_{fit} + \frac{rank(f_{fit}, C_s)}{\sum i = 100} \tag{4.20}$$

$$f_{accuracy} = \frac{\sum^{n=4} x}{n} \tag{4.21}$$

4.2.3 Phase three: Extrapolation

Discretised scheme

A new discretised scheme was created, which represented a section of a hypothetical anode chamber extending from the surface of a flat anode to a second flat anode (Figure C.5). The biofilm was situated in one layer of cells on each side of the scheme, whilst the bulk community was present in all other cells. Cell thickness was the same as the previous scheme at 0.5mm. Inputs were transferred from the selected 'best fit' indexes and outputs were compared to the previous discretised scheme. Mesh independence tests were conducted to ascertain errors in the discretisation of the scheme and to assess convergence on the final extrapolation results. Three cell thicknesses were considered: the original 0.5mm, as well as two finer resolutions of 0.25mm and 0.125mm. Biofilm thickness was adjusted to be one cell thick and the corresponding biofilm concentrations were adjusted to keep biofilm mass equivalent across comparisons. Filters were used to extrapolate a range of calibration model outputs based on their accuracies. All filters only took into account model permutations that were within calibration ranges. The filters first chose fitness scores (>95%) and mean accuracies (>95%), however extrapolation predictions were highly variable. Further specification was used to filter models who had very similar end and starting concentrations >90%, with reasonably high accuracies for each of the observed parameters (>80%). A further filter was used to remove models whose selected inputs had reached the limits of the input ranges during calibration. This ensured that the results were not skewed due to the arbitrary nature of each of these limits.

Projections

Substrate concentration and the anode interstices distance were adjusted to determine the affect on model outputs. Output parameters were determined for the first timestep after 90% substrate removal. Outputs for mean substrate degradation rates (Equation 4.15), maximum current density (Equation 4.16), coulombic efficiency (Equation 4.18) and current degradation rate (Equation 4.17) were calculated as in the calibration process. ORR were calculated across time (t_{90}) and reported for a substrate removal of 90% (ΔC_s, Equation 4.22).

$$ORR = \frac{\Delta C_s}{t_{90}} \tag{4.22}$$

The specific energy required to support the MEC (E_{elec}, Equation 4.23) was calculated using the applied voltage (V_{app}, 1.0V), retention time (t_{90}), concentration of substrate (C_s) removed (90%), coulombic efficiency (Ce_{an}) at 90% removal, Faraday's constant (F) and the number of electrons released during oxidation (n=8). Energy was converted from joules to kWh. Annual costs for electricity divided the energy consumed (E_{elec}) by the retention time (t_90) in days and scaled up-to 365 days (Equation 4.24). Electricity costs assumed £0.10/kWh (Business Electricity Prices, 2016).

$$E_{elec} = V_{add} 0.9 C_s \frac{Ce_{an} F}{n} / 3.6e6 \tag{4.23}$$

$$cost = £0.10 \frac{E_{elec}}{t_{90}} 365 \tag{4.24}$$

Maximum achievable hydrogen yields and energy production were determined from intermediary 'hydrogen concentration' values (C_{H_2}). Hydrogen concentrations were found by adapting the equations for current production from organic matter (Logan, 2008) and Faraday's law of electrolysis. Coulombic efficiencies were taken as the coulombic efficiency at 90% removal Ce_{an} for each individual model, cathodic efficiency (Ce_{cat}) was assumed to be 50%. Molecular weights of 2.016g/mol and 32g/mol were used for hydrogen (M_{H_2}) and oxygen (M_{O_2}), respectively. The valency (z) of hydrogen was 2 and the number of electrons supplied from organic mater oxidation (n) was 4.

$$C_{H_2} = \frac{0.9 C_s Ce_{cat} Ce_{an} M_{H_2} n}{M_{O_2} z} \tag{4.25}$$

The specific energy (E_{H_2}, kWh/m^3, Equation 4.26) produced from hydrogen gas assumed that 1.23V (V_{hfc}) of energy was produced in a downstream air-hydrogen fuel cell with a maximum conversion efficiency (ν) of 75.7% (Haseli, 2018). Faraday's constant (F) was taken as 96,485C/mol. Valency (z) and molecular weight (M_{H_2}) were 2 and 2.016g/mol, respectively.

$$E_{H_2} = \frac{z F V_{hfc} \nu}{Ce_{cat} M_{H_2} 3.6 \cdot 10^6} C_{H_2} \tag{4.26}$$

Hydrogen yields (Y_{H_2}, L/m^3/d, Equation 4.27) describe hydrogen volume produced over time per

volume of influent. This was calculated from hydrogen concentrations (C_{H_2}), 90$ removal times (assumed to be equivalent to retention times) and hydrogen density (ρ = 0.8988g/l).

$$Y_{H_2} = \frac{C_{H_2}}{t_{90}\rho} \tag{4.27}$$

Annual hydrogen revenue (Equation 4.28) was found from the mass of hydrogen produced over 365 days. Hydrogen pricing was assumed to be £3.55/kg, a market target price in the EU for 2020 (Europa, 2008).

$$revenue = £3.55\frac{C_{H_2}}{t_{90}1000}365 \tag{4.28}$$

Net energy compared the amount of potential energy available in the hydrogen produced (E_{H_2}) and the energy required to supply the voltage (E_{elec}). The comparative net energy (E_{comp}, Equation 4.30) was found by adding the energy saved from replacing aeration (E_{AS} = 0.23kWh/m^3 Shi (2011)) to the net energy from the MEC (E_{MEC}). Annual equivalent carbon dioxide emission (CO_2e, Equation 4.31) was calculated using the comparative net energy (E_{comp}) and the CO2 emission factor for the UK (0.309kg-CO_2e/kWh, BEIS (2018)) for 365 days in a year.

$$E_{MEC} = E_{H_2} - E_{elec} \tag{4.29}$$

$$E_{comp} = E_{MEC} + E_{AS} \tag{4.30}$$

$$CO_2e = 0.309E_{comp}365 \tag{4.31}$$

Penultimately, I computed anode area requirements per unit-flowrate (A_Q) from the time until 90% removal (t_{90}, Equation 4.32), the distance between the centre of the bulk liquid and the biofilm (w_{int}/2), and the thickness of the anode (w_{an}) - equivalent to specific surface area on a 'flat' anode. The capital costs per metre squared of anode (anode area costs) were calculated as the product of the costs per unit flowrate ($Cost_Q$) and the inverse of the anode area requirements (A/Q, Equation 4.33).

$$A_Q = t_{90}/(0.5w_{int} + w_{an}) \tag{4.32}$$

$$Cost_A = \frac{Cost_Q}{A_Q} \tag{4.33}$$

Scenarios

Two main scenarios were considered: a 'no growth' scenario and a 'linear biofilm growth' scenario, designed to represent upper and lower limits on the state of the biofilm following increases in the organic loading rate (OLR). The no growth scenario used all inputs as found during the calibration process for the basis of the extrapolation of substrate concentration and interstices width. The second scenario considered a linear correlation of biofilm biomass with respect to acetate concentration.

4.3 Results and Discussion

4.3.1 Organic removal rates

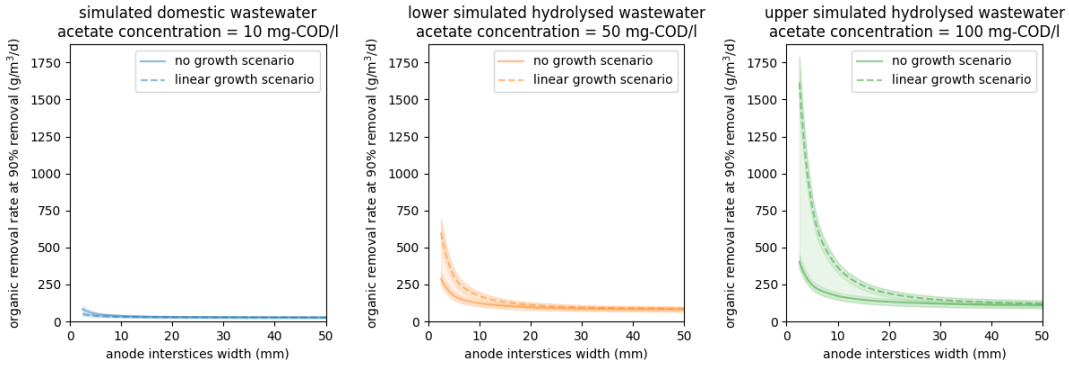

Figure 4.1: ORR at 90% substrate removal and anode chamber width under no growth and linear growth scenarios fed with three different acetate concentrations

Local ORR from biofilm activity were higher than in the bulk community due to higher biomass concentrations (Figure 4.10). ORR were thus higher when anode interstices were narrower (Figure 4.1). Differences in microbial activity were required to calibrate numerical methods against observations (Section 4.3.4). Under the 'simulated domestic wastewater' scheme (Ac = 10mg-COD/l), the highest ORR for both scenarios (102g-COD/m^3/d) was found with an anode gap of 2.5mm. In the 'real-world', domestic wastewater contains other lipids, carbohydrates and proteins (Huang et al., 2010) that contribute to ORR but are not directly oxidised by electrogenic species (Speers and Reguera, 2012) and thus higher ORR can be expected.

Pilot MEC with cassette style designs and anode chamber widths of >10mm have reported higher ORR (130-940g-COD/m^3/d, 1.1) than with comparable model chambers (>10mm, 24-45g-COD/m^3/d),

though coulombic efficiencies have been low when hydrogen cycling is ignored (13-31%). This suggests that most of the ORR in these reactors is not through direct electrogenic uptake by the biofilm. Moreover, pilot MEC employ '3 dimensional' anode structures such as carbon felt (Baeza et al., 2017, Cotterill et al., 2017, Escapa et al., 2015, Heidrich et al., 2013) and carbon brushes (Cusick et al., 2011), which increase the surface area of the anode and create smaller interstices between their surfaces. Regardless, ORR are lower than those provided by activated sludge (AS) (450-1,425g-BOD/m^3/d) (Stanbury et al., 2017) and lower still than ORR targets for financial competitiveness (800-1,400g-COD/m^3/d) (Aiken et al., 2019).

ORR increased with acetate concentration. Previously, acetate concentrations of 100mg/l have been achieved by hydrolysing domestic wastewater (Ligero et al., 2001), though unreliably. When anodes were 20-50mm apart ORR were low (89-213g-COD/m^3/d). Decreasing interstices widths to 10mm increased ORR to 354$\pm$50g-COD/m^3/d under the 'linear growth' scenario and 168$\pm$34g-COD/m^3/d under the 'no growth' scenario. Further reducing interstices to 5mm increased ORR for both the 'linear growth' and 'no growth' scenarios (740$\pm$101g-COD/m^3/d, 241$\pm$38g-COD/m^3/d). And, the highest ORR, again, occurred when interstices were 2.5mm (1530$\pm$240g-COD/m^3/d, 389$\pm$57g-COD/m^3/d) (Figure 4.1). The highest ORR predicted (2.5mm, 100mg-COD/l, 'linear growth') surpassed ORR targets (800-1,400g-COD/m^3/d) (Aiken et al., 2019) and was more than double the ORR when widths were twice as broad.

At 50mg-COD/l with an interstices width of 2.5mm, ORR were 570$\pm$112g-COD/m^3/d under the 'linear growth' scenario: 63% lower than when concentrations were 100mg-COD/l. Furthermore, interstices widths will need to be relatively consistent due to the high sensitivity that width has on ORR, a significant engineering challenge. A conservative width estimation of 5mm interstices, and an acetate concentration of 50mg-COD/l, predicts a maximum ORR of 300$\pm$57g-COD/m^3/d. Whilst this figure alone is lower than requirements for a viable reactor (Aiken et al., 2019), an increase in ORR due to the removal of other chemical species is likely and thus MEC may compete with the lower end of AS ORR under these conditions.

The difference in ORR between the 'no growth' scenario and 'linear growth' scenario shows that MEC performance is largely dependent on the relationship of the biofilm's biomass to acetate concentration. In the laboratory, Monod parameters were found when biofilms had had sufficient time to grow and stabilise (c.3 weeks) in an open, batch system. Typically, biofilms undergo growth, plateau and death phases and thus mean acetate removal is likely lower than predictions. This process may be slower in electrogenic biofilms than in AS as anaerobes, typically, produce 2 ATP molecules per glucose, whilst aerobic organisms produce 38 ATP molecules per glucose (Kolmos, 2012). High performance is therefore likely to be unstable as anaerobic organisms will need to consume more substrate to gain the same amount of energy. This is supported by observations

of pilot MEC, which could not, consistently, treat effluent to standard (Baeza et al., 2017, Cotterill, 2017, Heidrich et al., 2014). Moreover, pre-treatments are unlikely to provide stable acetate concentrations. Conservative estimates are therefore needed.

If biofilms fail to grow and biomass concentrations do not scale linearly with acetate concentrations ('no growth' scenario), MEC would still have ORR (389 ± 57g-COD/m^3/d) similar to the lower end of AS (450g-BOD/m^3/d, Stanbury et al. (2017)). Reducing interstices widths to 2.5mm and increasing acetate concentrations to more than 100mg-COD/l should therefore allow for an MEC that can compete with AS in terms of ORR when accounting for additional substrate. However, narrower interstices ($<$10mm) are likely to cause blockages with 'real' domestic wastewater (Aelterman et al., 2008). Up-flow hydrolysis reactors can retain some, but likely not all, suspended solids (SS). Further pre-treatment will be required to remove and dispose of SS, increasing costs. If the 'linear growth scenario' is achievable and further increases in ORR can be achieved from the removal of other chemical species, MEC may begin to compete with the lower-end of AS with anodes only 10mm apart but biofilms would have to scale with acetate concentrations and remain consistent. Regardless, ORR was higher when interstices widths were 2.5mm for all concentrations and any successful reactor will need to design anode chambers accordingly.

Biofilms in narrow interstices (2.5mm) will need to be as concentrated as observed in broader chambers for these projections to hold weight. This width (2.5mm) may provide a limit to MEC ORR. The model failed to compute ORR for the 'linear growth' scenario when interstices widths of $\leq$2mm. Local ORR were high and substrate mass was low, leading to negative concentration projections, unbounding the model. Empirically, Chen et al. (2012) observed MEC current production declining when interstices were $<$2.2mm and not before. Chong et al. (2019) conducted a review of 71 papers and found that the greatest reduction in planar current densities occurred when pore sizes were $<500\mu$m due to pH inhibition. This was further speculated as an important limiting factor by Logan et al. (2006). However, only 5 out of the 71 papers had anode interstices with widths $>500\mu$m and broader chambers ($>$1mm) were not considered. Access to substrate appears to be a more likely limiting factor to high performance biofilms when interstices are narrow (0.5-2.5mm) and concentrations high ($>$50mg-COD/l). However, all of these studies, including the empirical observations used for the basis of this model, were conducted on a small scale and the same effects may not apply to a large-scale MEC. Access to substrate will be a larger problem in larger anode chambers, particular when widths are narrow. Large MEC may require either a modular design or increased convection to remove waste products and supply substrate to biofilms living in deeper recesses of anode chambers.

In reality, a continuous system is likely to be used, as they are typically more economically efficient at larger scales (Gorsek and Glavic, 2000). Although, the 'break-even point' between batch-run and

continuous-run MEC is yet to be determined. In a 'continuous system' biofilm development will likely vary along the length of a 'continuous reactor' and supply of substrate and thus biofilm concentration may be, on average, higher closer to the influent due to the continuous nature of supply. The optimal length (and viable removal capacity) of the reactor under these conditions would therefore be a function of the concentration and consistency of acetate and the subsequent biofilm response.

4.3.2 Energy recovery

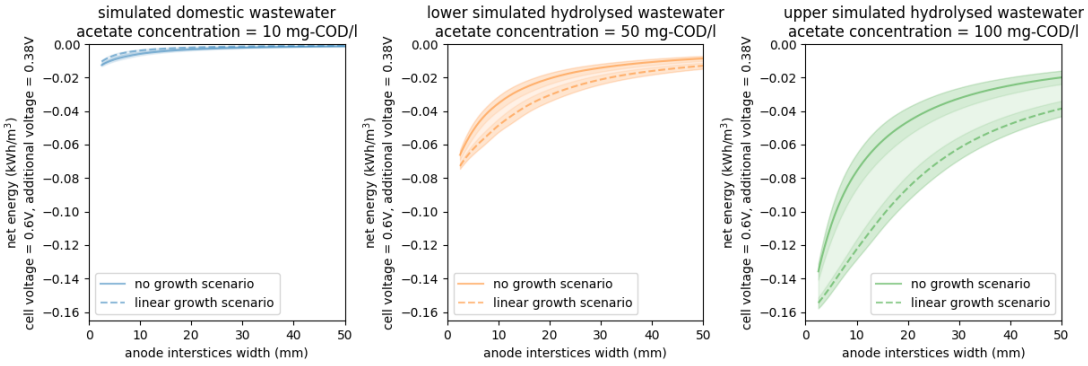

Figure 4.2: Net energy projections with an additional voltage of 1.0V

More energy was supplied to MEC through the power supply than was retrieved by the reduction of hydrogen, in all models (Figure 4.2). In theory, MEC can produce more energy than they require. Acetate is oxidised at -280mV (vs.H^+/H^2) and anodes can reach a potential of -220mV once potential losses at the electrodes surface are accounted for (Lim et al., 2018), whilst hydrogen is reduced at -420mV. The minimum additional voltage is thus 140mV, however potential losses in MEC are typically high due to the low conductivity of wastewater. Pilot studies have had applied potentials of 0.6-1.5V with higher voltages attaining higher cathodic efficiencies (Baeza et al., 2017, Cotterill et al., 2017, Cusick et al., 2011, Escapa et al., 2013, Heidrich et al., 2013). All models assumed an applied voltage of 1.0V, a cathodic efficiency of 50% and that all hydrogen was converted in a downstream air-hydrogen fuel cell producing 1.23V with a conversion efficiency of 75.7% (Haseli, 2018). Only 54% of the energy inputted was recovered. As the power supplied to the MEC was higher than that recovered, more energy was used as ORR and current increased (Figure 4.2). If all hydrogen can be recovered with a maximum downstream conversion efficiency of 75.7% and generate a voltage of 1.23V then energy recovery will reach 100% with an input voltage of 0.93V and a cathodic efficiency of 100%. More likely, an input voltage of 0.46V will be required for a cathodic efficiency of 50%, or some linear extrapolation between the two.

MEC required more energy when performance was high due to high potential losses. Nevertheless, the comparative net energy for wastewater utilities shows that switching to MEC can save energy

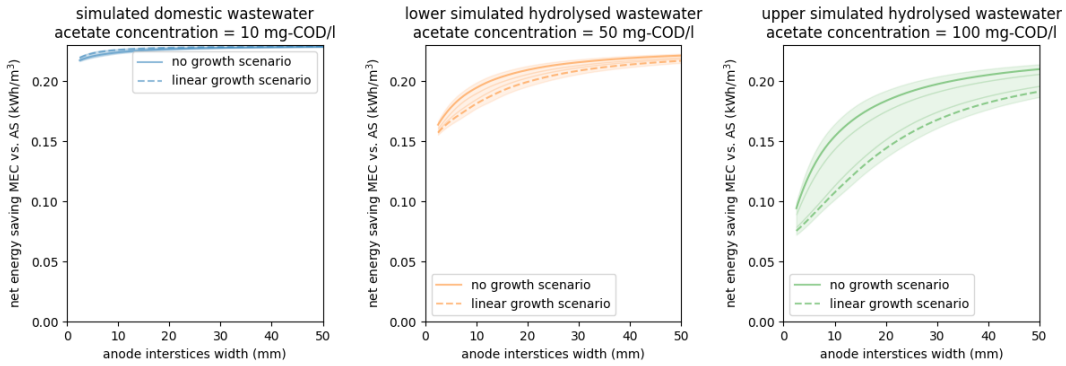

Figure 4.3: Comparative net energy projections for MEC vs. AS

even at high performance (Figure 4.3). The highest net energy losses for MEC were -0.16kWh/m^3, whilst the specific energy consumption for wastewater (0.23kWh/m^3) was marginally higher. Previously, higher applied voltages (1.1-1.5V) have been used to increase hydrogen production (Baeza et al., 2017, Cotterill et al., 2017, Heidrich et al., 2013) and thus MEC may end up using more energy than AS if potential losses are too great, performances are sufficiently high (100mg-COD/l, 2.5mm) and applied voltages exceed 1.44V. In the short-term most wastewater utilities will be able to reduced their energy expenditure by around 50% ((Shi, 2011)), however in the medium-long-term MEC are likely to reduce energy consumption further. If potential losses can be sufficiently reduced, with better electrochemical designs, then MEC could be net energy producers.

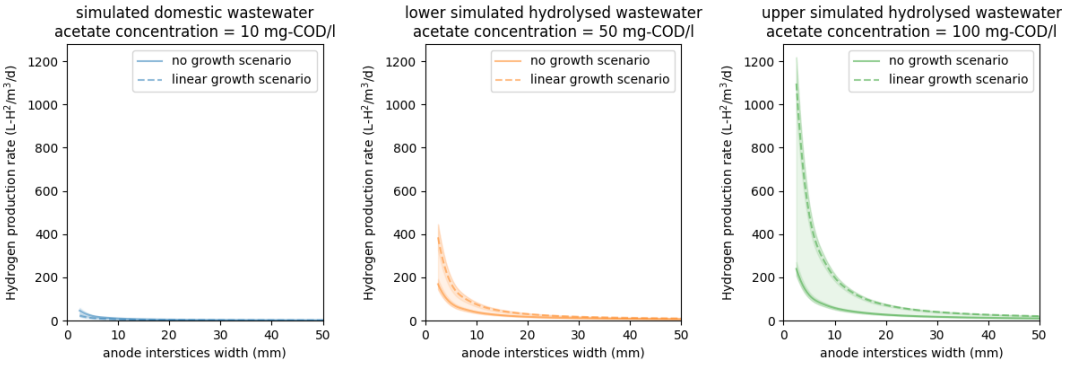

Figure 4.4: Projected hydrogen yields from MEC

Hydrogen yields were highest when concentrations were high and widths narrow. The highest hydrogen yields (207-1219L-H_2/m^3/d) were with an interstices width of 2.5mm with a width and a concentration of 100mg-COD/l. At a more achievable acetate concentration of 50mg-COD/l and width of 5mm, hydrogen yields were 69-202L-H_2/m^3/d. For the domestic wastewater scenario (10mg-COD/l) and broad widths (10mm) were 4-12L-H_2/m^3/d, marginally lower than the yields found in recent pilots (15L-H_2/m^3/d) (Heidrich et al., 2013), which did not measure acetate concentrations and had other chemical species present. Recently, very high yields (20,000L-H_2/m^3/d)

have been achieved with fermented corn starch products (Satinover et al., 2020) where OLR were very high (30g-COD/l/d). A rough comparison shows that yields were around two thirds of the OLR, similar to the yields predicted under the 'linear growth' scenario and the ORR at 2.5mm and 100mg-COD/l: 1036L/m^3/d vs. 1530g/m^3/d, giving further empirical weight to these numerical predictions.

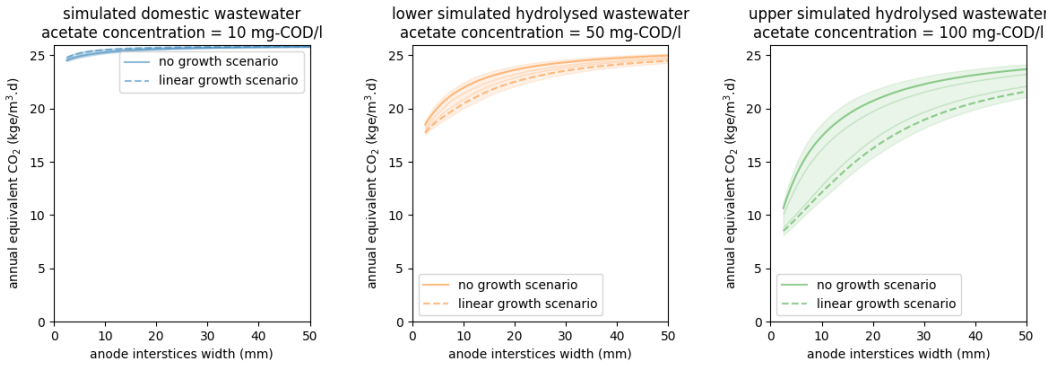

Figure 4.5: Projected CO2 equivalent emissions removed with 1.0V applied

Greenhouse gas emissions (GHG) are produced directly and indirectly by wastewater treatment. Direct emissions caused by microbial oxidation reactions are dependent upon the growth yield. Lower growth yields will generate more carbon dioxide, whilst higher growth yields will generate lower emissions. Conversely, lower yields generate less sludge, as less of the carbon in the wastewater is used to grow new cellular structures. MEC may have lower growth yields than AS, though this has yet to be determined fully (Heidrich et al., 2011). In AS, growth yields are typically dependent upon sludge age (Sherrard and Schroeder, 1973). Reduced sludge production would reduce the amount of transportation needed and could thus save indirect emissions from transportation. If further anaerobic treatments are also applied then the carbon in the waste sludge could eventually be released anyway, meaning that lower yields would be ultimately beneficial, though a thorough analysis will be required in future to determine the 'cross-over' point and to determine potential costs savings from potential sludge reductions once a functioning high-performance pilot is available to study.

Indirect emissions can be either inbuilt in the materials required for each treatment system or produced by the energy inputs. As MEC require more materials than AS, the choice of electrode materials and the production methods used in the supply chain will have a varying effect. Ignoring inbuilt emissions, annual equivalent CO_2 saved by MEC when compared with AS energy expenditure was dependent upon acetate concentration and coulombic efficiency (Figure 4.5). Due to higher energy requirements when widths were narrow at 100mg-COD/l the greatest CO_2 equivalent saving (26kge/m^3/d) was with an interstices width of 50mm. The lowest CO_2 equivalent saving at 100mg-COD/l (8kge/m^3/d) occurred with a width of 2.5mm. The UK produces 11Mm^3/d

of wastewater (Skellet, 1992). Although not all of this is currently treat by AS, treating the UK's wastewater would save 88-286kton-CO_2e annually, 0.02-0.13% of the 364.1Mt-CO_2e produced by the UK in 2018 (BEIS, 2019). Achieving higher CO_2 savings would require MEC to have lower potential losses.

Other gases may be produced by MEC such as hydrogen sulphide (Cotterill et al., 2017). Care should be taken to protect operators against harmful gases. Anodes should be sealed and has carefully extracted. Most MEC do not denitrify wastewater. However if this is included (Zheng et al., 2020) then nitrous oxide may also be produced.

4.3.3 Capital costs and design

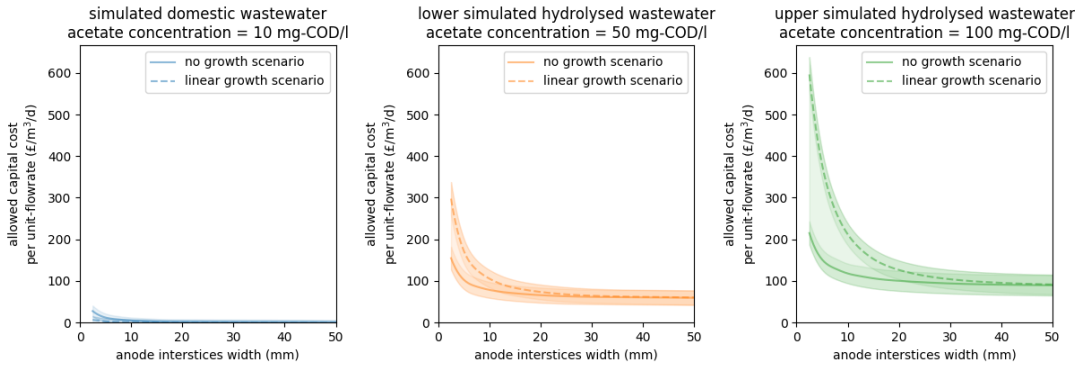

Figure 4.6: Allowable unit costs to break-even over a 20 year lifetime

The higher the ORR, the higher the allowed capital cost of a financially viable MEC (Aiken et al., 2019). Higher flowrate-costs are thus permissible under the 'linear growth' scenario when interstices are narrow and concentrations are high (Figure 4.6). For the 'simulated hydrolysed wastewater' scheme (100mg-COD/l) with an interstices width of 2.5mm, allowed capital costs were £584±54/m^3/d if MEC can operate for 20 years. Allowable costs reduce to £365±45/m^3/d and £207±40/m^3/d and £125±39/m^3/d for interstices of 5mm, 10mm and 20mm respectively. As allowable costs are much higher when interstices are narrow (2.5mm), the additional costs associated with additional screening will likely be worthwhile. Under conservative predictions (50mg-COD/l, 5mm width) allowable costs were £168±37/m^3/d, 71% less than the highest predictions. Contrarily, increasing acetate concentrations to 200mg-COD/l, increased allowable costs to £723±39/m^3/d (2.5mm). However, if biofilm biomass does not scale with concentration, then maximum allowable capital costs for 20-year lifetime are predicted to be £210±33/m^3/d (100mg-COD/l, 2.5mm). Attaining a steady, high concentration of acetate with quality controlled interstices widths and a relatively stable biofilm will be imperative to designing a financially viable reactor. Alternatively, applying MEC technology to industrial or agricultural waste streams with much higher acetate con-

centrations (Min et al., 2005), and which currently use aeration, may prove more achievable. However, the precision of the model reduced when acetate concentrations were >200mg-COD/l.

Whilst costs per unit flowrate are useful for budgeting, they are less helpful when designing a cost-effective reactor. Choosing cost-effective components requires an understanding of the allowable anode area costs to break-even. The anode is particularly important as it supports the electrogenic biofilm and is currently the most expensive component (Aiken et al., 2019) and is therefore the most important to cost correctly. Overall capital costs were standardised to the anode to give anode area costs. Whilst reducing interstices width increases allowable costs per unit flowrate, reducing the width requires additional anode material per unit volume thus the allowable costs per metre-squared of anode is dependent upon not only the cost per unit-flowrate but the width of the anode chamber and the time it takes to, confidently, achieve 90% COD removal.

Time until 90% substrate removal reduced with concentration and width (Figure 4.7). Target removals (90%) were achieved in less than 24 hours when concentrations were <100mg-COD/l and widths <50mm. Under the 'linear growth' scenario, when widths were >20mm increases in acetate concentration increased the time it took for substrate to be removed, whereas when widths <15mm, the time decreased. In the 'no growth' scenario, concentration always increased the time it took for substrate to be removed, though width still reduced removal times at all concentrations. The fastest, and thus the smallest reactor is predicted to achieve 90% removal in 1h26±13min when anodes were 2.5mm apart and concentrations were 100mg-COD/l. Under 'no growth', the same scheme had a removal time of 5h37±46min.

For a conservative estimation with 50mg-COD/l and 5mm interstices, removal times were 2h56±39min and 6h±25min for the 'linear growth' and 'no growth' scenarios, respectively. These removal times are at the lower range for typical AS HRTs (5-14h) (Stott, 2003) and thus anode chambers may fit into aeration lanes, provided anode material is sufficiently narrow, allowing a good proportion of the MEC to be retrofitted. Removal times however, will be wholly dependent on biofilm development, which has so far been unpredictable in the 'real-world' (Cotterill et al., 2017). Removal rates will likely vary as substrate varies and biofilms undergo growth and death cycles (Judd, 2013). Moreover, not all substrate will likely be converted to acetate in pre-treatment and either: retention times will

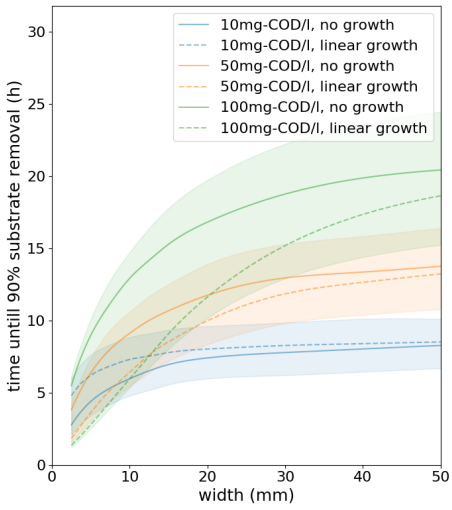

Figure 4.7: Time until 90% substrate removal

have to be extended, cheaper post-treatments will be required to 'polish' effluent to standard or waste streams will need to be split by chemical species and treated by other, yet defined, renewable technologies. Previous MEC have achieved 6-62% removal in continuous systems (Baeza et al., 2017), but has been highly variable. (Ligero et al., 2001) achieved 50% COD removal and retained 80% of soluble COD. If MECs can remove nearly all of the soluble COD then COD removal may be greater than 75%, a European standard (European Economic Community Council, 1991).

Anode surface area required increased as width decreased and decreased as removal time decreased. Densely packed reactors require more material and faster reactors require less (Figure 4.8). As narrower anode chambers have shorter removal times than broader chambers (Figure 4.7), a trade-off occurs. The 'linear growth' scenario showed that material requirements reduced when widths were narrow ($<$10mm) and concentrations high ($>$50mg/l) due to a decrease in removal time and thus reactor size, which outweighs the increase in material packing density (Figure 4.8). This relationship did not hold when widths were $>$10mm and when concentrations were low (10mg-COD/l, 'simulated domestic wastewater'). Area requirements are $47.6\pm7.0 m^2/m^3/d$ for the optimistic scenario (2.5mm, 100mg-COD/l) and $60.7\pm11 m^2/m^3/d$ for the conservative scenario (5mm, 50mg-COD/l), assuming 'linear growth'. If biofilms do not develop fully ('no growth') then area requirements are projected to be $213 m^2/m^3/d$, creating a more expensive reactor. In addition to access to substrate (Judd, 2013) and electron-accepting surfaces (Reguera and Kashefi, 2019), biofilms will be dependent upon the mass transport of metabolic products, such as protons, away from the biofilm (Logan et al., 2006), the chemical species present in the wastewater (Kadier et al., 2014, Zhao, 2018), pH, temperature (Roger et al., 2008), prior microbial communities (Ishii et al., 2015), shear forces (Fink et al., 2016) and the time with which it has had to develop. Whilst, these factors can be controlled to some extent, microbial communities are vastly complex and ultimate biofilm development cannot be definitively known, and will vary over time.

Engineers should focus on optimistic but conservative scenarios. A conservative measure, taking biofilm stability into account, could be in the region of 75-220$m^2/m^3/d$, depending on the material, the cost, prior testing and risk tolerance, however increased material requirements will reduce the allowable material unit prices proportionally. Material surface area should only count towards area requirements if the surface is accessible and capable of supporting an electroactive biofilm. Materials with very high specific surface areas, such as activated carbon cannot have the majority

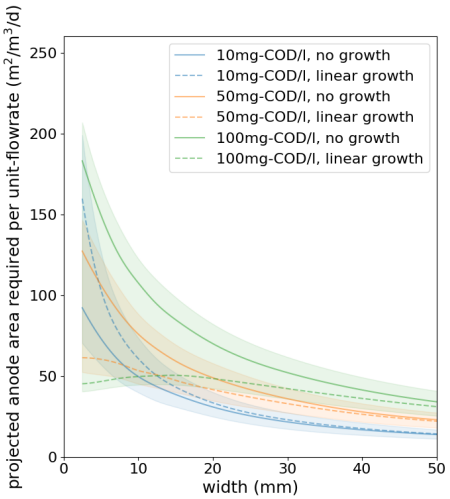

Figure 4.8: Anode surface area required per volume per hour

of their surface counted, as the high surface area is predominantly from a multitude of pores with small diameters $<50\mu$m. The most suitable materials will be flat carbon surfaces that can be packed together tightly and porous carbon materials with pores $>$2mm.

Anode area costs (the allowable capital costs standardised to the anodes surface) were dependent upon the allowable capital costs (per unit flowrate) and the anode surface area required (per unit flowrate). Initial cost predictions were based on a 20-year period (Aiken et al., 2019). For an acetate concentration of 100mg-COD/l, an interstices width of 2.5mm and a 20-year lifetime, allowable anode area costs were £24.70$\pm$6.40/m^2 and £2.26$\pm$£0.70/m^2, whilst for a conservative design (50mg-COD/l, 5mm) allowable costs reduced to £5.65$\pm$2.35/m^2 and £1.91$\pm$0.40/m^2 for the 'linear growth' and 'no growth' scenarios, respectively (Figure 4.9).These costs may be achievable if sufficiently cheap electrode materials can be found. The cheapest membranes currently cost £1/m^2 (Aiken et al., 2019), under the 'no growth' conservative scenario this leaves £0.51-£1.31/m^2 for electrode and treatment components, a significant supply chain challenge unless a membraneless system is used. However, if interstices widths are carefully controlled, acetate supply is stable and biofilms are relatively stable then allowable costs significantly increase. This cost will however have to take into account the cost of pre and post-treatments as well as any replacement costs and maintenance (Aiken et al., 2019). Bioanodes and cathodes must not foul over their operational lifetime (Aiken et al., 2019) despite being in a chemically complex environment (Stott, 2003) - biofilms will need to be relatively stable despite requiring weeks to months for biofilms to grow (Kumar et al., 2017) - treatments systems will need to consistently treat varying OLR and meet environmental standards - sludge will need to be removed from the narrow spaces in the anode compartment - and pre-treatments will need to be of sufficient quality to prevent clogging and to provide a stable supply of acetate.

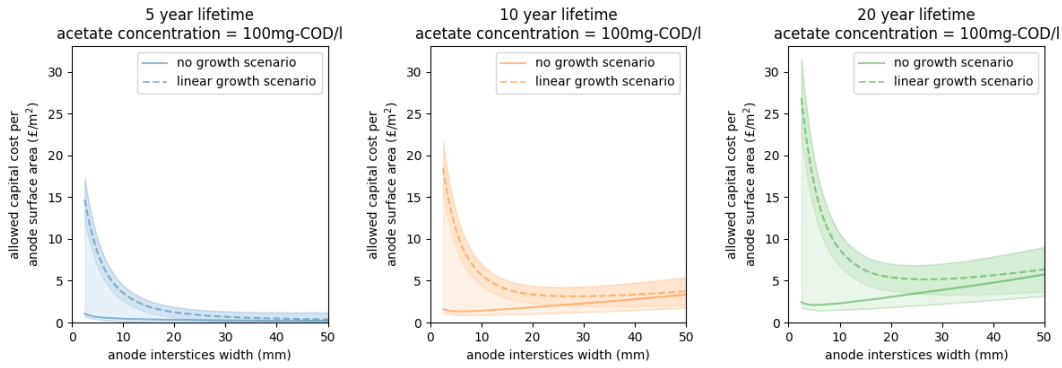

Figure 4.9: Allowable anode area costs to break-even over a 5, 10 and 20 year lifetimes.

Moreover, industry leaders will likely require a shorter time-frame to break-even. In the UK, water industry budgets typically cover a 5-year period. If MEC can be shown to break-even within this time-frame then appetite for MEC research will likely be higher. For an optimistic 'simu-

lated hydrolysed wastewater' scenario (2.5mm, 100mg-COD/l) under 'linear growth', allowable cost predictions were £13.50±3.50/m^2 and £17.00±4.40/m^2 for 5 and 10 year time-frames. For the conservative scenario (5mm, 50mg-COD/l) allowable costs reduced to £2.06±1.13/m^2 and £3.67±1.56/m^2 for a 5 and 10 years, respectively Figure 4.9. Accounting for the instability of biofilms, allowable anode area costs reduce to £0.32-1.18m^2 over a 5-10 year period for the conservative 'no growth' scenario and £0.96-1.49/m^2 with a width of 2.5mm and 100mg-COD/l, which are highly unlikely to break-even. Ensuring biofilms grow and remain relatively stable is therefore of the upmost importance for commercial viability. Contrarily, increasing acetate concentration to 200mg-COD/l (2.5mm width) showed that allowable costs can significantly increase to £21.80±3.50m^2. However, as costs will be determined prior to performance, reactors should be designed as cheaply as possible, whilst providing the highest quality control on anode interstices widths and pre-treatment.

I propose that the best chance of success is to strive to design an MEC with interstices widths of 2.5mm and material costs of £5/m^2 and should be applied to a waste-stream that when hydrolysed can produce a sufficiently consistent supply of acetate (>100mg-COD/l). This lower cost would leave some financial tolerance for additional material requirements due to biofilm variability, maintenance, operation and constructing pre and post-treatment systems. However, this cost will depend upon risk tolerance and higher or lower costs may be necessary depending upon financial leniency, the conventional system with which the MEC is competing with and the ultimate mean performance. Removal rates will need to be demonstrated empirically, with 'real' wastewater, over a long time period before implementing on an industrial scale. The longest studies to date have been around one year (Heidrich et al., 2013). Longer studies will require a significant time commitment. Initial demonstration of high removal rates over a shorter timeframe within a pilot system may provide the impetus to invest the necessary time and resources to develop a commercial system.

4.3.4 Input parameters

MEC performance is typically variables. Ranges were found during calibration for each of the Monod parameters. This provided robust predictions for ORR, allowable costs and net energy production. Specific growth rates of electrogens have been observed as high as 0.06/h (Marozava et al., 2014*a*), and as low as 0.002/h (Marozava et al., 2014*a*, Velasquez-orta and Yu, 2011). The algorithm found mean specific growth rates for the biofilm of 0.0295±0.0061/h, around half of the maximum observed. Bulk community specific growth rates were marginally lower at 0.0221±0.0159 but had much higher variability and were thus within one standard deviation of the biofilm's mean. Death rates were also marginally higher in the biofilm (0.0175±0.0065/h) than in the bulk com-

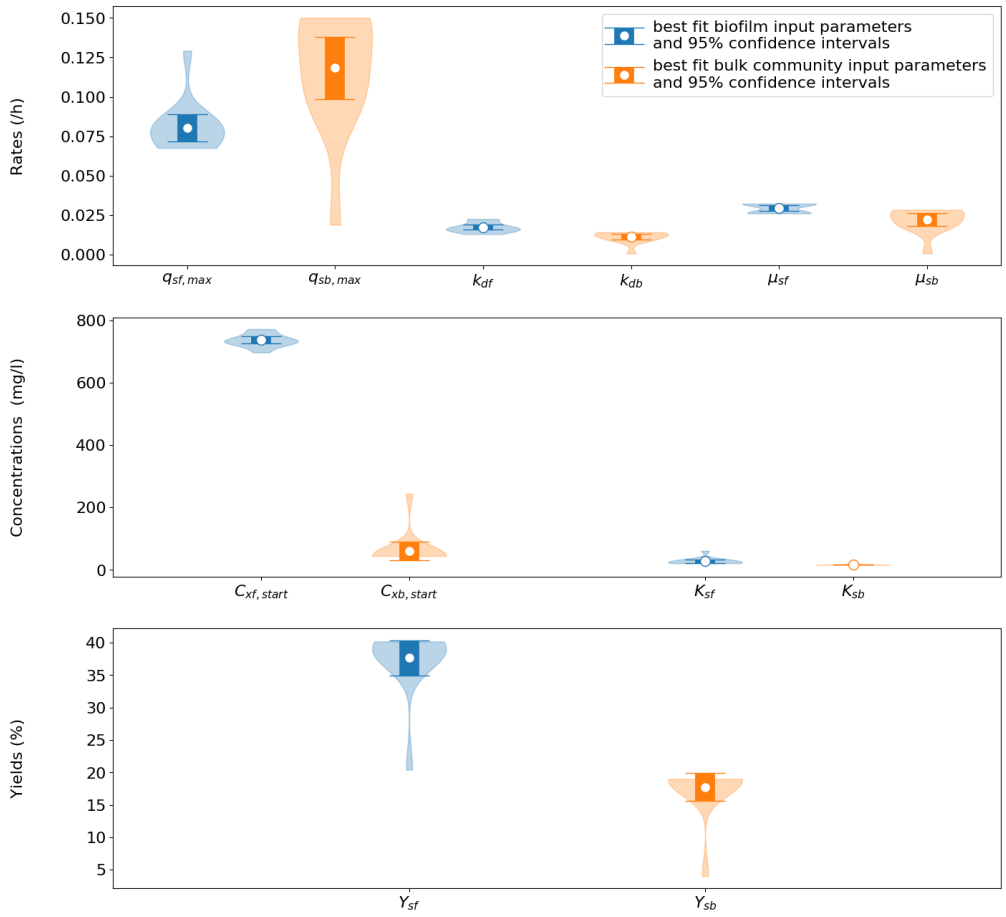

Figure 4.10: Violin plot of input ranges for models with good fit to all observation means

munity (0.0114±0.0074/h). Accurate model permutations were negatively skewed for both fields (Figure 4.10). Skew is graphically described by the violin plot (Figure 4.10) where the width of the plot is representative of the frequency density of parameter values found by the algorithm. A negative skew shows that numerically more solutions were viable when death rates were lower.

Yields were higher in the biomass (37.6%±10.2) than in the bulk community (17.7%±8.1). Higher variability in bulk community parameters suggests that the bulk community field may have played a smaller roll in determining model outputs. As such specific degradation rates were lower in the biofilm (0.0803±0.0321/h) than in the bulk community (0.1184±0.0740), despite the fact that overall substrate degradation rates were higher in the biofilm. Higher substrate degradation rates were due to the biomass having order of magnitude higher in the biofilm (0.539±0.405mg/l vs. 0.060±0.108mg/l). Biofilm concentrations were a function of the cells width. As the cell width (0.5mm) was somewhat arbitrary, biomass concentrations can be universally represented in terms of area (0.270mg/m^2).

Monod constants were higher, but more uncertain, in the biofilm (100±78mg/l vs. 60±11mg/l).

If Monod constants are higher in the biofilm then it should take longer for the biofilm to reach maximum substrate uptake rates and the species in the bulk community would have a competitive advantage in terms of uptake rates. This may explain why coulombic efficiencies are lower when concentrations are low, although the uncertainty in biofilm parameters is too high to assert this definitively. Nevertheless, the biofilm has a clear advantage in terms of substrate uptake rate once a biofilm had fully developed due to much higher biomass concentrations. This agrees with Zhao (2018)'s observation of >90% counts of *Geobacter spp.* when acetate concentrations were high and Ren et al. (2014)'s observation that BES can outcompete AS in terms of removal rates under certain conditions. Hypothetically, higher Monod constants may be due to the limiting effects of diffusion. As the biofilm is situated on a flat anode surface it takes time for substrate to reach the surface for uptake and thus enzyme activity will be limited by this process. Regardless of the reason this further illustrates that high biomass concentrations are paramount to MEC viability. Sufficient time and stable, high substrate supply will be needed to allow biofilms to develop. If possible it would be best to enrich communities with second generation consortia Baudler et al. (2014), Mathuriya (2013). Further, increasing temperature may speed up biofilm growth, though this may have the unwanted effect of increasing methanogenic competition (Kumar et al., 2017, Patil et al., 2010).

4.3.5 Calibration accuracy

The algorithm was able to find reasonably accurate numerical representations of reality with high computational efficiency (Figure 4.11). A total of 15,000 permutations were modelled out of a possible 2.51 x 10^{24} permutations. Of these permutations, 3028 fit within calibration parameter ranges, 745 had a fitness greater than 90% and 647 of these were within input ranges. However, in each of these high accuracy models, in most models only a subsection of parameters reached a very high accuracy, at the expense of others. As such, only 13 models had accuracies >80% in each of the four calibration parameters and >90% similarity between the starting biomass concentrations and the end biomass concentrations. Mean fitness was 94.8% and mean accuracy to the means of the four parameters was 89.9%. Out of the 13 models used in extrapolation, 6 had mean accuracies >90% with the most accurate model having a mean accuracy of 93.2%.

The scheme used during the extrapolation was simpler than the scheme used for calibration as it represented a section of a hypothetical larger reactor (Figure C.5). Substrate degradation rates, maximum current density and current degradation rates were almost identical to the calibration scheme (-0.8%, -1.8% and -0.9%). Coulombic efficiency was reduced (-35.5%), presumably due to the increase in the mean distance of the total substrate after the removal of the left hand side of the compartment. The mesh independence test showed no significant difference in any of the outputs

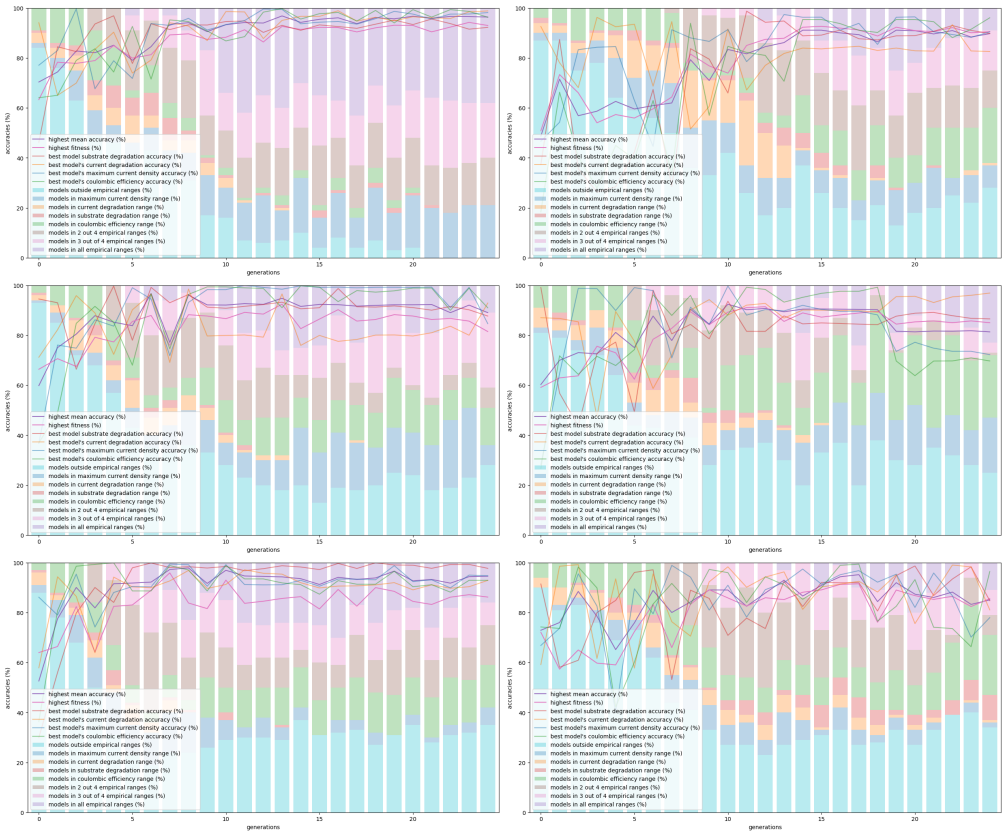

Figure 4.11: Model accuracies found during calibration process

for all three cell thicknesses (Figure C.6). The scheme was convergent due to the predominance of the Monod source terms in determining the performance in a relatively 'still' batch reactor. The ORR with a cell width of 0.5mm 100mg-COD/l was 99.8±4.5% the value of ORR for cell widths of 0.25mm and 0.125mm. In the 'no growth' scenario there was tendency for for the ORR to be lower at 0.5mm than when interstices were narrow (minimum = 92.9% at 2.5mm), whereas in the 'linear growth' scenario the ORR tended to be marginally higher at 0.5mm when interstices were narrow (maximum = 103.2% at 2.5mm). When interstices were broader (50mm) the schemes were highly convergent (99.6% 'no growth' vs. 100.2% 'linear growth').

Substrate degradation rates had a good mean accuracy (92.2±11.8%) in the final model permutations used during extrapolation, with the highest accuracy of 99.7%. When acetate concentrations were ≤100mg-COD/l and widths were broad (65mm) there was good agreement at 10-COD/l and 50mg-COD/l between the 'no growth' scenario(1.4±0.2, 4.3±1.2) and the 'linear growth' scenario (1.4±0.2, 4.6±1.2). At 100mg-COD/l the two scenarios begin the diverge with the linear growth scenario (6.6±1.6g-COD/l.h) having a higher maximum degradation rate than the 'no growth' scenario (5.4±1.6g-COD/l.h). Under the 'linear growth' scenarios there was an order of magnitude increase in the concentration of biofilm biomass from 10mg-COD/l to 100mg-COD/l, whilst the

biofilms mass in the 'no growth' scenario was static. As little difference was observed in substrate degradation rates for these scenarios at these concentrations, it is likely that the substrate degradation rate did not actively assist the algorithm in determining biofilm parameters. Substrate degradation rates, which consider the rate of change of the reactant, cannot therefore be used to determine biofilm kinetics in BES chambers with large open sections, due to the confined location of the biofilm on the anode surface and the limiting affects of mass transport. Higher acetate concentrations may have mitigated this effect.

The number of electrons released in an electrogenic reaction (current density) and the rate of change of release (current degradation rate) directly measure the rate of change of the product of the electrogenic reaction and thus hypothetically better predictors of biofilm kinetics and may explain why growth rates in the bulk community are more uncertain (Section 4.3.4). Mean accuracies of maximum current densities and current degradation rates were 92.2±11.8% and 89.0±7.8%, respectively. Maximum current densities were not predicted to be affected by the width of the anode chamber, agreeing with other empirical observations (Chen et al., 2012).

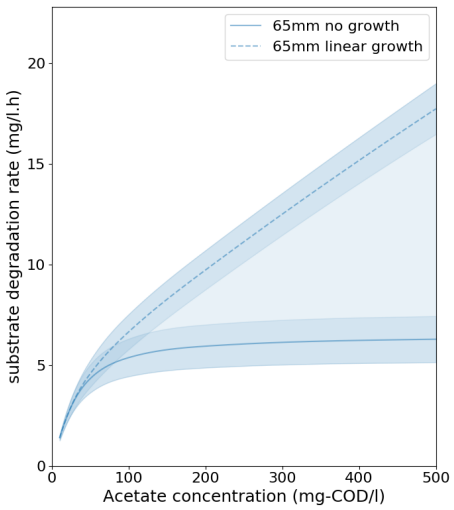

Figure 4.12: Substrate degradation rate

The 'linear growth' scenario more accurately predicted maximum current densities when concentrations were high. Under 'linear growth' maximum current density had an approximately linear relationship with acetate concentration, as seen in the laboratory (Chapter 3), whilst the 'no growth' scenario predicted this to be logistical. At 500mg-COD/l maximum current density predictions were 2.16±0.71A/m^2. Previous studies using 1,200mg-COD/l of acetate found planar current densities around 6-7A/m^2 (Chen et al., 2012, Liu et al., 2013), scaling linearly this would translate to around 2.5-3A/m^2 at 500mg-COD/l. Linear growth predictions thus had a good agreement with other empirical observations and tend towards conservatism (useful for design). This may also be a property of inoculating with a mixed community. Under 'no growth',

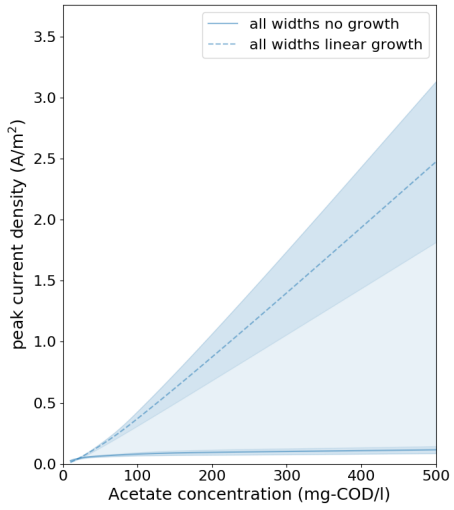

Figure 4.13: Maximum current densities

current degradation rates were unstable at ≥100mg-COD/l (Figure 4.14). This may be due to the biofilm having insufficient mass to stay competitive with the bulk community. However, as *Geobacter spp.* counts typically increase when acetate concentrations are high (Zhao, 2018) this seems unlikely, giving further weight is given to the 'linear growth' scenario which showed current degradation rates progressively increasing.

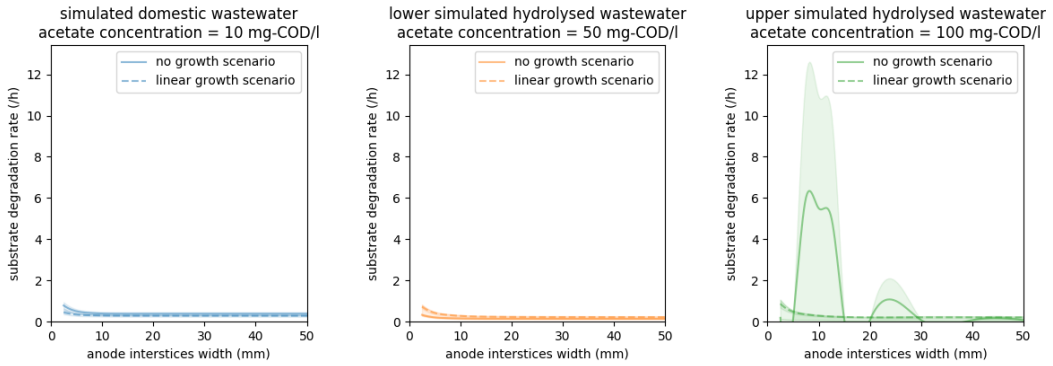

Figure 4.14: Current degradation rate

At high concentrations (500mg-COD/l) and broad widths (65mm) the 'linear growth' scenario (17.9±1.9g-COD/l.h) over predicted maximum substrate degradation rates observed in the laboratory (9.2mg-COD/l/h) and by Zhao (2018) (10mg/l/h), whilst the 'no growth' scenario (6.4±2.0g-COD/l.h) under-predicted. Presumably, a better numerical scenario may have taken into account reduction in the bulk community biomass in response to a more active biofilm. This would have lowered substrate degradation rates and increased coulombic efficiencies, without affecting maximum current densities.

However, this point may be moot. When interstices are narrow the biofilm occupies a larger proportion of the space and contributes more towards overall removal rates due to an increase in mass transport. This is confirmed by coulombic efficiency (accuracy = 88.6±10.3%), which increased when interstices were narrow in both scenarios (Figure 4.15). As the bulk community occupies a significantly reduced amount of space, projections at narrower interstices are therefore already determined primarily by the activity of the biofilm and are the most important to predict. As the biofilm's activity was primarily due to high biomass concentrations (Section 4.3.4), the greatest impediment to the predictions provided by this model are viable at

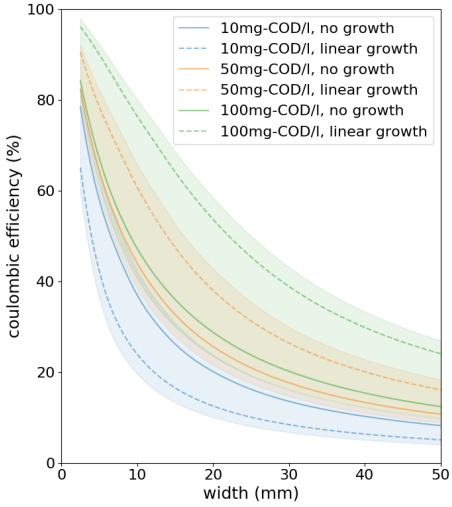

Figure 4.15: Coulombic efficiency

high concentrations and low interstices widths is whether biomass concentration will be reduced by mass transport limitations or pH inhibition. If Chen et al. (2012)'s observations are to be believed, this should not occur until interstices widths are $<$2.2mm but further empirical testing over a long period of time ($>$12 months) in 'real-world' conditions will be required to confirm.

In future modelling work a continuous chamber should be considered. Influents and effluents will need to be described and the effect of changes in velocity and reactor dimensions on MEC cost-performance should be considered. 3D models should be considered if influent ports are of different dimensions to reactor chambers. Further work could also investigate the effect of different substrates on MEC cost-performance as wastewater is composed of a multitude of biodegradable compounds and electrogens can consume both acetate, formate and hydrogen (Speers and Reguera, 2012). Acetate has previously been shown to facilitate the highest current densities (Zhao, 2018) and thus the effect of other compounds should be considered to improve model accuracy. Moreover MEC do not currently reduce the nutrient content of wastewater. Further work could consider tying in nitrogen removal, otherwise separate treatments will be required.

4.4 Conclusion

The algorithm predicted (with 93.2% agreement to mean observations) that the biofilm had higher ORR in its local vicinity than the microorganisms in the bulk community, due to higher biomass concentrations in the biofilm. As such, the highest performing models occurred when substrate concentrations were high and interstices narrow. Domestic wastewater contains contains too little acetate (10mg-COD/l), in its typical form, for MEC to be a viable alternative to AS. An achievable design using conservative estimates, which can compete with AS, would see an MEC be cost-effective when material costs are reduced to $<$£5/m^2 standardised to the anode's surface, wastewater is pre-treated to obtain a steady supply of acetate $>$100mg-COD/l and anode interstices widths are carefully controlled so that anodes are 2.5mm apart. At this level ORR may be high enough to compete with the lower end of AS. However, biofilms must be stable maintained and quality control must be of a high standard. Higher costs may be permissible if acetate concentrations are higher, biofilms remain relatively stable and quality control is of a high standard. Unfortunately, MEC will remain net energy negative so long as potential losses remain high and as performance increases, so too will energy costs. Reducing potential losses by half may allow MEC to be net energy producers, generating further revenue, reducing financial risk and significantly improving CO2 emission removal equivalents. Full-scale deployment as a treatment technology could see MEC reduce national (and the future potential of international) indirect GHG emissions on the order of 0.01-0.1%, depending on potential losses.

Chapter 5. Conclusion

5.1 Background

The total number of publications regarding microbial fuel cells (MFC) and microbial electrolysis cells (MEC) has been increasing at a rate of 12-20% per year, an above average rate, for the past 23 years (1.1) - and yet no commercially viable design has been produced. Often studies have used educated guesses when designing reactors, whilst this method benefits from empirical observation, it does not necessarily tell the observer how these bio-electrochemical systems (BES) would behave under different conditions. Furthermore, previous pilot reactors situated on wastewater treatment sites have had variable COD removal and Hydrogen production, a property that requires extended study length to correctly diagnose the solutions to problems. A predictive approach allows engineers and scientists to better understand how and where to apply the technology, and improve design, although any numerical predictions will need to be demonstrated empirically before development can occur on an industrial scale. Most empirical studies used high concentrations of acetate, not typically found in domestic wastewater. Reported maximum current densities were higher when using acetate ($<$33.3A/m^2) (Nam et al., 2011) than when using wastewater ($<$1.1A/m^2) (Hays et al., 2011) 1.2. Pilot reactors, have had similarly low current densities (0.22-0.37A/m^2)(Baeza et al., 2017, Cotterill et al., 2017, Escapa et al., 2015, Gil-Carrera et al., 2013, Heidrich et al., 2013), the larger size of the electrodes may increase ohmic losses, but the effect appears to be small 1.2 and are highly variable, which is not suitable for an industrial setting. Whilst, high current densities will be necessary for high energy retrievable, current densities are still very low in acetate reactors compared to typical electrolysis, which are 10,000A/m^2 (Schalenbach et al., 2016). Moreover, previous capital costs have been shown to be financially intolerable (Aiken et al., 2019, Escapa et al., 2012, Rozendal et al., 2008). To be cost-effective MEC are thus be required to provide additional cost benefits, predominantly by reducing energy consumption, which is the second highest cost the wastewater sector (Curtis, 2010, US EPA, 2006). To convince wastewater utility executives of the applicableness of BES technology for wastewater treatment, standards must be met rigorously and electrochemical systems must not foul.

5.2 The challenge

The three major challenges currently facing MEC development are: low energy recovery in domestic wastewater, limited organic removal rates (ORR) as compared to conventional treatments, and the use of expensive electrochemical materials. This thesis has sought to quantify: cost-performance targets for a commercially viable reactor; achievable ORR; the necessary acetate concentrations to achieve high ORR and high energy retrieval; the anode design that would be most effective in terms of ORR, energy retrieval and the allowable capital costs for a commercially viable design. Secondary findings have investigated the degradation rates of electrogenic communities and the effectiveness of potentiostats in conditions analogous to domestic wastewater. Further work will need to demonstrate the findings of this thesis in an empirical manner and ensure the stability of such systems over the long-term.

5.3 Commercial viability and other findings

Initial cost predictions

The majority of the financial incentive for implementing MEC in a wastewater treatment plant is through the reduction of energy after removing aeration. The revenue retrieved from hydrogen production is too small to cover the high capital costs due to high potential losses from low conductivity waste-streams. As aeration rates are tied to the organic loading rates, removal rates in MEC are the biggest determinant of commercial viability alongside the quantity of electrode materials. Combined, the anode and current collector accounted for 96% of the electrochemical component costs in recent MEC pilot designs (Aiken et al., 2019). Reducing the cost of the anode will therefore have a large impact on viability. Initial recommendations presupposed a 90% reduction in anode and current collector cost, and an increase in OLR from 140mg-COD/m^3/d to between 800–1,400g-COD/m^3/d: an order of magnitude higher than presently achievable. Annual membrane replacement and additional staff did not greatly effect targets, but regular replacement of the cathode was highly detrimental to MEC competitiveness. Reusing the anode significantly reduced OLR targets, but to for this to be feasible, anodes would be required to function after 20 years of operation, and the longest studies to date have been around one year (Gil-Carrera et al., 2013, Heidrich et al., 2013). Furthermore, convincing industry leaders of the financial benefits of MEC will likely require a shorter time-frame to break-even, though the current zeitgeist encouraging companies towards more sustainable and innovative practices may provide some financial leeway.

Cost-effectiveness of potentiostats

The use of potentiostats was shown to be not cost-effective. Substrate degradation rates were not

effected by the posed anode potential, as has been observed in other studies (Commault et al., 2013, Cucu et al., 2013, Nam et al., 2011). It is possible that the low conductivity reduced the benefit that high anode potentials derive by attracting negatively charged acetic acid ions. Power requirements were considerably higher when poising anode potential at +300mV. This is due to the additional voltage required to achieve hydrogen reduction at -420mV. Furthermore, the systems used in this experiment cost approximately £825 per reactor and could only support up to 10mA (personal communication, Whistonbrook, UK). Applying potentiostats to MEC at large-scale and scaling up the current carrying capacity would unneccesarily increase MEC's already high costs.

Electrogenic removal rates

Mean coulombic efficiencies were observed to increase with respect to concentration (10-50mg-COD/l). A promising hypothesis is that the electrogenic biofilm outcompetes its neighbours for resources in proximity to the anode, but is limited by diffusion due to its planar existence on a flat anode surface. This is further supported by modelling efforts. The algorithm used in model validation, showed that to achieve the observed current productions, substrate degradation rates and coulombic efficiencies, local removal rates from the electrogenic biofilm had to be higher than was found in the bulk liquid and that this was predominantly due to higher biomass concentrations. In models with Monod parameters that fit observations well, higher Monod constants were found in the biofilm, though uncertainty for this parameter was high. If true, then higher acetate concentrations will be required for biofilms to compete with the bulk community, though this may be influenced by the anode chamber size.

In other studies, Zhao (2018) found that high acetate concentrations (300mg/l) produce high proportions of electrogenic species (90%), however Sleutels et al. (2011) observed that coulombic efficiency decreased from 96% to 52% when acetate concentration increased from 60mg-COD/l to 2,100mg-COD/l over a 30 day period. One explanation could be that there is an optimum acetate concentration to achieve high coulombic efficiency, which is likely effected by the microbial community, temperature and reactor design. Alternatively, biofilms are not stable phenomena and both studies did not observe coulombic efficiency for much longer following 'steady-state': longer studies have observed variable performances (Baeza et al., 2017, Cotterill et al., 2017, Heidrich et al., 2014), which could be explained by the community undergoing a growth and death phase (Judd, 2013, Kolmos, 2012). Moreover, coulombic efficiency is predicted to increase with reduced anode interstices as mass transport time of substrate to the biofilm is reduced, though biomass concentrations in the biofilm will be dependent upon mass transport of chemical species both to and from the biofilm (Logan et al., 2006).

Cost-performance predictions

Maximum acetate degradation rates were 9.2mg-COD/l at 10°C, once current production stabilised,

similar to values found in the literature at higher temperatures. MEC are therefore suited for use in temperate climates. Performances were extrapolated to higher acetate concentrations and varying anode width chambers using numerical methods with a mean accuracy of 93.2%. To achieve the observed current production and substrate degradation rates observed in the laboratory, the algorithm predicted that removal rates were higher in the vicinity of the biofilm than in the bulk liquid. As such, a combination of high acetate concentration and narrow anode chamber widths were shown to have a positive impact on ORR. For typical domestic wastewater (10mg-Ac-COD/l), it is unlikely that any anode design can be financially viable. Previously, acetate concentrations have been increased to 100mg-COD/l (Ligero et al., 2001) through hydrolysis. At this concentration, ORR may begin to compete with the lower end of AS, particularly when anode interstices are narrow ($<$10mm).

The impact of anode interstices distance

Numerical predictions showed that for anodes with interstices of 2.5mm, provided sufficient pre-treatment can be implemented to remove suspended solids and biofilms remain relatively stable, a property that has yet to be demonstrated, ORR (1,530$\pm$240g-Ac-COD/m^3/d) can surpass initial targets (800–1,400g-COD/m^3/d) and AS (450-1,425mg-BOD/l/d, Stanbury et al. (2017)). Thus MEC anode chambers may be retrofitted to pre-existing aeration lanes. However performance is highly dependent upon biofilm development. Anodes will require high quality control to ensure that interstices are somewhat homogeneously wide (2.5mm), a stable supple of acetate with high concentration ($>$100mg-COD/l) and anode chambers will require sufficient time for biofilms to grow. Even if this is achieved, performance will likely be less than upper predictions due to growth, plateau and death phases that microorganisms typically experience (Judd, 2013). For an optimistic 'simulated hydrolysed wastewater' scenario (2.5mm, 100mg-COD/l) under 'linear growth', allowable cost predictions standardised to the anodes surface were £13.50$\pm$3.50/m^2, £17.00$\pm$4.40/m^2 and £24.70$\pm$6.40/m^2 for 5, 10 and 20 year time-frames, respectively. This cost includes all of the materials, pre-treatment and maintenance. Under a more conservative prediction, accounting for poor anode interstices quality control and unstable acetate supply (5mm, 50mg-COD/l) anode area costs were £2.06$\pm$1.13/m^2, £3.67$\pm$1.56/m^2 and £5.65$\pm$2.35/m^2 for 5, 10 and 20 year time-frames, respectively. Moreover, these costs are predicated on the surface area of the material and therefore if quality control is poor allowable costs will be even lower, as the material chosen will have been overvalued. Furthermore, performance is highly dependent upon biofilm growth and therefore if biofilms fail to grow then the value of such systems to utilities will be negative.

I propose that the best chance of designing a commercially viable system that can financially compete with AS, would be to design an MEC with material costs £5/m^2 standardised to the anode's surface. Although higher costs may be permissible if biofilms remain stable, performance is high

and the financial risk is tolerable. This would allow some tolerance for additional material input to cover the variable nature of biofilm stability, and would also allow some costs for maintenance and installation of post and pre-treatment systems. Further reiterating the points made above, anode interstices will need to be carefully controlled, acetate supplies must be consistently >100mg-COD/l, electrodes must not foul and post-treatment will likely be needed to ensure standards are met.

The impact of full-scale MEC deployment

In their current design, MEC cannot be energy positive when applied to typical domestic wastewater due to high potential losses, though this may be less of an issue in cities that use sea-water flushing such as Hong Kong. However, compared with AS MEC will be net energy savers for all the scenarios modelled. Although direct emissions are likely to be the same as AS, as carbon removal should be the same, MEC are predicted to reduce equivalent CO2 emissions by 8-26kge/m^3. If MEC were applied on a full scale to all wastewater treated in the UK (11Mm^3/d) (Skellet, 1992), this would be on the order of magnitude of 0.01-0.1% of all national emissions. Around 80% of global wastewater (330km^3, Drechsel et al. (2015)) is still released into the environment without adequate treatment (WWAP, 2017), applying MEC to all regions that do not currently have adequate treatments, instead of AS, could prevent 2-7billion tons of CO2 equivalent emissions per year. Decreasing potential losses would ensure that the higher end of these predictions could be reached and may allow MEC to be net energy positive. For MEC to achieve net energy production the maximum voltage input applied should be no more than 0.46V (if combined cathodic efficiencies and hydrogen capture are 50%).

Globally, our species currently emits 36billion tons of CO2, however in 1950 we only emitted around 5billion tons of CO2 (Ritchie and Roser, 2020). Whilst, the current phase of the solar cycle may have increased recent temperatures temporarily by about a third (Booth, 2018, Laut and Gundermann, 1998*a*,*b*), it is extremely likely that our emissions are having on the climate (IPCC, 2014) and the rate at which emissions are increasing is unprecedented in at least the last 800,000 years (Le Floch et al., 2018). Moreover, populous regions such as Africa and India are only just beginning to increase their emissions (Ritchie and Roser, 2020), if these continue inline with the exponential trends observed over the last century then we may accelerate our affect on the climate to a point at which we may find it difficult to safely adapt.

5.4 Review

This doctoral thesis has been an attempt to provide answers to the viability of the use of microbial electrolysis cells as a sustainable treatment for domestic wastewater. I conclude that implementation of the technology for domestic wastewater treatment may be commercially viable if material costs can be reduced to £5/m^2, pre-treatments can produce sufficient acetate concentrations, re-

moval rates can reach environmental regulations and electrode fouling and blockages are prevented. As far as I am aware no study to date has investigated the combined effect that reactor design and acetate concentration have on both the cost and the performance of the reactor. However, during the course of the study simplifications were made to make the task more time-efficient and to better illustrate certain limits. Acetate was used as the basis of numerical predictions as acetate was shown in the meta-analyses to produce the highest current densities and thus the highest performances. In reality, domestic wastewater will contain a max of substrates, which will each have their own degradation rates. Furthermore, biofilm communities and bulk communities were assumed to be homogeneous, in reality each of these will contain a plethora of microbial species. Nevertheless, modelled predictions mapped empirical observations on current density, current degradation rates, coulombic efficiency and substrate degradation with a mean accuracy of 93.2%. Real-world studies will be required to confirm removal rates with biofilms fed with high acetate concentrations ($>$100mg/l) in narrow spaces (2.5mm) over a long period of time and in changing environmental conditions.

The mass transport of substrate to the biofilm is the driving force in BES. Therefore, the combined relationship that concentration and anode chamber width have on biofilm performance is applicable to other BES. Commercial viability of alternative BES will be impacted by: the costs offset by applying the technology in other industries; the cost-benefit of alternative cathode products; and the effect of substrates on biofilm development and anode potential. To achieve high-performance reactors high concentrations of biofilm biomass will need to produced, although current generation will probably remain orders of magnitudes less than a typical electrolysis cells. Therefore application of bio-electrochemical systems is limited to areas that currently have replaceable high operational costs, preferably higher than activated sludge, and stronger organic waste.

5.5 Further research

Anode materials

Development and use of cheap anode materials is perhaps the most important factor in the commercial viability of MEC in the treatment of wastewaters. Porous materials with widths 0.5-2.5mm may provide the highest removal rates at the lowest cost. However, the impact that mass transport limitation plays on biofilm development and current production will require further investigation. Materials will also need to be inordinately cheap to procure. Waste products from other industrial and commercial processes may provide the most cost-effective solution, such as waste carbon fibre.

Wastewaters and pre-treatment

Future research may investigate the impacts of waste-streams containing much higher concentra-

tions of organic matter (>500mg-COD/l). Potential avenues could include waste activated sludge (Xin et al., 2018), agricultural (Min et al., 2005) and food waste streams (Cardeña et al., 2018) that are currently treated using energetically costly methods. To retrieve the energy content stored in organic matter pre-treatments will be required. Possible technologies include: hydrolysis reactors and dark fermentation (Cardeña et al., 2018). Upflow hydrolysis reactors (Ligero et al., 2001) may be of particular interest as they can remove suspended solids and have short retention times to prevent methanogenesis. Additionally, domestic wastewater may be a feasible stream for implementation if food can be concentrated cost-effectively.

Mass transport of chemical species

Higher uncertainties were found when widths were reduced. This is due to the unknown response of the biofilm community in respect to reduced widths and high acetate concentrations. Further research could be conducted to determine the ORR and energy recovery in bio-electrochemical systems with anode interstice of 0.5-2.5mm and high acetate concentrations. Focus should be on the effects that reducing width, at varying concentrations, has on the mass transport of substrate to the biofilm, as well as mass transport of products from the biofilm and the effect on species growth. Empirically determining the limiting combined effect of width and concentration has on electrogenic biomass will provide limits to the applicability of MEC technology. Further attention could be given on the impact that flow and anode surface charge have on the mass transport of chemical species. Other means of improving mass transport to the biofilm may also be considered, the impact that turbulence has on biofilm growth was not considered in this study. Other means of improving mass transport may include attracting charged chemical species towards the biofilm through poised potentials. However, for this to be successful ionic conductivity will need to greatly improved and the costs will have to be justified.

Modelling

Modelling was conducted using a batch reactor. Acetate was fed every 48h at the same organic loading rate, which degraded over time. Under these conditions the biofilm was allowed to grow and stabilise over a three week period. Continuous reactors will effect the growth of the biofilm, as concentration will be more consistent near to the influent and degrade through the length of the reactor, as opposed to degrading over time. Furthermore, increasing turbulence through increased velocity should improve mass transport to and from the biofilm. Efforts were made during the course this research to model the effect that flowrate would have on the biofilm, however this significantly increased the computational time. Future research in this area should look to investigate the effects of flowrate in continuously fed reactors and simplify the modelling procedure to be time-efficient. Additionally, the model was simplified by assuming an homogeneous starting biofilm concentration attached to the anode and an homogeneous biomass concentration in the bulk

liquid. Accuracy could be improved by modelling the growth of the biofilm over time. This would be highly computationally intensive and again modelling procedure would have to be adapted to be more time-efficient. Additional substrates and species differentiation could also be integrated into modelling efforts to improve removal rate accuracies.

Potential losses

Assuming that combined cathodic efficiency and hydrogen capture is 50% then applied voltages must not exceed 0.46V for MEC to be energy positive. Potential losses are high due to the low conductivity of domestic wastewater. Adding salts into wastewater is likely to be a hazardous and expensive endeavour and therefore better s cell designs will be needed to overcome this. The challenge is therefore in designing an MEC that has reduced gaps between electrodes but that can still boast a high accessible anode surface area, which can received sufficient amounts of substrate to support a biofilm.

Microbial fuel cell design

Alternatively to MEC, MFC are energy positive (Rabaey and Verstraete, 2005), but design constraints surround the aeration of cathode chambers and bioanode corrosion is a common phenomenon due to cell reversal (Li et al., 2017). Further work may find easier progress in applying anode design and cost recommendations described here to an MFC with improved electrochemical designs.

Bibliography

Aelterman, P., Versichele, M., Marzorati, M., Boon, N. and Verstraete, W. (2008), 'Loading rate and external resistance control the electricity generation of microbial fuel cells with different three-dimensional anodes', *Bioresource Technology* **99**, 8895–8902.

Aiken, D. C., Curtis, T. P. and Heidrich, E. S. (2019), 'Avenues to the financial viability of microbial electrolysis cells [MEC] for domestic wastewater treatment and hydrogen production', *International Journal of Hydrogen Energy* **44**(5), 2426–2434.
URL: *https://doi.org/10.1016/j.ijhydene.2018.12.029*

Aiken, D. C., Curtis, T. P., Jones, C., Dolfing, J. and Heidrich, E. (2018), Microbial Electrolysis Cells and Copper Anodes: High current, low cost, high risk, *in* 'ISMET-EU 2018', Newcastle-upon-Tyne.

APHA (2017), *Standard Methods for the Examination of Water and Wastewater*, 23rd edn, American Public Health Association, Washington, D.C.

Arden, E. and Lockett, W. (1914), 'Experiments on the Oxidation of Sewage without the Air of Filters', *J. Soc. Chem. Ind* **33**(523).

Baeza, J. A., Martinez-Miro, A., Guerrero, J., Ruiz, Y. and Guisasola, A. (2017), 'Bioelectrochemical hydrogen production from urban wastewater on a pilot scale', *Power Sources* **356**, 500–509.

Baudler, A., Riedl, S. and Schröder, U. (2014), 'Long-term performance of primary and secondary electroactive biofilms using layered corrugated carbon electrodes', *Frontiers in Energy Research* **2**(30), 1–6.

Baudler, A., Schmidt, I., Langner, M., Greiner, A. and Schroder, U. (2015), 'Does it have to be carbon? Metal anodes in microbial fuel cells and related bioelectrochemical systems', *Energy and Environmental Science* **8**, 2048–2055.

BEIS (2018), Goverment GHG conversion factors for company reporting, Technical Report July, Department for Business, Energy & Industrial Strategy, London, UK.
URL: *www.nationalarchives.gov.uk/doc/open-government-licence/*

BEIS (2019), 2018 UK greenhouse gas emissions, provisional figures, Technical Report March, Department for Business, Energy & Industrial Strategy, London, UK.

URL: *https://assets.publishing.service.gov.uk/government/uploads/system/uploads/attachment_data/file/790626/2 provisional-emissions-statistics-report.pdf*

Booth, R. J. (2018), 'On the influence of solar cycle lengths and carbon dioxide on global temperatures', *Journal of Atmospheric and Solar-Terrestrial Physics* **173**(October 2016), 96–108.
URL: *https://doi.org/10.1016/j.jastp.2018.01.026*

Box, G. E. P. (1976), 'Science and statistics', *Journal of the American Statistical Association* **71**(356), 791–799.

Brown, R., Schmidt, U., Harnisch, F. and Schroder, U. (2017), 'Combining hydrogen evolution and corrosion data - A case study on the economic viability of selected metal cathodes in microbial electrolysis cells', *Journal of Power Sources* **336**, 473–483.

Business Electricity Prices (2016), 'Business and Commercial Electricity Prices'.
URL: *http://www.businesselectricityprices.org.uk/*

Caccavo, F., Lonergan, D. J., Lovley, D. R. and Davis, M. (1994), 'Acetate- Oxidizing Dissimilatory Metal-Reducing Microorganism', *Microbiology* **60**(10), 3752–3759.
URL: *http://aem.asm.org/content/60/10/3752.full.pdf*

Callahan1, B. J., McMurdie, P. J., Rosen, M. J., Han, A. W., Johnson, A. J. A. and Holmes, S. P. (2016), 'DADA2: High resolution sample inference from Illumina amplicon data', *Nature Methods* **13**(7), 4–5.

Cardeña, R., Moreno-Andrade, I. and Buitrón, G. (2018), 'Improvement of the bioelectrochemical hydrogen production from food waste fermentation effluent using a novel start-up strategy', *Journal of Chemical Technology and Biotechnology* **93**(3), 878–886.

Champigneux, P., Renault-Sentenac, C., Bourrier, D., Rossi, C., Delia, M. L. and Bergel, A. (2018), 'Effect of surface nano/micro-structuring on the early formation of microbial anodes with Geobacter sulfurreducens: Experimental and theoretical approaches', *Bioelectrochemistry* **121**, 191–200.
URL: *https://doi.org/10.1016/j.bioelechem.2018.02.005*

Chaudhary, A., Kauser, I., Ray, A. and Poretsky, R. (2018), 'Taxon-Driven Functional Shifts Associated with Storm Flow in an Urban Stream Microbial Community', *American Society for Microbiology* **3**(4).

Chen, S., He, G., Liu, Q., Harnisch, F., Zhou, Y., Chen, Y., Hanif, M., Wang, S., Peng, X., Hou, H. and Schröder, U. (2012), 'Layered corrugated electrode macrostructures boost microbial bioelectrocatalysis', *Energy and Environmental Science* **5**(12), 9769–9772.

Chong, P., Erable, B. and Bergel, A. (2019), 'Effect of pore size on the current produced by 3-dimensional porous microbial anodes: A critical review', *Bioresource Technology* **289**(February).

Christensen, P. and Hamnet, A. (1994), *Techniques and Mechanisms in Electrochemistry*, Springer Netherlands.

Christgen, B., Scott, K., Dolfing, J., Head, I. M. and Curtis, T. P. (2015), 'An Evaluation of the Performance and Economics of Membranes and Separators in Single Chamber Microbial Fuel Cells Treating Domestic Wastewater', *PLoS ONE* **10**(8), 1–13.
URL: *http://dx.doi.org/10.1371/journal.pone.0136108*

Commault, A. S., Barrière, F., Lapinsonnière, L., Lear, G., Bouvier, S. and Weld, R. J. (2015), 'Influence of inoculum and anode surface properties on the selection of Geobacter-dominated biofilms', *Bioresource Technology* **195**, 265–272.
URL: *http://dx.doi.org/10.1016/j.biortech.2015.06.141*

Commault, A. S., Lear, G., Packer, M. A. and Weld, R. J. (2013), 'Influence of anode potentials on selection of Geobacter strains in microbial electrolysis cells', *Bioresource Technology* **139**, 226–234.
URL: *http://dx.doi.org/10.1016/j.biortech.2013.04.047*

Cotterill, S. E. (2017), Scale up and Development of a Microbial Electrolysis Cell for Domestic Wastewater Treatment and Energy Recovery, PhD thesis, Newcastle University.

Cotterill, S. E., Dolfing, J., Jones, C., Curtis, T. P. and Heidrich, E. S. (2017), 'Low Temperature Domestic Wastewater Treatment in a Microbial Electrolysis Cell with 1m2 Anodes: Towards System Scale Up', *Fuel Cells* **17**(5), 584–592.

Cselovszky, J., Wolf, G. and Hammes, W. P. (1992), 'Production of formate, acetate, and succinate by anaerobic fermentation of Lactobacillus pentosus in the presence of citrate', *Applied Microbiology and Biotechnology* **37**(1), 94–97.

Cucu, A., Costache, T. A., Divona, M., Tiliakos, A., Stamatin, I. and Ciocanea, A. (2013), 'Microbial Electrolysis Cell: Hydrogen production using microbial consortia from romanian waters', *Digest Journal of Nanomaterials and Biostructures* **8**(3), 1179–1190.

Curtis, T. P. (2010), Low-Energy Wastewater Treatment: Strategies and Technologies, *in* R. Mitchell and J. Gu, eds, 'Environmental Microbiology', Wiley-Blackwell, chapter 13.

Cusick, R. D., Bryan, B., Parker, D. S., Merrill, M. D., Mehanna, M., Kiely, P. D., Liu, G. and

Logan, B. E. (2011), 'Performance of a pilot-scale continuous flow microbial electrolysis cell fed winery wastewater', *Bioenergy and Biofuels* **89**, 2053–2063.

Cusick, R. D., Kiely, P. D. and Logan, B. E. (2010), 'A monetary comparison of energy recovered from microbial fuel cells and microbial electrolysis cells fed winery or domestic wastewaters', *International Journal of Hydrogen Energy* **35**(17), 8855–8861.

Dai, Z., Heidrich, E. S., Dolfing, J. and Jarvis, A. P. (2019), 'Determination of the Relationship between the Energy Content of Municipal Wastewater and Its Chemical Oxygen Demand', *Environmental Science and Technology Letters* **6**(7), 396–400.

Dewan, A., Beyenal, H. and Lewandowski, Z. (2008), 'Scaling up microbial fuel cells.', *Environmental science & technology* **42**(20), 7643–7648.

Dhar, B. R. and Lee, H. S. (2014), 'Evaluation of limiting factors for current density in microbial electrochemical cells (MXCs) treating domestic wastewater', *Biotechnology Reports* **4**(1), 80–85.

Dobrzyńska, A. and Bernat, K. (2004), 'Carbon Removal by Activated Sludge under Fully Aerobic Conditions at Different COD / N Ratio', *Polish Journal of Environmental Studies* **13**(1), 33–40.

Drechsel, P., Qadir, M. and Wichelns, D. (2015), *Wastewater: Economic asset in an urbanizing world*, Springer.

Escapa, A., Gil-Carrera, L., García, V. and Morán, A. (2012), 'Performance of a continuous flow microbial electrolysis cell (MEC) fed with domestic wastewater.', *Bioresource technology* **117**, 55–62.

Escapa, A., Mateos, R. and Morán, A. (2015), 'Scaling-up of membraneless microbial electrolysis cells (MECs) for domestic wastewater treatment: Bottlenecks and limitations', *Bioresource Technology* **180**, 72–78.
URL: *http://dx.doi.org/10.1016/j.biortech.2014.12.096*

Escapa, A., Moreno, R. and Morán, A. (2013), 'Reduced energy consumption during low strength domestic wastewater treatment in a semi-pilot tubular microbial electrolysis cell', *Journal of Environmental Management* **122**, 1–7.
URL: *http://dx.doi.org/10.1016/j.jenvman.2013.03.001*

Europa (2008), HyWAYS the European Hydrogen Roadmap Contract. SES6-502596, Technical report.

European Economic Community Council (1991), 91/271/EEC of 21 May 1991 concerning urban waste-water treatment, Technical Report L.

Fink, R., Oder, M., Rangus, D., Raspor, P. and Bohinc, K. (2016), 'Microbial adhesion capacity. Influence of shear and temperature stress', *International Journal of Environmental Health Research* **25**(6), 656–669.
URL: *http://dx.doi.org/10.1080/09603123.2015.1007840*

Fornero, J. J., Rosenbaum, M. and Angenent, L. T. (2010), 'Electric Power Generation from Municipal , Food , and Animal Wastewaters Using Microbial Fuel Cells', *Electroanalysis* **22**(7-8), 832–843.

Gardner, E. L. W., Luca, A. D. and Udrea, F. (2017), '2D and 3D Thermal Flow Sensor Modelling – A Comparative Analysis', *University of Cambridge* pp. 1–4.

Ge, Z. and He, Z. (2016), 'Long-term performance of a 200 liter modularized microbial fuel cell system treating municipal wastewater: treatment, energy, and cost', *Environmental Science: Water Research & Technology* **2**(2), 235–406.

Gil-Carrera, L., Escapa, A., Carracedo, B., Morán, A. and Gómez, X. (2013), 'Performance of a semi-pilot tubular microbial electrolysis cell (MEC) under several hydraulic retention times and applied voltages.', *Bioresource technology* **146**, 63–9.

Glöckner, F. O., Yilmaz, P., Quast, C., Gerken, J., Beccati, A., Ciuprina, A., Bruns, G., Yarza, P., Peplies, J., Westram, R. and Ludwig, W. (2017), '25 years of serving the community with ribosomal RNA gene reference databases and tools', *Journal of Biotechnology* **261**, 169–176.

Gorsek, A. and Glavic, P. (2000), 'Part III: Extended Analysis of Cost Parameters', *Chemical Engineering Research and Design* **78**, 231–244.

Green Investment Back (2015), 'The UK anaerobic digestion market'.
URL: *http://greeninvestmentgroup.com/media/*

Gummer, J., Chater, N., Hoskins, B., Johnson, P., Brown, Quere, C. L. and Skea, J. (2017), Energy Prices and Bills - impact of meeting carbon budgets, Technical report, Committee on Climate Change.

Guterres, A. (2019), Special edition: progress towards the Sustainable Development Goals, Technical Report May, United Nations, Economic And Social Council.

Hamelers, H. V. M., Stein, N., Rozendal, R. A. and Buisman, C. J. N. (2011), 'Butler – Volmer – Monod model for describing bio-anode polarization curves', *Bioresource Technology* **102**, 381–387.

Hasany, M., Mardanpour, M. M. and Yaghmaei, S. (2015), 'Biocatalysts in microbial electrolysis cells : A review', *International Journal of Hydrogen Energy* **41**(3), 1477–1493.

Haseli, Y. (2018), 'Maximum conversion efficiency of hydrogen fuel cells', *International Journal of Hydrogen Energy* **43**(18), 9015–9021.
URL: *https://doi.org/10.1016/j.ijhydene.2018.03.076*

Hays, S., Zhang, F. and Logan, B. E. (2011), 'Performance of two different types of anodes in membrane electrode assembly microbial fuel cells for power generation from domestic wastewater', *Journal of Power Sources* **196**(20), 8293–8300.
URL: *http://dx.doi.org/10.1016/j.jpowsour.2011.06.027*

Heidrich, E. (2012), Evaluation of Microbial Electrolysis Cells in the treatment of domestic wastewater, PhD thesis, Newcastle University.

Heidrich, E. S., Curtis, T. P. and Dolfing, J. (2011), 'Determination of the Internal Chemical Energy of Wastewater', *Environ. Sci. Technol* **45**(2), 827–832.

Heidrich, E. S., Dolfing, J., Scott, K. and Edwards, S. R. (2013), 'Production of hydrogen from domestic wastewater in a pilot-scale microbial electrolysis cell', *Environmental Biotechnology* **97**, 6979–6989.

Heidrich, E. S., Edwards, S. R., Dolfing, J., Cotterill, S. E. and Curtis, T. P. (2014), 'Performance of a pilot scale microbial electrolysis cell fed on domestic wastewater at ambient temperatures for a 12 month period', *Bioresource Technology* **173**, 87–95.

Henze, M. and Comeau, Y. (2008), Wastewater Characterization, *in* 'Biological Wastewater Treatment: Principles, Modelling and Design', IWA Publishing, London, UK, pp. 33–52.

Hillier, D., Ross, S., Westerfield, R., Jaffe, J. and Jordan, B. (2013), *Corporate Finance*, 2nd ed. edn, Maidenhead: McGraw-Hill Education.

Huang, M.-h., Li, Y.-m. and Gu, G.-w. (2010), 'Chemical composition of organic matters in domestic wastewater', *Desalination* **262**(1-3), 36–42.
URL: *http://dx.doi.org/10.1016/j.desal.2010.05.037*

IPCC (2014), 'Climate Change 2014 Synthesis Report Summary Chapter for Policymakers'.

Ishii, S., Suzuki, S., Tenney, A. and Norden-krichmar, T. M. (2015), 'Microbial metabolic networks in a complex electrogenic biofilm recovered from a stimulus-induced metatranscriptomics approach', *Nature Scientific Reports* **5**(14840).
URL: *http://dx.doi.org/10.1038/srep14840*

ITM Power (2013), 'Hydrogen Cost Structure Update'.
URL: *http://www.itm-power.com/news-item/hydrogen-cost-structure-update*

Janicek, A., Fan, Y. and Liu, H. (2015), 'Performance and stability of different cathode base materials for use in microbial fuel cells', *Journal of Power Sources* **280**, 159–165.
URL: *http://dx.doi.org/10.1016/j.jpowsour.2015.01.098*

Judd, S. (2013), *watermaths*, second edn, Judd and Judd Ltd., Bedfordshire, UK.

Kadier, A., Simayi, Y., Kalil, M. S., Abdeshahian, P. and Hamid, A. A. (2014), 'A review of the substrates used in microbial electrolysis cells (MECs) for producing sustainable and clean hydrogen gas', *Renewable Energy* **71**, 466–472.
URL: *http://dx.doi.org/10.1016/j.renene.2014.05.052*

Karthikeyan, R., Wang, B., Xuan, J., Wong, J. W., Lee, P. K. and Leung, M. K. (2015), 'Interfacial electron transfer and bioelectrocatalysis of carbonized plant material as effective anode of microbial fuel cell', *Electrochimica Acta* **157**, 314–323.

Katuri, K. P., Scott, K., Head, I. M., Picioreanu, C. and Curtis, T. P. (2011), 'Microbial fuel cells meet with external resistance', *Bioresource Technology* **102**(3), 2758–2766.
URL: *http://dx.doi.org/10.1016/j.biortech.2010.10.147*

Kim, H. J., Park, H. S., Hyun, M. S., Seop, C. I., Kim, M. and Kim, B. H. (2002), 'A mediator-less microbial fuel cell using a metal reducing bacterium , Shewanella putrefaciens', **30**, 145–152.

Kim, J. R., Min, B. and Logan, B. E. (2005), 'Evaluation of procedures to acclimate a microbial fuel cell for electricity production', *Applied Microbiology and Biotechnology* **68**(1), 23–30.

Kolmos, H. J. J. (2012), *Brock biology of microorganisms*, 13th edn, Benjamin Cummings, San Francisco, CA.

König, J., Mühlenhoff, S., Eckert, K., Büttner, L., Odenbach, S. and Czarske, J. (2011), 'Velocity measurements inside the concentration boundary layer during copper-magneto-electrolysis using a novel laser Doppler profile sensor', *Electrochimica Acta* **56**, 6150–6156.

Kumar, G., Bakonyi, P., Zhen, G., Sivagurunathan, P., Koók, L., Kim, S. H., Tóth, G., Nemestóthy, N. and Bélafi-Bakó, K. (2017), 'Microbial electrochemical systems for sustainable biohydrogen production: Surveying the experiences from a start-up viewpoint', *Renewable and Sustainable Energy Reviews* **70**, 589–597.

Kundu, A., Sahu, J. N., Redzwan, G. and Hashim, M. A. (2013), 'An overview of cathode material and catalysts suitable for generating hydrogen in microbial electrolysis cell', *International Journal of Hydrogen Energy* **38**(4), 1745–1757.
URL: *http://dx.doi.org/10.1016/j.ijhydene.2012.11.031*

Larrosa-Guerrero, A., Scott, K., Head, I. M., Mateo, F., Ginesta, A. and Godinez, C. (2010), 'Effect of temperature on the performance of microbial fuel cells', *Fuel* **89**(12), 3985–3994.

Laut, P. and Gundermann, J. (1998*a*), 'Does the correlation between solar cycle lengths and Northern Hemisphere land temperatures rule out any significant global warming from greenhouse gases?', *Journal of Atmospheric and Solar-Terrestrial Physics* **60**(1), 1–3.

Laut, P. and Gundermann, J. (1998*b*), 'Solar cycle length hypothesis appears to support the IPCC on global warming', *Journal of Atmospheric and Solar-Terrestrial Physics* **60**(18), 1719–1728.

Le Floch, D., Bereiter, B., Blunier, T., Barnola, J.-M., Siegenthaler, U., Raynaud, D., Jouzel, J., Fischer, H., Kawamura, K., Stocker, T. and J.R.Petit (2018), '800,000-year Ice-Core Records of Atmospheric Carbon Dioxide (CO2)', *Carbon Dioxide Intormation Analysis Center* pp. 1–5.

Leaist, D. G. and Lyons, P. A. (1984), 'Diffusion in dilute aqueous acetic acid solutions at 25°C', *J. Solution Chem.* **13**, 77–85.

Leung, R. W. K., Li, D. C. H., Yu, W. K., Chui, H. K., Lee, T. O., van Loosdrecht, M. C. M. and Chen, G. H. (2012), 'Integration of seawater and grey water reuse to maximize alternative water resource for coastal areas: the case of the Hong Kong International Airport.', *Water science and technology : a journal of the International Association on Water Pollution Research* **65**(3), 410–7.
URL: *http://www.ncbi.nlm.nih.gov/pubmed/22258669*

Li, J. and He, Z. (2016), 'Development of a dynamic mathematical model for membrane bioelectrochemical reactors with different configurations', *Environmental Science and Pollution Research* **23**(4), 3897–3906.

Li, J., Li, H., Fu, Q., Liao, Q. and Zhu, X. (2017), 'Voltage reversal causes bioanode corrosion in microbial fuel cell stacks', *International Journal of Hydrogen Energy* **42**(45), 27649–27656.

Liao, Q., Zhang, J., Li, J., Ye, D., Zhu, X. and Zhang, B. (2015), 'Increased performance of a tubular microbial fuel cell with a rotating carbon-brush anode', *Biosensors and Bioelectronics* **63**, 558–561.
URL: *http://dx.doi.org/10.1016/j.bios.2014.08.014*

Ligero, P., Vega, A. and Soto, M. (2001), 'Pretreatment of urban wastewaters in a hydrolytic upflow digester', *Water SA* **27**(3), 399–404.
URL: *http://www.wrc.org.za*

Lim, S. S., Fontmorin, J.-M., Izadi, P., Daud, W. R. W., Scott, K. and Yu, E. H. (2018), 'Impact of applied cell voltage on the performance of a microbial electrolysis cell fully catalysed

by microorganisms for the production of hydrogen', *International Journal of Hydrogen Energy* **45**(4), 2557–2568.

Liu, C., Li, J., Zhu, X., Zhang, L., Ye, D., Brown, R. K. and Liao, Q. (2013), 'Effects of brush lengths and fiber loadings on the performance of microbial fuel cells using graphite fiber brush anodes', *International Journal of Hydrogen Energy* **38**(35), 15646–15652.
URL: *http://dx.doi.org/10.1016/j.ijhydene.2013.03.144*

Liu, Y., Harnisch, F., Fricke, K., Sietmann, R. and Schroder, U. (2008), 'Improvement of the anodic bioelectrocatalytic activity of mixed culture biofilms by a simple consecutive electrochemical selection procedure', *Biosensors and Bioelectronics* **24**(4), 1006–1011.

Logan, B. (2008), *Microbial Fuel Cells*, John Wiley & Sons, Inc, Hoboken, New Jersey, USA.

Logan, B. E. and Rabaey, K. (2012), 'Conversion of Wastes into Bioelectricity and Chemicals by Using Microbial Electrochemical Technologies', *Science* **337**, 686–690.

Logan, B. E., Rossi, R., Ragab, A. and Saikaly, P. E. (2019), 'Electroactive microorganisms in bioelectrochemical systems', *Nature Reviews* **17**, 3017–319.

Logan, B. E., Wallack, M. J., Kim, K. Y., He, W., Feng, Y. and Saikaly, P. E. (2015), 'Assessment of Microbial Fuel Cell Configurations and Power Densities', *Environmental Science and Technology Letters* **2**(8), 206–214.

Logan, B. E., Zikmund, E., Yang, W., Rossi, R., Kim, K. Y., Saikaly, P. E. and Zhang, F. (2018), 'Impact of Ohmic Resistance on Measured Electrode Potentials and Maximum Power Production in Microbial Fuel Cells', *Environmental Science and Technology* **52**(15), 8977–8985.

Logan, B., Hamelers, B., Rozendal, R., Schroder, U., Keller, J., Freguia, S., Aelterman, P., Werstraete, W. and Rabaey, K. (2006), 'Critical Review Microbial Fuel Cells: Methodology and Technology', *Environmental Science and Technology* **40**(17), 5181–5192.

Lothongkum, G., Vongbandit, P. and Nongluck, P. (2006), 'Experimental determination of E-pH diagrams for 316L stainless steel in air-saturated aqueous solutions containing 0-5,000 ppm of chloride using a potentiodynamic method', *Anti-Corrosion Methods and Materials* **53**(3), 169–174.

Lovley, D. R. and Phillips, E. J. P. (1988), 'Novel Mode of Microbial Energy Metabolism: Organic Carbon Oxidation Coupled to Dissimilatory Reduction of Iron or Manganese', *Appl. Envir. Microbiol.* **54**(6), 1472–1480.
URL: *http://aem.asm.org/cgi/content/long/54/6/1472*

Lu, L., Xing, D., Ren, N. and Logan, B. E. (2012), 'Syntrophic interactions drive the hydrogen production from glucose at low temperature in microbial electrolysis cells', *Bioresource Technology* **124**, 68–76.

Madani, S., Gheshlaghi, R., Mahdavi, M. A., Sobhani, M. and Elkamel, A. (2015), 'Optimization of the performance of a double-chamber microbial fuel cell through factorial design of experiments and response surface methodology', *Fuel* **150**, 434–440.
URL: *http://dx.doi.org/10.1016/j.fuel.2015.02.039*

Mahadevan, R., Bond, D. R., Coppi, M. V., Palsson, B. O., Schilling, C. H. and Lovley, D. R. (2006), 'Characterization of Metabolism in the Fe(III)-Reducing Organism', *Applied and Environmental Microbiology* **72**(2), 1558–1568.

Malovanyy, M., Shandrovych, V., Malovanyy, A. and Polyuzhyn, I. (2016), 'Comparative Analysis of the Effectiveness of Regulation of Aeration Depending on the Quantitative Characteristics of Treated Sewage Water'.

Marozava, S., Röling, W. F. M., Seifert, J., Küffner, R., Von Bergen, M. and Meckenstock, R. U. (2014*a*), 'Physiology of Geobacter metallireducens under excess and limitation of electron donors. Part I. Batch cultivation with excess of carbon sources Sviatlana', *Systematic and Applied Microbiology* **37**(4), 287–295.

Marozava, S., Röling, W. F. M., Seifert, J., Küffner, R., Von Bergen, M. and Meckenstock, R. U. (2014*b*), 'Physiology of Geobacter metallireducens under excess and limitation of electron donors. Part II. Mimicking environmental conditions during cultivation in retentostats', *Systematic and Applied Microbiology* **37**(4), 287–295.
URL: *http://dx.doi.org/10.1016/j.syapm.2014.02.005*

Mathuriya, A. S. (2013), 'Inoculum selection to enhance performance of a microbial fuel cell for electricity generation during wastewater treatment', *Environmental Technology* **34**(13-14), 1957–1964.
URL: *http://www.tandfonline.com/doi/abs/10.1080/09593330.2013.808674*

McMurdie, P. J. and Holmes, S. (2013), 'Phyloseq: An R Package for Reproducible Interactive Analysis and Graphics of Microbiome Census Data', *PLoS ONE* **8**(4).

Metcalf & Eddy, Revised by: Tchobanoglous, G., Burton, F. L. and Stensel, H. D. (2003), *Wastewater Engineering: Treatment and Reuse*, 4th ed. edn, McGraw-Hill, New York, USA.

Min, B., Kim, J. R., Oh, S. E., Regan, J. M. and Logan, B. E. (2005), 'Electricity generation from swine wastewater using microbial fuel cells', *Water Research* **39**(20), 4961–4968.

Mortia, M., Malvankar, N., Franks, A., Summers, Z., Giloteaux, L., Rtoaru, A., Rotaru, C. and Lovley, D. (2011), 'Potential for Direct Interspecies Electron Transfer in Methanogenic', *mbio* **2**(4), 5–7.

Nam, J.-y., Tokash, J. C. and Logan, B. E. (2011), 'Comparison of microbial electrolysis cells operated with added voltage or by setting the anode potential', *International Journal of Hydrogen Energy* **36**.

OECD (2006), 'Public Investment in the United Kingdom', *OECD Journal on Budgeting* **6**(4), ISSN 1608–7143.

OFWAT (2019), PR19 initial assessment of plans : Overview of company categorisation, Technical Report January, OFWAT.

Olsson, G. (2012), *Water and Energy: Threats and Opportunities*, IWA Publishing, London.

Pant, D., Singh, A., Van Bogaert, G., Gallego, Y. A., Diels, L. and Vanbroekhoven, K. (2011), 'An introduction to the life cycle assessment (LCA) of bioelectrochemical systems (BES) for sustainable energy and product generation: Relevance and key aspects', *Renewable and Sustainable Energy Reviews* **15**(2), 1305–1313.

Patil, S. A., Harnisch, F., Kapadnis, B. and Schröder, U. (2010), 'Electroactive mixed culture biofilms in microbial bioelectrochemical systems : The role of temperature for biofilm formation and performance', *Biosensors and Bioelectronics* **26**(2), 803–808.
URL: *http://dx.doi.org/10.1016/j.bios.2010.06.019*

Patricia, G. L., Adba, M., Edgar, M., Alejandro, P., Manuel, M. J. and Robles, N. (2011), A comparative life cycle assessment of a wastewater treatment technology considering two inflow scales ., Technical report, Instituto de Ingeniería.
URL: *http://hdl.handle.net/10625/48608*

Picioreanu, C., Head, I. M., Katuri, K. P., Loosdrecht, M. C. M. V. and Scott, K. (2007), 'A computational model for biofilm-based microbial fuel cells', *Water Research* **41**, 2921–2940.

Pinto, R. P., Srinivasan, B., Manuel, M. F. and Tartakovsky, B. (2010), 'A two-population bio-electrochemical model of a microbial fuel cell', *Bioresource Technology* **101**(14), 5256–5265.
URL: *http://dx.doi.org/10.1016/j.biortech.2010.01.122*

Pinto, R. P., Tartakovsky, B. and Srinivasan, B. (2012), 'Optimizing energy productivity of microbial electrochemical cells', *Journal of Process Control* **22**(6), 1079–1086.
URL: *http://dx.doi.org/10.1016/j.jprocont.2012.04.005*

Potter, M. C. (1910), 'On the Difference of Potential due to the Vital Activity of Micro- organisms', *Durham Univ. Phil. Soc. Proc.* **3**.

Potter, M. C. (1911), 'Electrical Effects accompanying the Decomposition of Organic Compounds', *Durham Univ. Phil. Soc. Proc.* pp. 260–276.

Rabaey, K. and Verstraete, W. (2005), 'Microbial fuel cells: Novel biotechnology for energy generation', *Trends in Biotechnology* **23**(6), 291–298.

Recio-Garrido, D., Perrier, M. and Tartakovsky, B. (2016), 'Combined bioelectrochemical-electrical model of a microbial fuel cell', *Bioprocess and Biosystems Engineering* **39**(2), 267–276.

Reguera, G. and Kashefi, K. (2019), 'The electrifying physiology of Geobacter bacteria, 30 years on', *Advances in Microbial Physiology* **74**, 1–96.

Ren, L., Zhang, X., He, W. and Logan, B. E. (2014), 'High current densities enable exoelectrogens to outcompete aerobic heterotrophs for substrate', *Biotechnology and Bioengineering* **111**(11), 2163–2169.

Rezaei, F., Richard, Ã. T. L., Bruce, Ã. Ã. and Logan, E. (2008), 'Enzymatic Hydrolysis of Cellulose Coupled With Electricity Generation in a Microbial Fuel Cell', *Biotechnology and Bioengineering* **101**(6), 1163–1169.

Ribot-Llobet, E., Nam, J. Y., Tokash, J. C., Guisasola, A. and Logan, B. E. (2013), 'Assessment of four different cathode materials at different initial pHs using unbuffered catholytes in microbial electrolysis cells', *International Journal of Hydrogen Energy* **38**(7), 2951–2956.
URL: *http://dx.doi.org/10.1016/j.ijhydene.2012.12.037*

Ritchie, H. and Roser, M. (2020), 'CO2 and Greenhouse Gas Emissions', *Our World in Data* pp. 1–54.
URL: *https://ourworldindata.org/co2-and-other-greenhouse-gas-emissions*

Roger, T., Bhakoo, M. and Zhang, Z. (2008), 'Bacterial adhesion and biofilms on surfaces', *Progress in Natural Sciences* **18**, 1049–1056.

Rozendal, R. A., Hamelers, H. V., Rabaey, K., Keller, J. and Buisman, C. J. (2008), 'Towards practical implementation of bioelectrochemical wastewater treatment', *Trends in Biotechnology* **26**(8), 450–459.

Ruiz, Y., Baeza, J. A. and Guisasola, A. (2015), 'Enhanced Performance of Bioelectrochemical Hydrogen Production using a pH Control Strategy', *ChemSusChem* **8**, 389–397.

Satinover, S. J., Schell, D. and Borole, A. P. (2020), 'Achieving high hydrogen productivities of 20 L/L-day via microbial electrolysis of corn stover fermentation products', *Applied Energy* **259**, 114126.
URL: *https://doi.org/10.1016/j.apenergy.2019.114126*

Satomi, M. (2014), Shewanella, *in* C. A. Batt and M. L. Tortorello, eds, 'Encyclopedia of Food Microbiology', Vol. 3, Elsevier, Cambridge, Massachusetts, United States, pp. 397–407.

Sawyer, D. T., Sobkowiak, A. and Roberts, J. L. (1995), *Experimental Electrochemistry for Chemists*, 2nd editio edn, American Chemical Society.

Schalenbach, M., Tjarks, G., Carmo, M., Lueke, W., Mueller, M. and Stolten, D. (2016), 'FOR I NCREASED Acidic or Alkaline ? Towards a New Perspective on the Efficiency of Water Electrolysis', *Journal ofThe Electrochemical Society* **163**(11).

Sherrard, J. H. and Schroeder, E. D. (1973), 'Cell yield and growth rate in activated sludge', *Journal of the Water Pollution Control Federation* **45**(9), 1889–1897.

Sherwood, T. K., Pigford, R. L. and Wilke, C. R. (1975), *Mass transfer*, Series: McGraw-Hill chemical engineering series.

Shi, C. Y. (2011), *Mass Flow and Energy Efficiency of Municipal Wastewater Treatment Plants*, IWA Publishing, London, UK.

Skellet, C. (1992), 'Better sewage treatment in the UK', *European Water Pollution Control* **2**(1), 39–41.

Sleutels, T. H. J. A., Darus, L., Hamelers, H. V. M. and Buisman, C. J. N. (2011), 'Effect of operational parameters on Coulombic efficiency in bioelectrochemical systems', *Bioresource Technology* **102**(24), 11172–11176.
URL: *http://dx.doi.org/10.1016/j.biortech.2011.09.078*

Sleutels, T. H. J. A., Heijne, T. and Buisman, C. J. N. (2012), 'Bioelectrochemical Systems : An Outlook for Practical Applications', *ChemSusChem* **5**, 1012–1019.

Speers, A. M. and Reguera, G. (2012), 'Electron donors supporting growth and electroactivity of geobacter sulfurreducens anode biofilms', *Applied and Environmental Microbiology* **78**(2), 437–444.

Stanbury, P. F., Whitaker, A. and Hall, S. J. (2017), Chapter 11 - Effluent treatment, *in* 'Principles of Fermentation Technology (Third Edition)', Butterworth-Heinemann, Oxford, UK, pp. 687–723.

Stott, J. and Abdullahi, A. (2018), Corrosion in Microbial Environments, *in* 'Materials Science and Materials Engineering', Elsevier, Amsterdam.

Stott, R. (2003), Fate and behaviour of parasites in wastewater treatment systems, *in* D. Mara and N. Horan, eds, 'Handbook of Water and Wastewater Microbiology', Academic Press, Cambridge, Massacusetts, USA, pp. 1–832.

Sultana, S. T., Babauta, J. T. and Beyenal, H. (2016), 'Electrochemical biofilm control : a review', *Biofouling* **31**(9-10), 745–758.
URL: *http://dx.doi.org/10.1080/08927014.2015.1105222*

Suzuki, S., Karube, I. and Matsunaga, T. (1978), 'Application of a biochemical fuel cell to wastewaters', *Biotechnol. Bioeng. Symp.* **8**.

Torres, I. T., Rittmann, B. E. and Marcus, A. K. (2007), 'Conduction-Based Modeling of the Biofilm Anode of a Microbial Fuel Cell', *Biotechnoogy and Bioengineering* **98**(6), 1171–1182.

US EPA (2006), 'Wastewater Management Fact Sheet [EPA 832-F-06-024]'.

US EPA (2014), Primer for Municipal Wastewater Treatment Systems, Technical Report January, US EPA.

Velasquez-orta, S. B. and Yu, E. (2011), 'Evaluation of hydrolysis and fermentation rates in microbial fuel cells', *Applied Microbiology and Biotechnology* **90**, 789–798.

Vignola, M., Werner, D., Wade, M. J., Meynet, P. and Davenport, R. J. (2018), 'Medium shapes the microbial community of water filters with implications for effluent quality', *Water Research* **129**, 499–508.

Wang, H., Qu, Y., Li, D., Zhou, X. and Feng, Y. (2015), 'Evaluation of an integrated continuous stirred microbial electrochemical reactor : Wastewater treatment , energy recovery and microbial community', *Bioresource Technology* **195**, 89–95.

Ware, M. and Mabe, M. (2015), The STM Report, Fourth Edition, Technical Report 5, International Association of Scientific, Technical and Medical Publishers.

WWAP (2017), 'The United Nations World Water Development Report - Wastewater: The Untapped Resource', *UNESCO* **5**(2), 80–81.

Xia, C., Zhang, D., Pedrycz, W., Zhu, Y. and Guo, Y. (2018), 'Models for Microbial Fuel Cells: A critical review', *Journal of Power Sources* **373**, 119–131.
URL: *https://doi.org/10.1016/j.jpowsour.2017.11.001*

Xin, X., He, J., Li, L. and Qiu, W. (2018), 'Enzymes catalyzing pre-hydrolysis facilitated the anaerobic fermentation of waste activated sludge with acidogenic and microbiological perspectives', *Bioresource Technology* **250**, 69–78.
URL: *https://doi.org/10.1016/j.biortech.2017.09.211*

Ye, Y. and Logan, B. E. (2018), 'he importance of OH- transport through anion exchange membrane in microbial electrolysis cells', *International Journal of Hydrogen Energy* **43**(5), 2645–2653.
URL: *https://doi.org/10.1016/j.ijhydene.2017.12.074*

Zhang, Y. and Angelidaki, I. (2016), 'Microbial Electrochemical Systems and Technologies: It is Time to Report the Capital Costs', *Environmental Science and Technology* **50**(11), 5432–5433.

Zhao, F. (2018), The effect of complex feed on Bioelectrochemical systems (BESs) performance, PhD thesis, Newcastle University.

Zhen, G., Lu, X., Kobayashi, T., Kumar, G. and Xu, K. (2015), 'Promoted electromethanosynthesis in a two-chamber microbial electrolysis cells (MECs) containing a hybrid biocathode covered with graphite felt (GF)', *Chemical Engineering Journal* **284**, 1146–1155.
URL: *http://linkinghub.elsevier.com/retrieve/pii/S138589471501342X*

Zheng, D., Gu, W., Zhou, Q., Zhang, L. and Wei, C. (2020), 'Bioresource Technology Ammonia oxidation and denitrification in a bio-anode single-chambered microbial electrolysis cell', *Bioresource Technology* **310**(May), 123466.
URL: *https://doi.org/10.1016/j.biortech.2020.123466*

Appendices

Appendix A. Supporting information for Chapter 1

Technology		
Activated sludge	Electrodeionization	Nanotechnology
Adsorption Bio-oxidation process	Electrodialysis	Oil-water separator
Advanced oxidation process	Electrolysis	Parallel plate oil-water separator
Aerated lagoon	Enhanced biological phosphorus removal	Photobioreactor
Aerobic granular sludge	Expanded granular sludge bed digestion	Reed bed
Anaerobic clarigester	Extended aeration	Regenerative thermal oxidizer
Anaerobic digestion	Facultative lagoon	Retention basin
Anaerobic filter	Fenton's reagent	Reverse osmosis
Anaerobic lagoon	Fine bubble diffusers	Rotating biological contactor
Anammox	Flocculation-sedimentation	Sand filter
API oil-water separator	Flotation process	Screen filter
Belt filter	Forward osmosis	Sedimentation
Capacitive deionization	Froth flotation	Septic tank
Carbon filter	Hydrocyclone	Sequencing batch reactor
Cesspit	Imhoff tank	Skimmer machine
Clarifier	Induced gas flotation	Slow sand filter
Coarse bubble diffusers	Ion exchange	Stabilization pond
Composting toilet	Lamella clarifier	Supercritical water oxidation
Constructed wetland	Living machines	Thermal hydrolysis
Cross-flow filtration	Maceration sewage	Treatment pond
Dark fermentation	Media filter	Trickle-bed reactor
Decentralized	Membrane bioreactor	Trickling filter
Desalination	Membrane distillation	Ultrafiltration
Diffuser sewage	Microalgae	Ultraviolet disinfection
Dissolved air flotation	Microbial electrolysis cell	Upflow anaerobic sludge blanket digestion
Dissolved gas flotation	Microbial electrosynthesis	Urine-diverting dry toilet
Distillation	Microbial fuel cell	Vacuum evaporation
Electro-oxidation	Microflotation	Vermifilter
Electrocoagulation	Moving bed biofilm reactor	Wet oxidation

Table A.1: technology search terms used for literature review. Search format: '"*technology*" wastewater'

Appendix B. Supporting information for Chapter 3

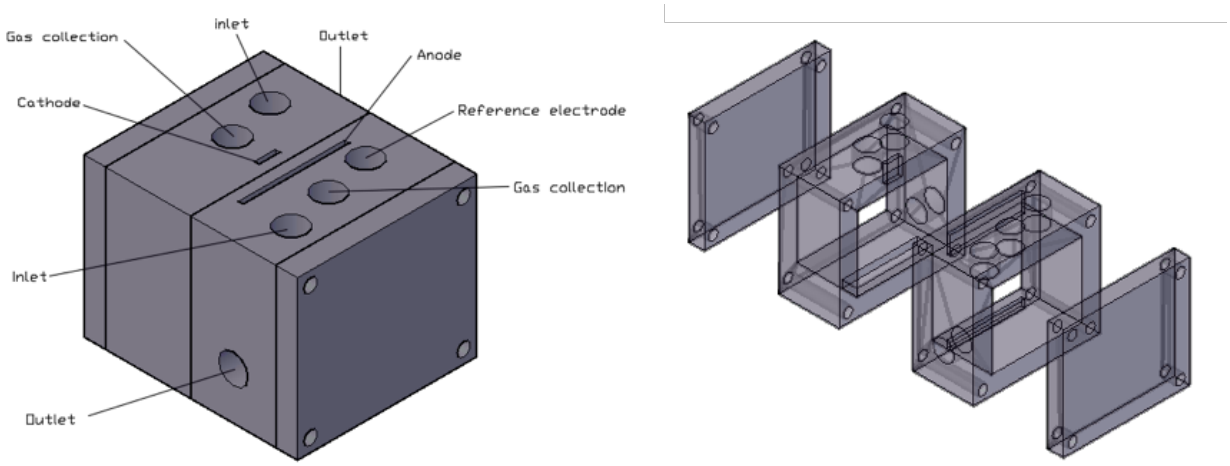

Figure B.1: Schematics for experimental 3D printed reactor chamber

Reference electrode	Voltage adjustment required
1	-0.012V
2	0.000V
3	-0.011V
4	-0.018V
5	-0.003V
6	0.000V
7	-0.006V
8 (Master)	0.000V

Table B.1: Voltage drift of reference electrodes and subsequent voltage corrections

Cell	Height (from bottom to tip) (mm)	Skew (From left to tip) (mm)	Distance (From anode to tip) (mm)
1	52	63	3
2	53	63	9
3	45	63	3
4	53	63	9
5	47	67	8
6	52	63	4
7	48	63	1
8	48	64	4

Table B.2: Placement of salt bridge tip in anode compartment

Cell	1kohm Resistor (kOhm)	2kohm Resistor (kOhm)
1	0.997	2.00
2	1.004	2.00
3	1.000	2.00
4	1.000	1.99
5	0.997	2.00
6	1.000	2.00
7	1.000	2.00
8	1.001	1.99

Table B.3: Measured resistance across cell to determine accuracy of current readings

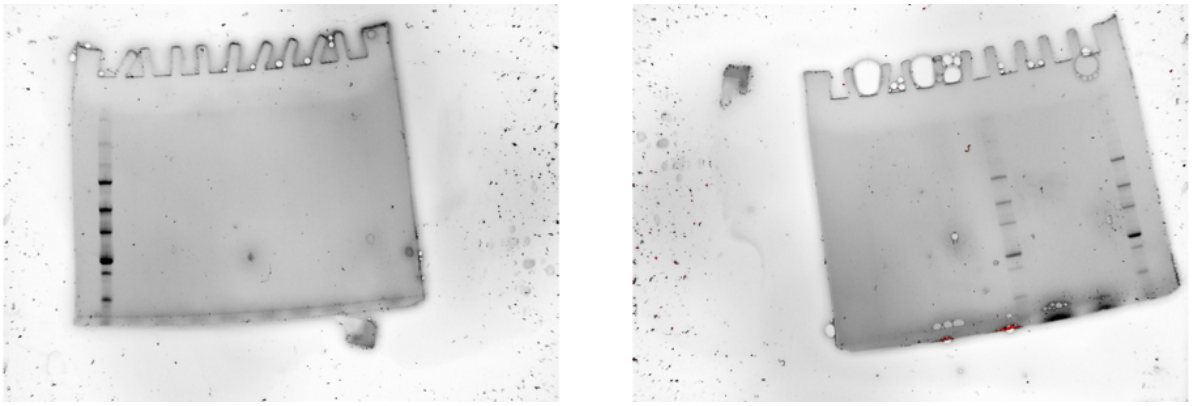

Figure B.2: Gel electrophoresis imaging to detect proteins in samples

Cell	Cathode	Anode
1	7.79	7.20
2	7.81	7.24
3	7.50	7.25
4	7.59	7.17
5	7.47	7.23
6	7.45	7.20
7	7.59	7.17
8	7.64	7.19

Table B.4: pH drift after 3 weeks of operation with mean concentration of 37.4mg/l

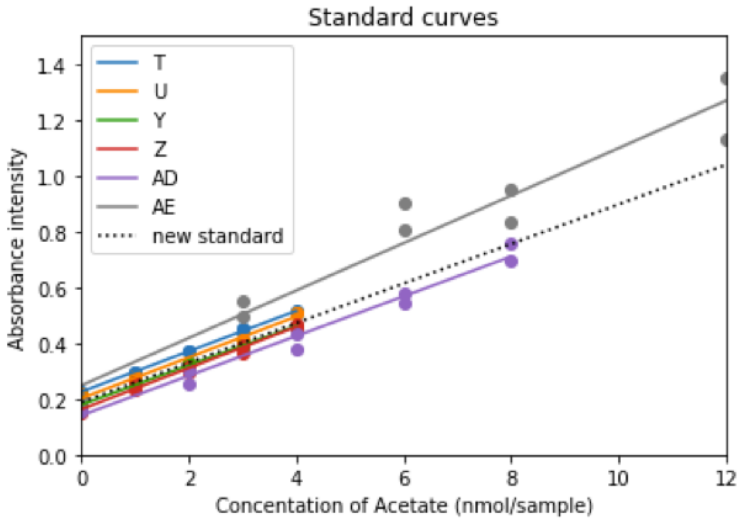

run	R^2	gradients	intercepts
T	0.998	0.072	0.225
U	0.984	0.073	0.202
Y	0.995	0.071	0.179
Z	0.988	0.074	0.162
AD	0.984	0.071	0.14
AE	0.949	0.085	0.248
new standard	0.91	0.071	0.188

Figure B.3: Standard curves used for acetate concentrations

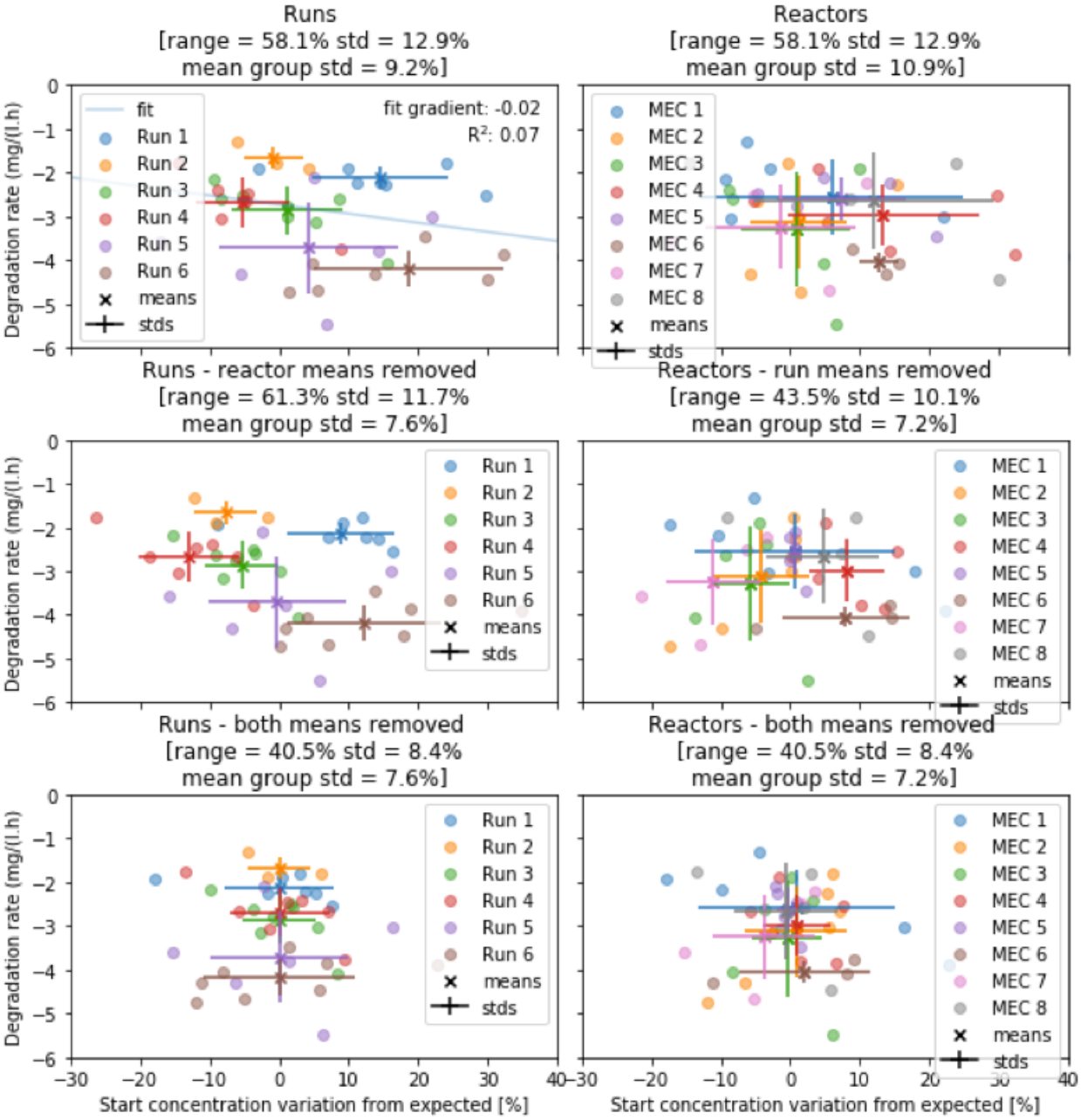

Figure B.4: Starting acetate concentration analysis into variation

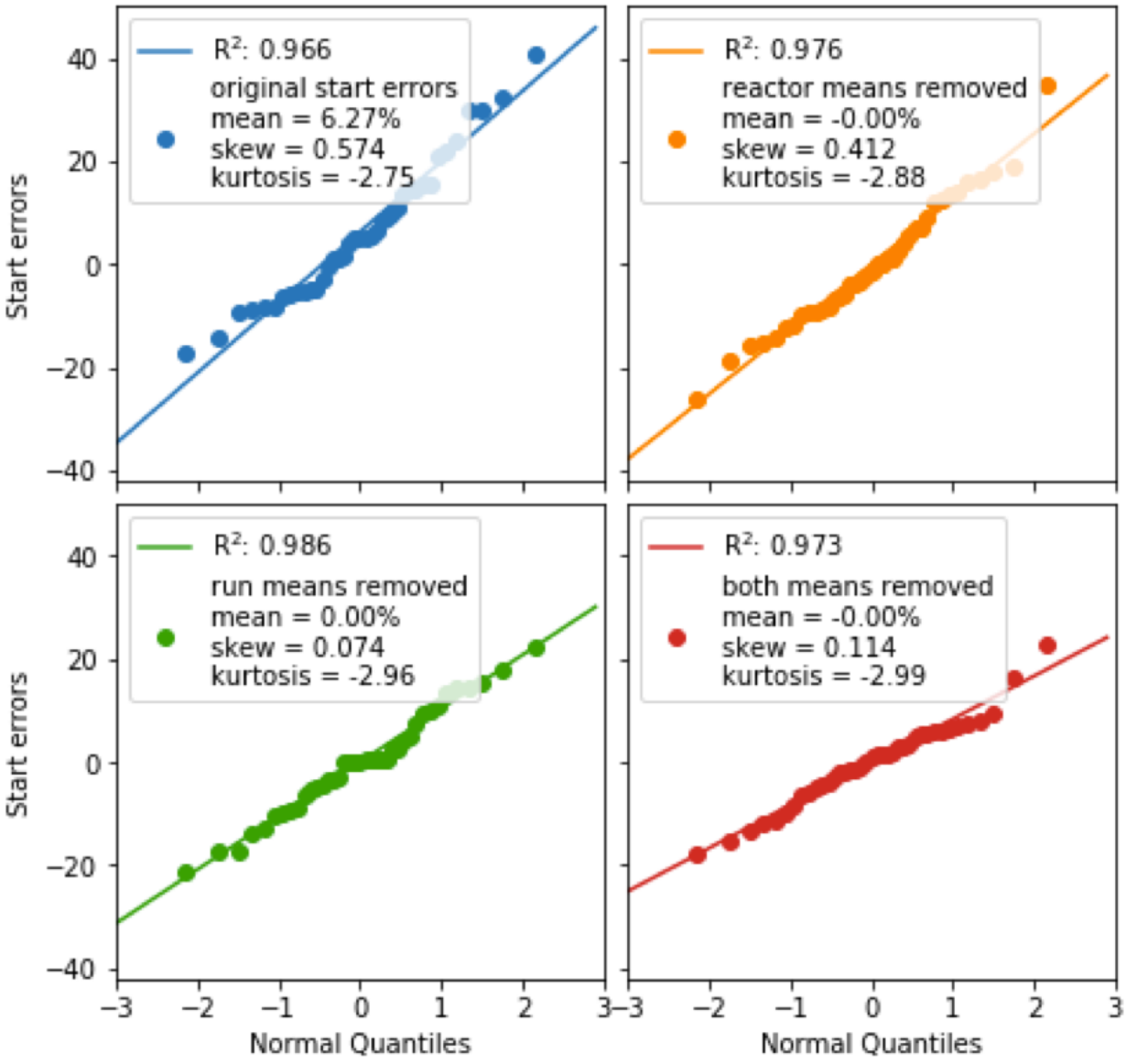

Figure B.5: Q-Q plot for substrate concentrations on raw data and with run means, and reactor means removed

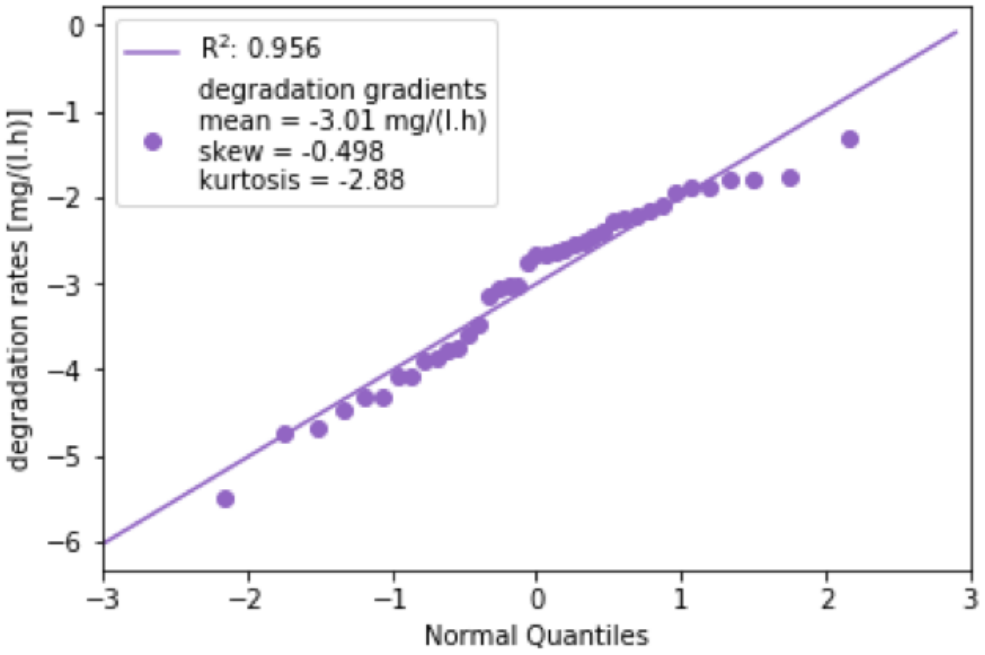

Figure B.6: Q-Q plot for substrate degradation rates

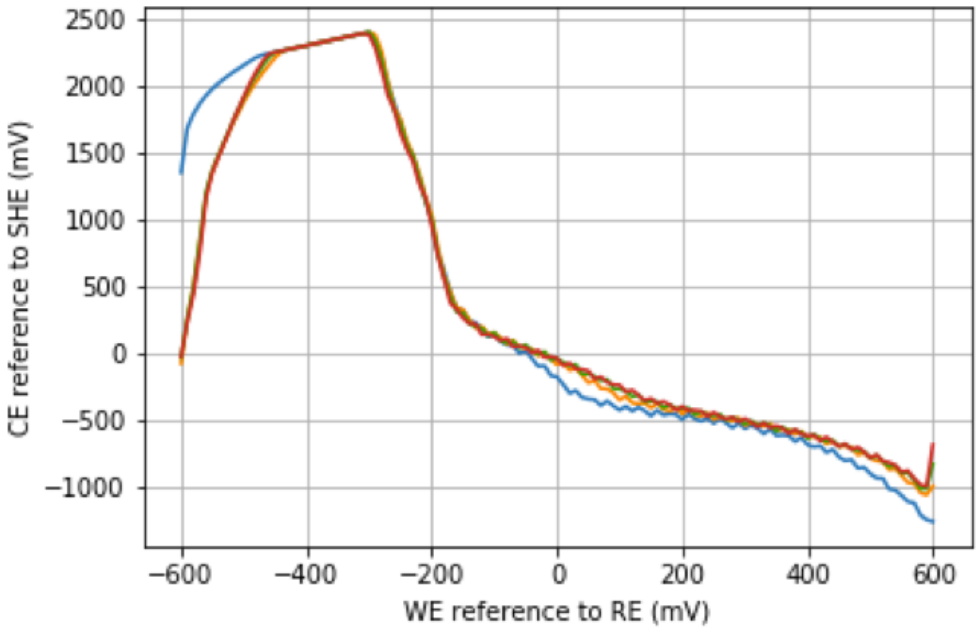

Figure B.7: Linear sweep voltammetry to determine stable potential range

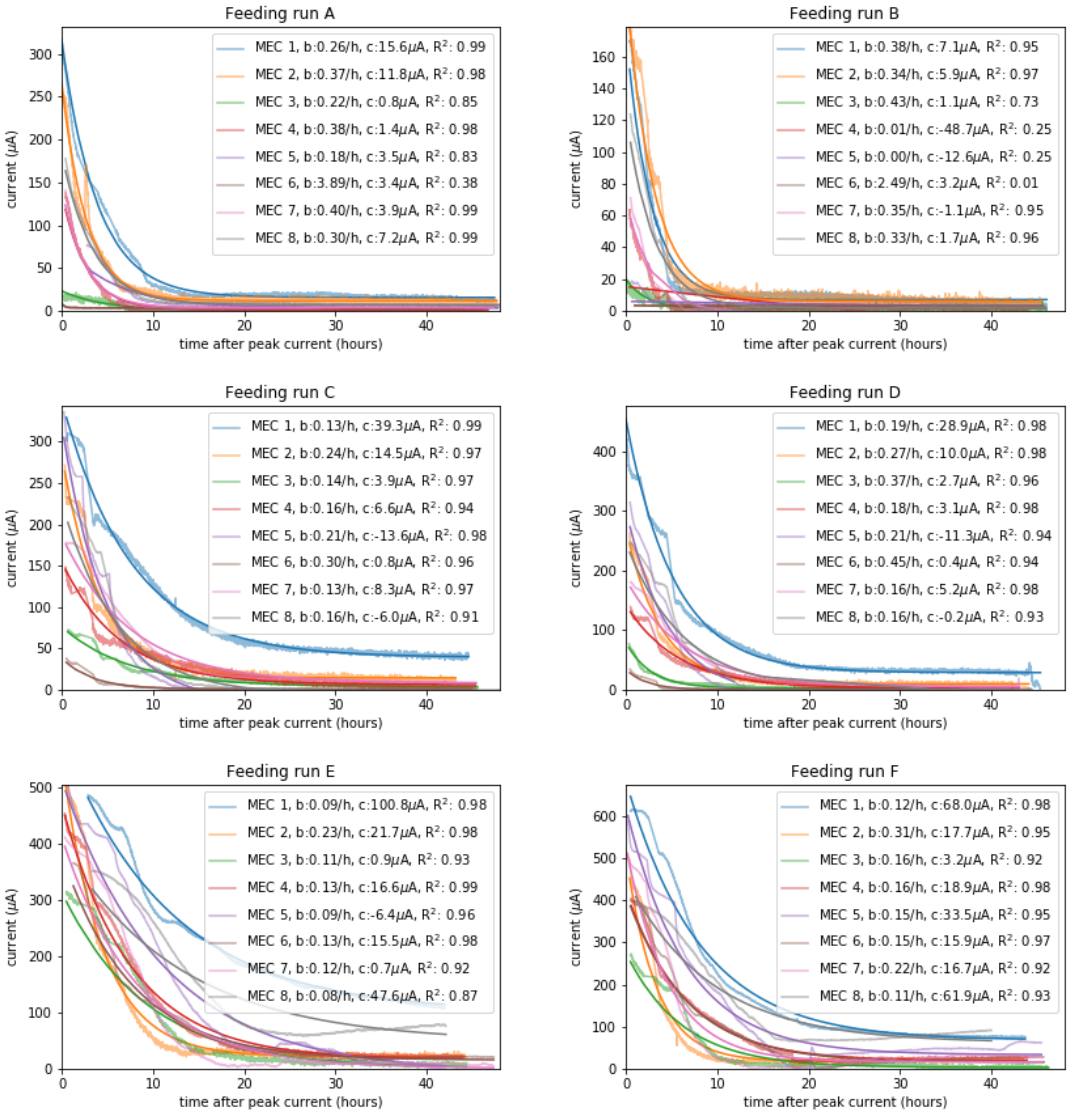

Figure B.8: Smoothed current dose-responses following feeding for all 6 runs and fit to exponential decay curves

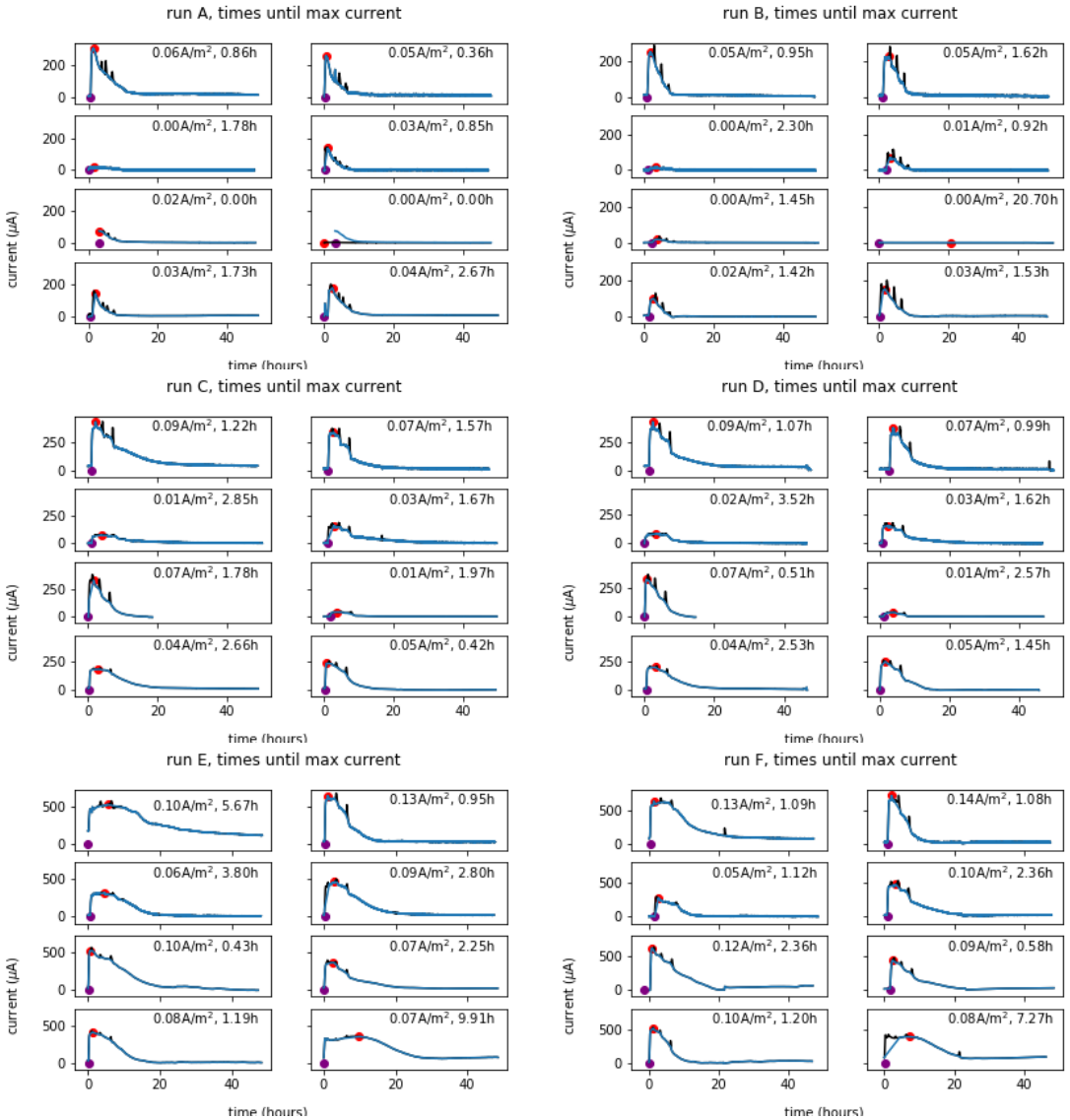

Figure B.9: Calculated feed times for each reactor over each run

Figure B.10: Profile qualities in forward runs

Figure B.11: Profile qualities in reverse runs

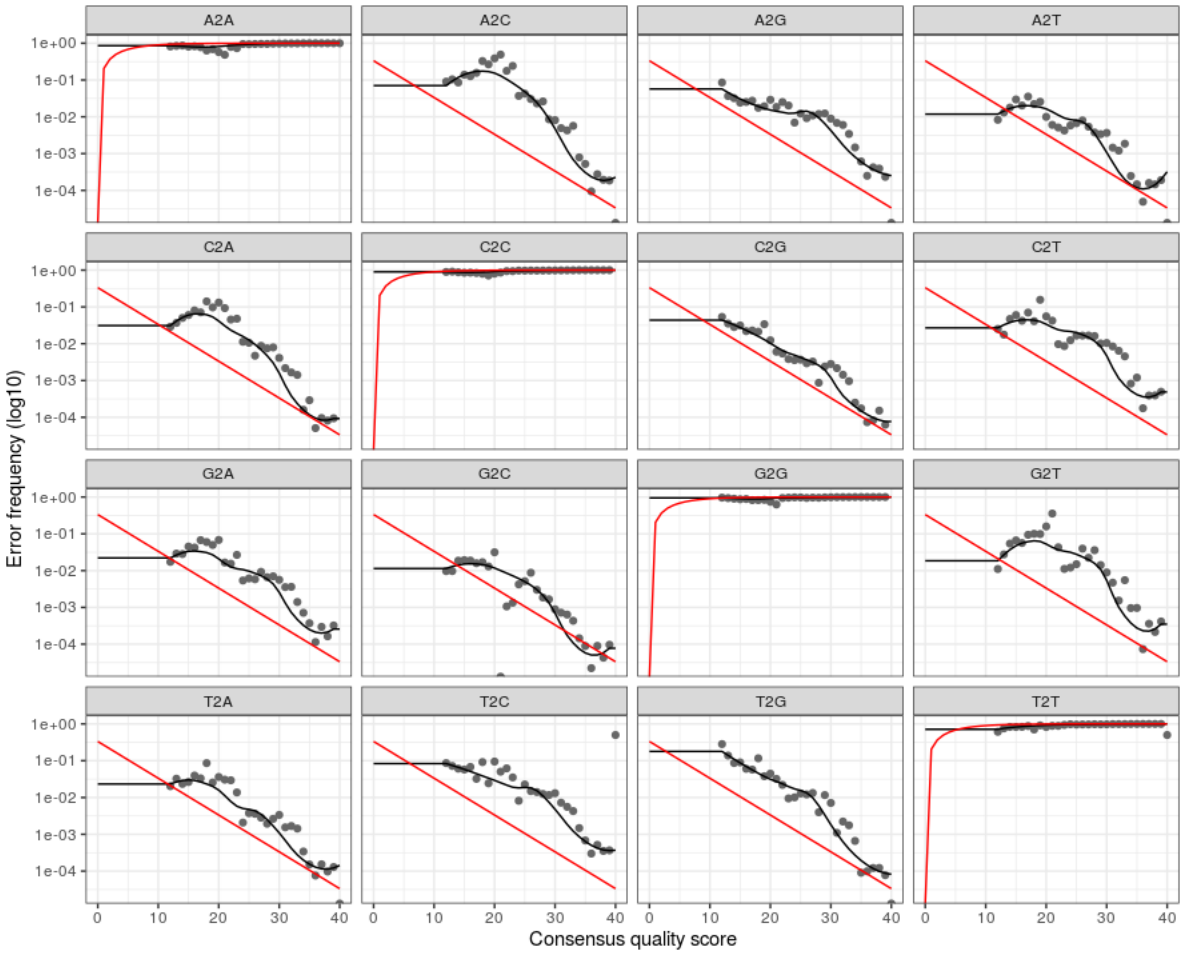

Figure B.12: Learning errors in forward runs

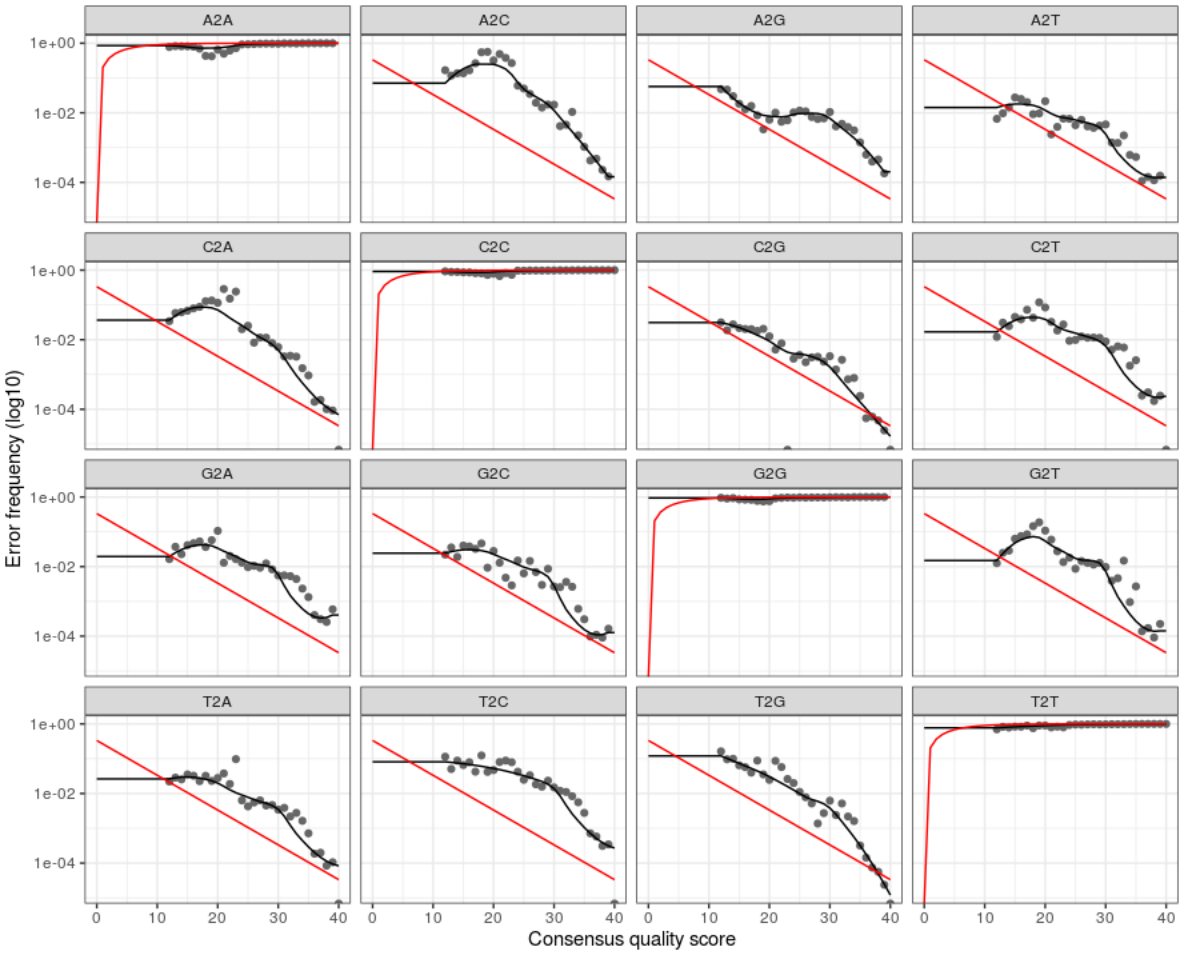

Figure B.13: Learning errors in reverse runs

Appendix C. Supporting information for Chapter 4

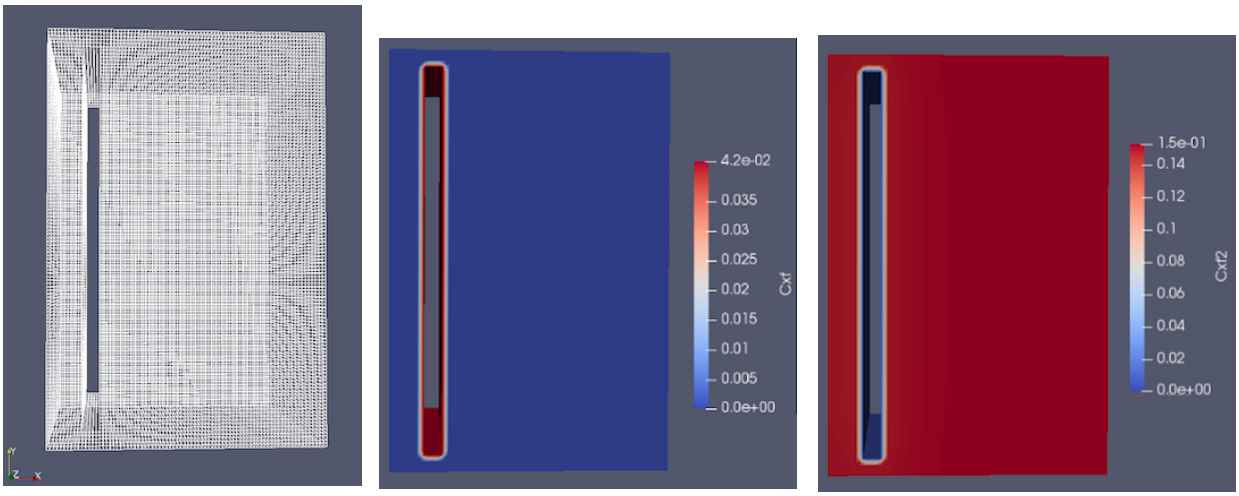

(a) Wireframe representation of discretised scheme

(b) Biofilm placement

(c) Bulk community placement

Figure C.1: Discretised scheme with biomass placements

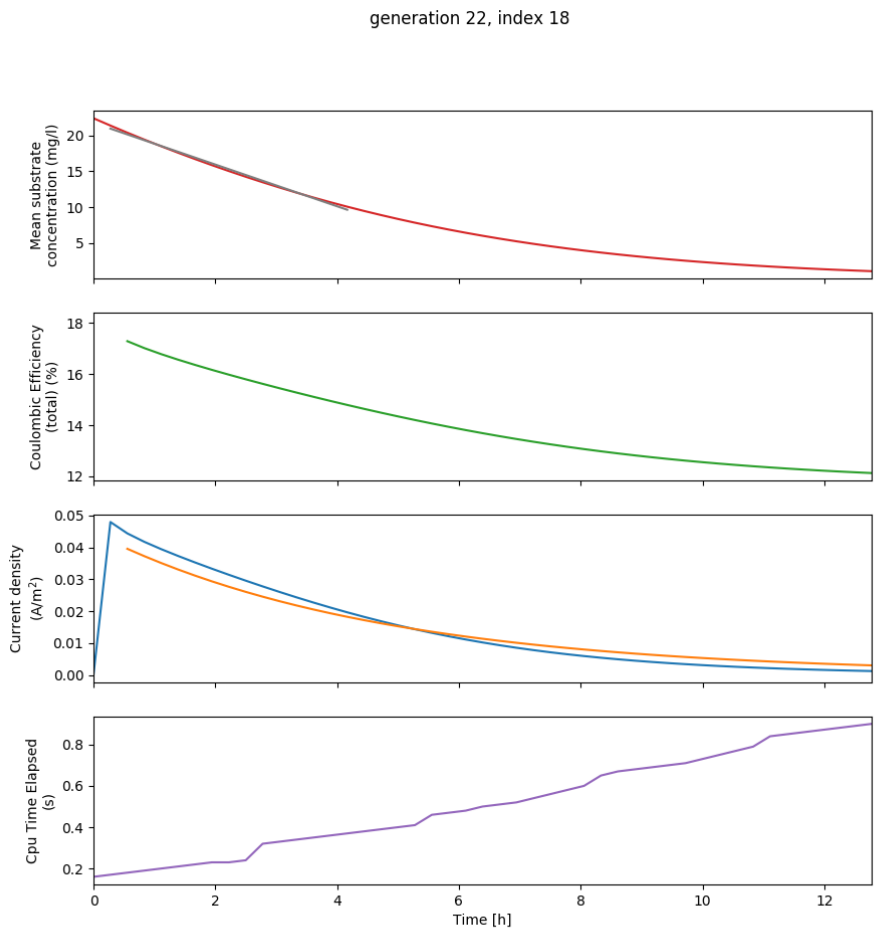

Figure C.2: Outputs for substrate, maximum current density, coulombic efficiency, and cpu time elapsed for most accurate permutation

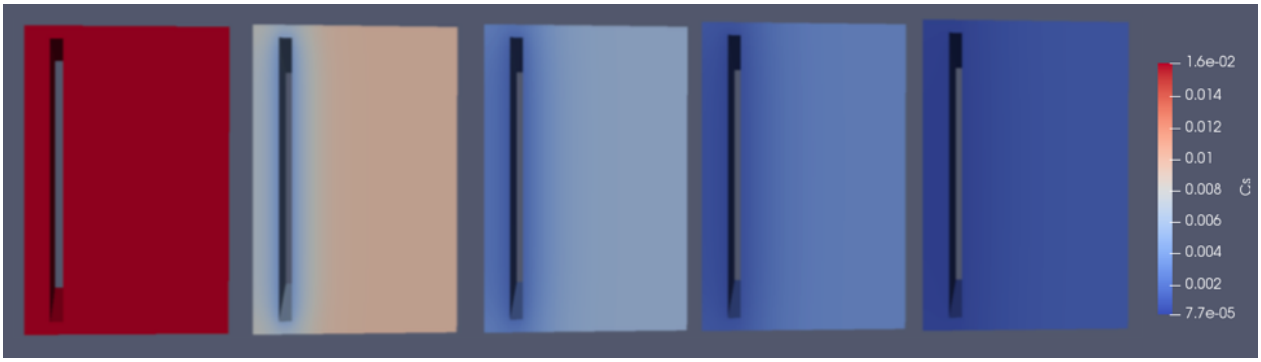

Figure C.3: Substrate removal over time in most accurate model

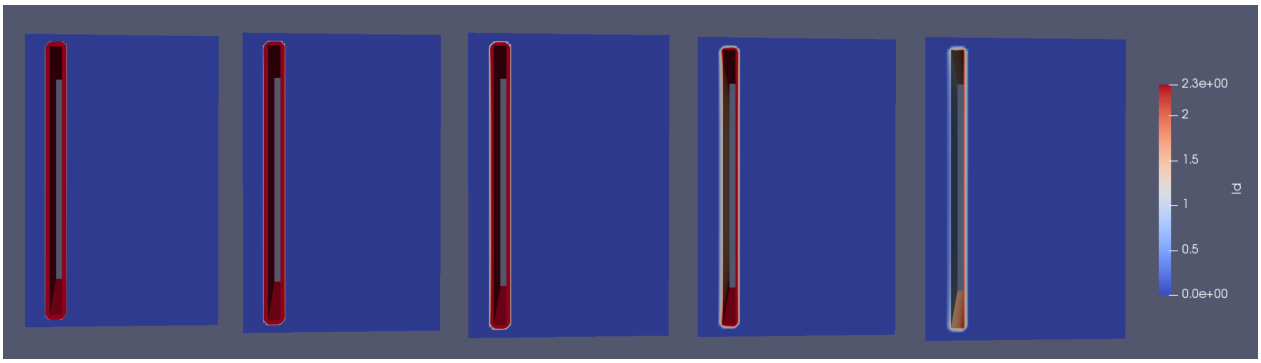

Figure C.4: Current production over time in most accurate model

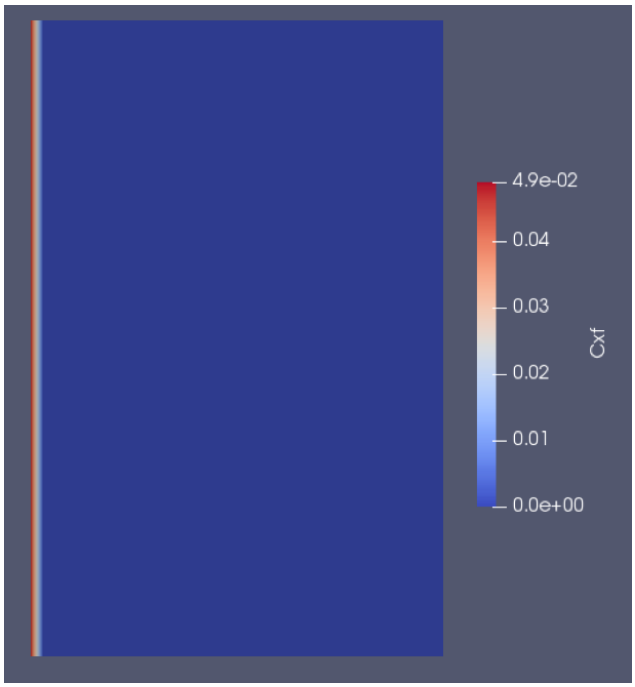

Figure C.5: Biofilm placement in new scheme

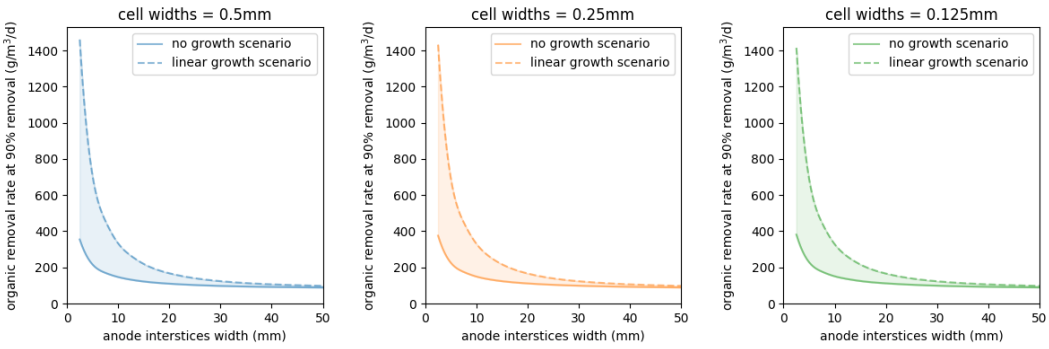

Figure C.6: Mesh independence test for a range of concentrations and widths